# Dimensional Analysis and Sub-scaling of Building Thermal Airflow Dynamics Based on Simple Analytical Models

Xin Zhang

A Thesis

in

the Department

of

Building, Civil and Environmental Engineering

Presented in Partial Fulfilment of the Requirements

for the Degree of

Master of Applied Science (Building Engineering) at

Concordia University

Montreal, Quebec, Canada

March 2019

# CONCORDIA UNIVERSITY

## SCHOOL OF GRADUATE STUDIES

This is to certify that the thesis prepared

By: Xin Zhang

Entitled: Dimensional Analysis and Sub-scaling of Building Thermal Airflow Dynamics Based on Simple Analytical Models

and submitted in partial fulfilment of the requirements for the degree of

**Master of Applied Science (Building Engineering)**

complies with the regulations of the University and meets the accepted standards with respect to originality and quality.

Signed by the final Examining Committee:

| | |
|---|---|
| Dr. H. Ge | Chair |
| *Chair's name* | |
| Dr. T-H. Kwok | Examiner |
| *Examiner's name* | |
| Dr. C. Alecsandru | Examiner |
| *Examiner's name* | |
| Dr. L. Wang | Thesis Supervisor |
| *Supervisor's name* | |

Approved by

Chair of Department or Graduate Program Director

_____ 2019

Dean of Faculty

# Abstract


**Dimensional Analysis and Sub-scaling of Building Thermal Airflow Dynamics Based on Simple Analytical Models**

Xin Zhang

Sub-scale model experiments are widely used in the design of natural/hybrid ventilation systems and the thermal mass of buildings to calibrate and validate simulation models, collect data, and guide preliminary designs. Defining a scaling law to relate a sub-scale model experiment to a full-size building is a good method to determine fabrication design and operation strategy. As a result, many previous studies have focused on airflow similarity between a sub-scale model and a full-size building in a steady state using dimensional analysis. These studies, however, lack integrated consideration of both airflow and heat transfer in a transient-state model. The purpose of this thesis is to build an analytical model for dimensional analysis in a simplified model and to define dimensionless numbers to consider integrated similarity. The thesis also discusses whether those dimensionless numbers can be applied to a complicated high-rise building. Both sub-scale and full-size simulation models are calibrated and validated using results of sub-scale model experiments. Subsequently, dimensionless results from both the sub-scale and full-size models are compared to verify the dimensionless numbers derived from the analytical model. Finally, counterpart results for a full-size model are calculated by the scaling law from sub-scale experiments for thermal mass application

## Acknowledgements

I would like to express my very great appreciation to my supervisor Dr. Liangzhu (Leon) Wang. Advice and supervision given by Dr. Wang has been a great help in completing this thesis. I would like to offer my special thanks for his valuable and constructive suggestions during planning and working of this research.

Secondly, I would like to express my special thanks to Dr. Jiwu Rao, who gave me advice and support for experiment device installation.

I would also like to thank various colleagues in the group, Dr. Dahai Qi, Ali Katal, Shu Chang, Cheng Zhang and Senwen Yang, for their assistance and support. In particular:

Dr. Dahai Qi helped to develop the scale method in dimensional analysis; Ali Katal assisted to build the simulation model; Shu Chang helped to check the equations and results in experiments and simulations; Cheng Zhang and Senwen Yang helped to build experiment model and install devices.

It is a joyful experience to work with them and learn research skills from them.

Finally, I wish to thank my wife and my parents for their support and encouragement, without their help, it is impossible to complete this research. I also wish to thank my friends in Canada, China and Japan, as it is helpful to have their support and encouragement.

## Contribution of Researchers

This study is conducted by a team, and Dr. Liangzhu Wang give us plenty of advice and suggestion. The contribution of researchers is following:

1. Dr. Dahai Qi first proposed this idea and building the analytical model in steady state [59], and he gave advice and suggestion when a transient model is developed with thermal mass in analytical model by the author (section 3.2).
2. PhD. student Ali Katal contributed mainly in the multizone-model coding (section 3.4). Setup, running simulation, and data analysis are conducted by the author, meanwhile, Ali Katal guide how to use his coding model.
3. MASc student Cheng Zhang and PhD. student Senwen Yang help to fabricate the experiment model and install experiment facility. The design, fabrication, setup, and data record of experiment are mainly conducted by the author.

All researchers have consented to participation of this thesis.

## Table of Contents

## List of Figures

## List of Tables

## Nomenclature

| | |
|---|---|
| $Q$ | Heat source (W) |
| $P$ | Pressure (Pa) |
| $\dot{m}$ | Mass flow rate (kg/s) |
| $T$ | Temperature (°C) |
| $j$ | Time Steps |
| $A$ | Area ($m^2$) |
| $R$ | Thermal resistance (($m^2 \cdot K$)/W) |
| $U$ | Overall heat transfer coefficient (W/($m^2 \cdot K$)) |
| $h$ | Convective coefficient (W/($m^2 \cdot K$)) |
| $L$ | Thickness (m) |
| $k$ | Conduction heat transfer coefficient (W/(m·K)) |
| $M$ | Mass (kg) |
| $\dot{M}$ | Mechanical mass flow rate (kg/s) |
| $C_p$ | Specific heat capacity of the air (J/(kg·°C)) |
| $C_{pw}$ | Specific heat capacity of the envelope (J/(kg·°C)) |

| | |
|---|---|
| $C_{pcm}$ | Specific heat capacity of the PCM (J/(kg·°C)) |
| $C_d$ | Discharge coefficient |
| $C$ | Flow coefficient |
| $\Delta t$ | Time span (s) |
| $\hat{t}$ | Dimensionless time |
| $n$ | Flow exponent |
| $S$ | Airflow source of certain zone |
| $H$ | Distance between top and bottom openings (m) |
| $V$ | Volume ($m^3$) |
| $Z$ | Floor elevation (m) |
| $g$ | Acceleration due to Earth's gravity ($m/s^2$) |
| $u$ | Speed of the fluid (m/s) |

*Greek symbols*

| | |
|---|---|
| $\theta$ | Dimensionless temperature |
| $\Pi$ | Dimensionless numbers |
| $\tau$ | Maximum time duration in test (s) |

| | |
|---|---|
| $\rho$ | Density ($kg/m^3$) |
| $\beta$ | Coefficient of thermal expansion (equal to approximately 1/T, for ideal gases) |
| $\nu$ | Kinematic viscosity ($m^2/s$) |

*Subscripts*

| | |
|---|---|
| *i* | Interior air |
| *o* | Outside air |
| *w* | Envelope |
| *s* | Sub-scale model |
| *f* | Full-size model |
| *e* | Effective |
| *z* | Zones |
| *pcm* | Phase change material |
| *max* | Maximum value of outside air |

# Chapter 1 Introduction

## 1.1. Statement of the problem

Economic development and growing population worldwide have resulted in increasing demands for energy and escalating generation of greenhouse gases (GHG). Among all sectors, the building sector has been a main contributor of energy use growth in Canada, most of which is due to increased needs for space cooling [1]. From 1990 to 2015, the total energy consumption for space cooling in both commercial/institutional and residential sectors increased by 116% [1]. Globally, from 1990 to 2016, space-cooling energy use has increased more than threefold to 2,020 TWh, which reached nearly 10% of the total electricity consumption (21,000 TWh) in whole building sectors [2]. Meanwhile, 40% of total carbon emissions are believed to be from buildings, a major contributor to global climate warming [3].

To reduce building energy demands and GHG generation, two common approaches have been often taken: 1) reducing energy usage through energy-efficiency measures, including using more-efficient energy systems, and 2) reducing the reliance on major energy expenders in buildings, such as mechanical systems, by taking advantage of passive systems, including passive solar energy and natural/hybrid ventilation. A well-designed natural ventilation system was found to be able to cut energy demands by 50% [4]. By adjusting window-to-wall ratio and window opening percentage, operational strategy can be optimized to increase energy savings through natural ventilation [5]. Furthermore, when outdoor air is cleaner than indoor air, by bringing in fresher

outside air and removing indoor contaminants (e.g., $CO_2$) [6], natural ventilation systems tend to reduce sick-building syndrome when compared to mechanical ventilation systems, as confirmed by a study of 42 buildings. On the other hand, in naturally ventilated buildings, thermal comfort seems a major concern: complaints of discomfort have been often reported due to the high sensitivity of indoor air to the exterior environment in hot or cold climates [7]. The thermal-comfort issue is therefore often addressed by combining mechanical and natural ventilation systems, so-called hybrid ventilation. It was found that hybrid ventilation could save 90% on cooling-system energy in extremely arid climates when proper control strategies were in place for the hybrid ventilation system in the tested building [8].

Given that its benefits outweigh its shortcomings, natural or hybrid ventilation is regaining its popularity as an effective passive cooling strategy [9].

Meanwhile, for regions with significant diurnal temperature variations, there often exists a mismatch between demand and response for a natural or hybrid ventilation system: that is, the peak cooling load may occur during the middle of the day, whereas the outdoor air conditions (e.g., outdoor temperature) are not suitable for natural or hybrid ventilation; on the other hand, when the outdoor air temperature is low at night, the indoor cooling load may become so low that natural ventilation becomes unnecessary. This problem can be solved by the use of load-shifting techniques, such as using the natural and/or man-made thermal masses of buildings for thermal storage. Therefore, a combination of thermal mass and hybrid ventilation becomes a reasonable

solution: the thermal mass provides a stored cold energy source to cool down the indoor environment during the daytime and is charged with the cooling energy at night [10]. The greater the natural thermal mass of a building, the more cooling energy can be stored and, therefore, the shorter the period of time the air-conditioning system needs to operate. The building thermal mass can also be increased with the addition of man-made thermal storage materials, such as phase-change materials (PCMs) [11]. Thermal mass storage has been proved to be an effective technology for buildings. It can be divided in two major types: sensible-heat and latent-heat storage (e.g., PCMs). PCMs are stable near their freezing/melting temperature and have a high thermal capacity. Takeda and Nagano applied a PCM to the floor in their air-PCM ventilation system [12][13]. They showed that the PCM floor is a practical option for increasing a building's thermal storage, experimentally increasing storage to 1.79 $MJ/m^2$ over the course of a single night in a test room.

Compared with natural building materials, such as wood or concrete, a PCM is often much more expensive, so its use could result in a substantial additional cost [14]. Therefore, the question of how to integrate thermal mass with natural/hybrid ventilation in the most cost-effective way remains a major challenge to promoting the wide application of hybrid ventilation. Frequently, air-PCM thermal energy storage systems have been combined with heating, ventilation, and air-conditioning (HVAC) systems [15].

Similar to other common building design and analysis problems, the design and operation of natural/hybrid ventilation systems with thermal mass often requires using several methods: analytical models, full-size experiments, scaled laboratory experiments, and numerical simulations, which can be further divided into multizone thermal models and the more detailed computational fluid dynamics (CFD) models [16].

When we compare experiments and numerical simulations, the latter require accurate material properties as inputs, which are often hard to find. For example, there is no standard set of accurate PCM properties provided by their manufacturers: some manufacturers provide only the "phase-change temperature," which means the substance's freezing and melting temperatures are identical, whereas others provide different freezing and melting temperatures [14]. Furthermore, powder and liquid PCMs are often mixed in building materials or are packed in containers of different shapes, so the variations in mixing percentages and container shapes result in vast property differences among different PCMs from different sources [17], which makes it quite difficult to conduct numerical simulations. Therefore, experiments are unavoidable when studying natural/hybrid ventilation systems with thermal mass. More than that, when relatively large openings are considered, indoor-outdoor interactions generate bidirectional exchange flows, which are difficult to simulate. However, bidirectional exchange flows also may reduce stack pressure and result in decrease of exchange flows, which may violate fire codes [18]. Moreover, numerical simulations

must be validated against reliable experimental data before drawing conclusions, especially for large buildings with more complicated thermal airflow situations [19].

Nonetheless, numerical simulations can be quite powerful if they have been properly validated. Compared to experiments, computational simulations have almost zero cost and can be extended to many situations and material parameters that cannot easily be tested experimentally, such as building structure, materials, operations strategy, and so on. As a result, taking the benefits of both experiments and simulations and avoiding their weaknesses, the study of thermal airflows within buildings needs an integrated approach that uses both methods: experiments provide quality measurement data that is used to validate simulations, and simulations can then be extended to study situations that are costly or impractical to study experimentally.

When it comes to experimental approaches, full-size experiments are more costly and are often impractical for large buildings in terms of time and space when compared to scaled tests [20]. In this study, therefore, scaled experiments are the main test approach used.

In many previous scaled experimental studies, general dimensionless numbers, such as the Reynolds number, the Froude number, or the Grashof number, were applied when designing scaled tests and when explaining the scaled results and extending them to other scales. It has been well accepted that it is impossible to conserve all types of similarities in such tests [16]. For example, when studying natural or hybrid ventilation systems, temperature similarity is the most significant objective, so the Grashof similarity is often applied. In hybrid ventilation, however, the

conservation of the Grashof similarity based on the generic Grashof definition may result in an unrealistically high temperature [21].

For these reasons, a sub-scale model of thermal performance needs an increased heat flux or needs to compensate for the variation by different boundary conditions after dimensional analysis to ensure integrated thermal performance similarity between prototype and sub-scale model [22]. Nevertheless, this similarity cannot match the fluid dynamic completely because the analytical model considers only the thermal performance, and the flow pattern will be distorted from that of the prototype. Similarly, due to different thermal masses of different materials between prototype and sub-scale model, time-dependence should also be considered by analytical models [23]. Consequently, in sub-scale model experiments, an appropriate transient-state scaling law is indispensable and, depending on the desired objective, could be derived by dimensional analysis.

For simulation approaches, the detailed models, such as the CFD models, often involve extensive computing costs and time [16], and stringent requirements from accurate boundary condition settings [24]. As a result, for most building designs, CFD simulations are often limited to fixed boundary conditions, such as temperature, heat flux, and airflow rate, instead of real, dynamic information [25]. An alternative solution is to use simpler numerical simulation models, such as multizone thermal airflow network models, which are based on the assumption that the thermal and airflow conditions in a space are well-mixed so that the large volumetric space can be considered as one zone with uniform temperature, pressure (at the same height), and species

concentrations [26]. For large buildings with complicated systems, multizone models are found to be quite effective and to provide adequate accuracy [27] [28], especially when long-term results such as annual energy simulations are required, which can never be done by CFD simulations. The current study, therefore, uses the multizone network model as the major simulation model. In summary, this study relies on combined multizone network simulations and scaled experiments to investigate natural/hybrid ventilation coupled with thermal mass in buildings.

## 1.2. Motivation

Natural ventilation and hybrid ventilation can effectively reduce space cooling demand, however, how to determine airflow rate is always challenging when natural ventilation and hybrid ventilation are combined with thermal mass (e.g. PCM). The reason for this challenge is disadvantage of simulation and experiment, i.e., it is difficult to simulate natural and hybrid ventilation in multizone model, to simulate thermal mass in transient state in CFD model. Due to those limitations, this thesis, therefore, intends to combine sub-scale experiment and analytical model to research natural and hybrid ventilation.

Through proposed method in the thesis, designer can quantify PCM thermal charge and discharge in natural and hybrid ventilation in preliminary more precisely. With thermal property uncertainty and high cost of PCM, the research is indispensable to guide PCM application in natural and hybrid ventilation system. The proposed natural and hybrid ventilation system, which combined with PCM, is suitable for commercial and institutional building, because residential building cannot afford it based on relatively lower price/performance ratio in residential building rather than commercial/institutional building. Therefore, the scope of proposed system application will be commercial/institutional building.

### 1.3. Objectives of this thesis

From the discussions in the previous section, the following challenges have been identified:

- When full-size experiments are not available, sub-scale tests need to be carried out. The typical dimensionless numbers from conventional dimensional analysis (e.g., from the Buckingham $\pi$ theorem or developed from partial differential equations) are often too general and are designed for conserving detailed, local fluid flow and heat transfer phenomena, but not for obtaining global information. Therefore, a new dimensionless analysis to identify new dimensionless numbers is required.

- These new dimensionless numbers are needed to aid in the design of sub-scale tests (i.e., to help scale down full-size test and boundary conditions), and to aid in extending the sub-scale test results to full-size scales (i.e., scaling up the scaled test results). Therefore, different test cases need to be carried out.

- The relationship needs to be well developed between the scaled-test results, the scaled-simulation results, and the full-size-simulation results (when the full-size experiments are impractical). A proper scaling process involving both experiments and simulations needs to be developed.

- This thesis intends to avoid and solve the previously indicated problems by deriving a new scaling law from dimensional analysis and to focus on the transient state with energy consumption

predictions for hybrid ventilation systems in high-rise buildings. This complex model would be difficult to achieve using any single method, therefore, the thesis combines dimensional analysis of an analytical model, sub-scale model experiments, and multizone simulations for sub-scale and full-size models. Limitations of this new scaling law are discussed in the methodology chapter.

To solve these challenges, the main objectives of this thesis are:

- Development of new dimensional analysis method

The new dimensional analysis method is meant to identify the dimensionless numbers specific to certain problems and to apply them to designing sub-scale experiments and to scaling up the results of these experiments. In this study, the dimensional analysis does not apply $\pi$ analysis or general partial differential equations to find the typical dimensionless numbers. Instead, we study the transient scaling law based on the lumped and simplified conservation equations of transient mass and heat balance equations for natural and hybrid ventilation systems coupled with thermal mass. The lumped models make it possible to capture global and homogeneous information, including temperature and pressure, and their relationships based on analytical models.

For a multizone model, it is difficult to find the ideal relationship between sub-scale and full-size models that simultaneously consider fluid motion, natural and mechanical ventilation, and heat transfer [16]. Therefore, it is assumed that dimensionless numbers derived from a simplified model can be used in a more complicated model. Then, the application of dimensionless numbers is discussed in the results.

- Sub-scale model experiments

In this thesis, the sub-scale model experiments cover two cases: single-zone natural ventilation and multizone hybrid ventilation, both of which are tested with and without PCMs. The first case is considered as the foundation for the second case, so the research plan follows the logic from natural ventilation to hybrid ventilation, from single zone to multiple zones, and from a simple model to a more complex model. Meanwhile, based on the new dimensionless numbers developed for each case, the measured sub-scale results are scaled up to those of the full-size models to evaluate the full-size performance of the hybrid ventilation both with and without PCMs.

- Multizone simulations of the sub-scale and full-size models

Numerical multizone simulations are conducted for both sub-scale and full-size scale models. The measured sub-scale model data are used to calibrate the multizone network model, which is then used to calculate the corresponding full-scale cases. The scaled-up full-size results are also compared to those obtained from the full-size simulations, which once again could help to verify the new scaling methods. A detailed schematic of the proposed method is found in Section 3.1.

# Chapter 2 Literature Review

## 2.1. Natural and Hybrid Ventilation

Hybrid ventilation is commonly employed in buildings when natural ventilation alone cannot satisfy the needs of air exchange or space cooling and mechanical fans are added as an assistant system. Going back to the 1950s, there were no HVAC systems in commercial buildings, therefore, natural ventilation was one of the few choices for space cooling [29].

A survey of 43,000 online questionnaires in 370 object constructions and 12 buildings with hybrid ventilation found better indoor air quality and higher thermal satisfaction with hybrid ventilation systems [30]. With relatively higher air-exchange rates, hybrid ventilation systems have been proven to reduce cases of sick-building syndrome [6]. At the same time, hybrid ventilation is also an effective energy-saving solution.

Brager et al. [29] proposed a framework for hybrid ventilation classification through 21 high-level case studies. They suggested that a hybrid ventilation system cannot be defined simply as an HVAC system with open windows. Instead, hybrid ventilation is an integrated system to reduce cooling loads by well-designed strategies. For example, combining thermal mass with nighttime hybrid ventilation can aid peak-load shifting to maximize the benefit of the system.

Ezzeldin and Rees [8] applied hybrid ventilation to space cooling in an extreme climate (i.e., a desert) area with diurnal temperature variation. A climate-responsive operation strategy was

designed that incorporated several technologies (i.e., direct evaporative cooling, borehole heat exchanger, night convective cooling strategy, and radiant cooling elements coupled to a cooling tower), resulting in a 90% reduction in energy demand. Hybrid ventilation was found to contribute to more than 40% of the total energy savings while at the same time providing a satisfactory thermal-comfort level. A higher temperature set point with a higher thermal mass used in the design reduced temperature fluctuations and thus improved thermal comfort in the building.

Spindler and Norford [31] indicated that although hybrid ventilation systems can contribute to reducing energy consumption, occupant satisfaction may become a major concern. It is, therefore, imperative to balance energy savings with thermal comfort. Using multizone modeling, they applied a black-box method (a kernel recursive least squares method and neural network) to solve the problem in designing a system. Although their method seemed to provide automatic control of the system, the model did not consider the wind effect, which is one of the most significant factors to consider in designing a hybrid ventilation system.

Simonetti et al. [32] proposed a regeneration system combined with a hybrid ventilation system. A natural air-conditioning wall was designed to connect the hybrid ventilation system with a building-integrated photovoltaic panel. It took advantage of both evaporative cooling and higher air exchange for dehumidification than conventional systems. The regeneration system used the solar heat stored in water tanks to increase the overall efficiency of the system.

A hybrid ventilation system was designed for a stack-effect-dominated building by Yang and Li [33]. They built an analytical model for the dimensional analysis to optimize natural and mechanical ventilation based on dimensionless numbers (ventilation performance indicator and atrium enhancement parameter). The analytical results were also validated by CFD simulations. Their paper showed that a dimensional analysis of the analytical model is an effective method for the design and analysis of hybrid ventilation systems.

Turner and Awbi [34] installed a hybrid ventilation system in a small residential test room inside an environmental chamber to collect full-size experimental data. Although a high air-exchange rate of 120 L/s existed, the inside-outside temperature difference could be kept within 10 °C under both heating and cooling conditions. The study also showed that a heat recovery ventilator could improve the performance of a hybrid ventilation system in an attic.

A whole-building hybrid ventilation study that integrated hybrid ventilation and building thermal mass was conducted in an institutional high-rise building. The researchers proposed that a lower operational temperature could be set during the pre-cooling of the exposed concrete floor in the corridors near the natural ventilation openings based on the weather prediction [9]. It was estimated that 11.7 MJ of space-cooling energy could be saved in the daytime after the concrete floors had been chilled by hybrid ventilation for four hours during the night.

For the same building, Karava et al. [35] conducted full-size measurements of air and concrete surface temperatures for the common spaces of the atrium and the corridor. They showed that there

was a temperature difference in the atrium air of approximately 3 °C between hybrid ventilation and only mechanical ventilation on a clear day because of solar irradiation. Meanwhile, hybrid ventilation was found to provide around 6,500 kWh of free cooling over three months, which was 30% of the total cooling demand.

From the literature review, it is apparent that hybrid ventilation can be well applied when combined with thermal mass and pre-cooling operations. For a large building with a high cooling demand, thermal mass with hybrid ventilation can play a significant role in energy savings. In this thesis, therefore, an energy-efficient thermal mass such as a PCM is integrated with a hybrid ventilation system to reduce energy consumption and improve occupants' thermal comfort.

### 2.2. Phase Change Materials

The earliest research on PCMs can be traced back to a 1978 study by Telkes of sodium sulfate decahydrate and water [36]. Therefore, PCM is not really a new technology and has been studied for more than 40 years. However, PCM is not commonly used in buildings as an affordable material due to the expensive pure paraffin waxes that are often the main ingredients in PCMs [37]. Therefore, designers and proprietors are prudent in their application of PCM and an optimized design is prerequisite.

Different encapsulation methods allow for different PCM applications. Macro-encapsulation refers to PCM packed in panels, tubes, and even spheres based on the customization needs, and micro-encapsulation refers to PCM particles in powder or liquid form mixed into building materials [14].

Therefore, various shapes, sizes, and mixing percentages may produce significantly customized PCM properties. How to determine these properties for accurate simulations often becomes a practical issue [14].

Figure 2-1. Micro-encapsulation and macro-encapsulation of PCM [14].

Although various studies have been conducted on PCM in the past 40 years, there is still a lack of research on the interaction of thermal airflow and PCM in real buildings [15], especially studies of systems combining hybrid ventilation with PCM as the thermal mass. When combined with hybrid ventilation, PCM is not restricted to space cooling but can also be used as an adjunct heating source with solar irradiation, HVAC, and heat pump systems [15].

Guarino et al. [38] tested a paraffin-based PCM wall in a small chamber for solar thermal storage in winter. The PCM wall, with paraffin waxes and an aluminum surface, melted and froze at approximately 19 °C. The test room was made with five PCM layers (Figure 2-2) on a wall facing the incoming solar radiation, which entered through a window on the opposite wall of a sealed room built inside a larger environmental chamber. The environmental chamber conditions were controlled to simulate the actual three-day weather of Montreal. The experiments and numerical simulations showed that the PCM could reduce annual heating energy consumption by 17%.

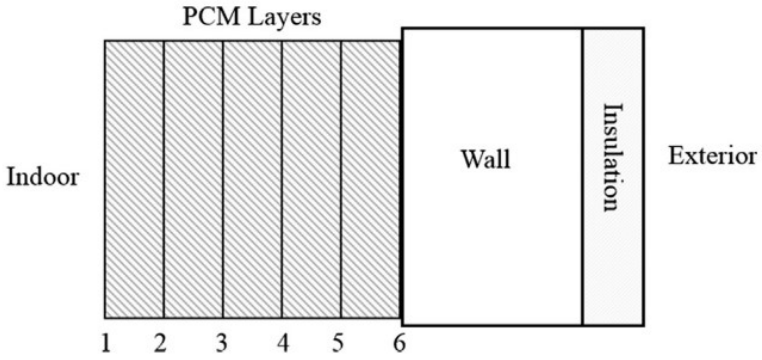


Figure 2-2. The design of an installed PCM wall [38].

Yanbing et al. [39] built an analytical model of a PCM-packed-bed storage system in a ceiling with nighttime ventilation (Figure 2-3). The model was further validated by experiments, which showed the convection coefficient between the PCM and capsule was 12–19 W/m$^2$. The researchers concluded that the analytical model was a suitable analysis model for the air-PCM system, and they suggested that the ceiling PCM system could reduce the space temperature and energy demand during cooling periods.

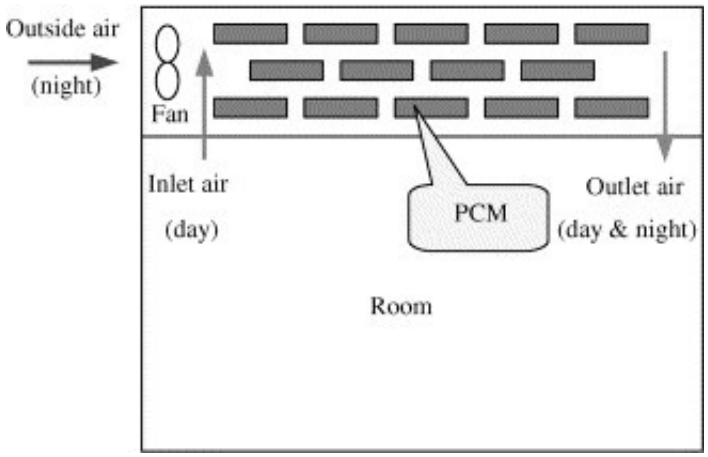


Figure 2-3. PCM-packed-bed storage system in a ceiling [39].

An in-floor supply air system (Figure 2-4) was proposed by Nagano et al. [13] and tested in a sub-scale office building. The PCM was installed over a supply air ventilation layer to charge the cooling load at night and discharge it during daytime. The melting and freezing temperature was approximately 20 °C, and the whole system reduced energy demand for space cooling by 89%.

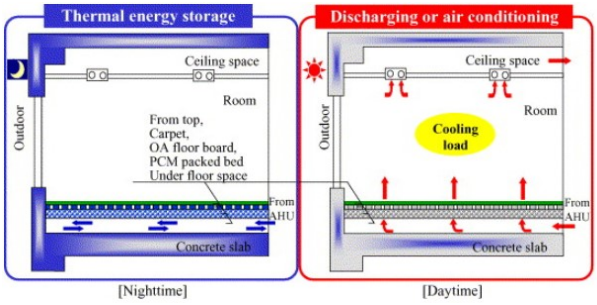


Figure 2-4. PCM-packed-bed in floor [13].

In conclusion, PCM can work effectively within building ventilation systems. Specifically, it can be charged with a larger free cooling or heating load when they are available than traditional construction materials. Therefore, a hybrid ventilation and PCM system is highly recommended for space cooling and heating near the material's phase-change temperature.

### 2.3. Numerical Modeling and Simulation

For thermal airflow modeling and simulations, two methods are commonly available: multizone network models and CFD modeling. Multizone simulation is based on a lumped model with the assumption that each room or zone has well-mixed air with uniform properties, including temperature, pressure, and species concentration [40]. In comparison, CFD models divide a room or zone into many control volumes, for which the well-known Navier-Stokes equations are solved

[16]. For both models, however, validation and calibration against experimental data are important to ensure simulation accuracy [22].

CFD is often more computationally intensive and time consuming but provides more detailed results than multizone network models [41][42]. To escalate the simulation speed, high-performance computer hardware and/or advanced numerical algorithms must often be used—for example, the use of graphics processing units (GPUs) and/or the development of new CFD methods, such as fast fluid dynamics [43], which are mostly still at the research stage. Therefore, it is still impractical to apply CFD to engineering analyses that model large cases (e.g., tens of millions of grids) or long-period simulations (e.g., on the scale of days, months, or years). In comparison, the multizone models have been commonly used for these situations. In the current study, therefore, we decided to use an in-house, multizone-based thermal airflow model [44] for the simulations of the building's hybrid ventilation system.

In the literature, multizone-based simulation models have been used to study natural/hybrid ventilation in buildings. A hybrid ventilation system for a residential building was modeled using a multizone model (TRNbuild and TRNflow) to determine energy savings under various combinations of indoor and outdoor conditions. It was found that while keeping the room CO2 concentration within allowable limits, the hybrid ventilation system used 20% less energy than a comparable mechanical system. The indoor $CO_2$ level was also controlled within an acceptable range. The study demonstrated the effectiveness of the multizone model for the study of hybrid

ventilation of buildings [45]. A large commercial building was simulated by Zhai et al. [46] with EnergyPlus which is a building energy simulation tool developed by the US Department of Energy labs. The study revealed several existing limitations of multizone simulation models for hybrid ventilation. The most significant one was the lack of trustworthy simulation settings, such as discharge coefficients, wind pressure, solar irradiation, and so on. The study agreed that it is possible to simulate a large building with hybrid ventilation, but the calibration and validation must be carried out for simulation accuracy.

In summary, for both CFD and multizone simulations, experimental calibration and validation are necessary. Compared to CFD, a multizone model is often faster and more appropriate for modeling large buildings with hybrid ventilation to analyze energy efficiency.

### 2.4. Sub-scale Model Experiment

Sub-scale modeling is a systematic method based on physics analysis for predicting the performance of a corresponding large-scale case for a given aspect serving a specific purpose [22]. In theory, the sub-scale model should replicate the physics phenomena of the prototype, in spite of different geometries and materials used at the two scales [47]. However, it is nearly impossible to reproduce all physics phenomena of the prototype. An effective alternative is to scale the problem for only those specific phenomena of interest, while neglecting other parameters.

Sub-scale tests are needed for new construction for which it is impossible to conduct full-scale tests before construction. They are also used to model existing buildings when full-scale tests are

limited by time, space, labor, or financial resources [22]. Properly designed and conducted, a sub-scale test can be an effective source of key inputs for numerical simulations, providing valuable data for validation and calibration, or guidelines and directions for simulation design. In addition, with recent developments in additive manufacturing technology—that is, 3D printing—it has become much easier to quickly prototype and fabricate an accurate sub-scale building model.

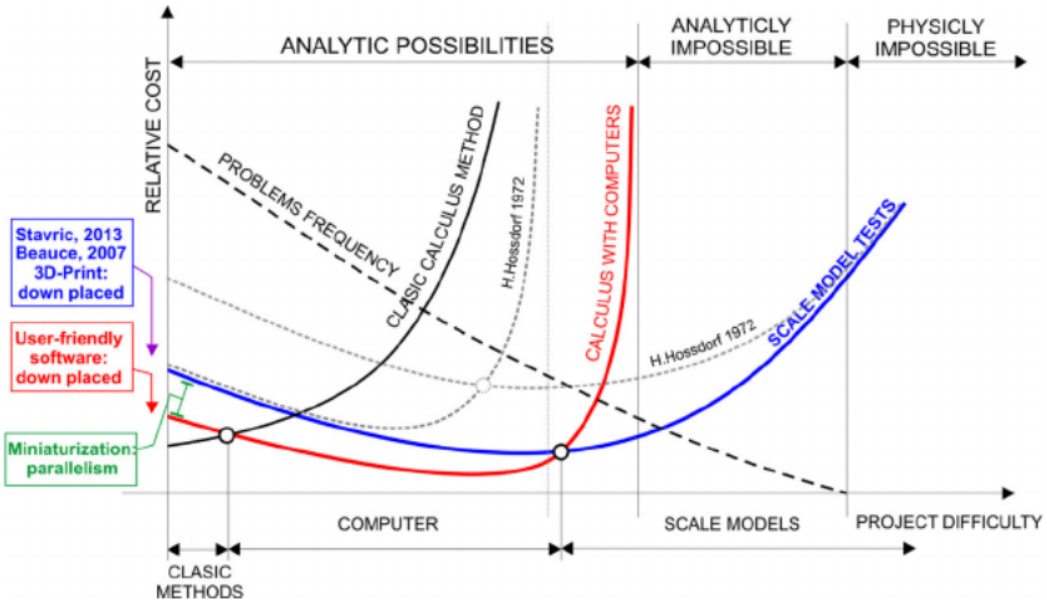


Figure 2-5. Project difficulty and relative cost for different modeling methods [22][48].

Relationships and trends among classic problem-solving methods—hand calculation, computer simulation, and scale-model experiment—are shown in Figure 2-5 graphed against project difficulty and relative cost. In 1972, Hossdorf and Hernández [48] discussed the relation between cost and difficulty for the first time, as shown by the dark lines. Lirola [22] modified and predicted

trends for newer technology developments, especially 3D printing and improvements in computing hardware and algorithms, as shown by the red and blue lines.

To conserve the similarity between sub-scale model and full-scale prototype of those physics phenomena of greatest interest, that is, the so-called "similarity analysis," the first step is to identify the associated dimensionless number or numbers that govern the phenomena in question—the so-called "dimensional analysis." Because these dimensionless numbers define the dominant forces and other parameters that reflect the underlying physics of complicated phenomena, and they are without dimensions, the similarity of the sub-scale and full-scale cases can be ensured by equating the associated dimensionless numbers between the two scales. When it is impossible to achieve equal dimensionless numbers because of limitations in test conditions and in materials available at both scales, the similarity analysis will try to identify those situations when the phenomena of interest become independent of the dimensionless numbers in question, so the similarity can be always satisfied (e.g., Reynolds Independence). There exist a few methods to conduct this dimensional analysis: 1) applying the Buckingham $\pi$ theorem; 2) deriving it from partial differential equations, such as the Navier-Stokes equations; or 3) deriving it from analytical models and their solutions.

A series of wind tunnel sub-scale experiments (Figure 2-6) were conducted by Cui et al. [49] to study temperature distribution and contaminant diffusion in urban areas governed by the Richardson and Reynolds numbers. It was found that within the region of Reynolds independence,

contaminant dispersion is governed by the Richardson number: its concentration increases with the Richardson number in the vertical direction of the street canyon in which the pollution distribution can affect indoor air quality simultaneously.

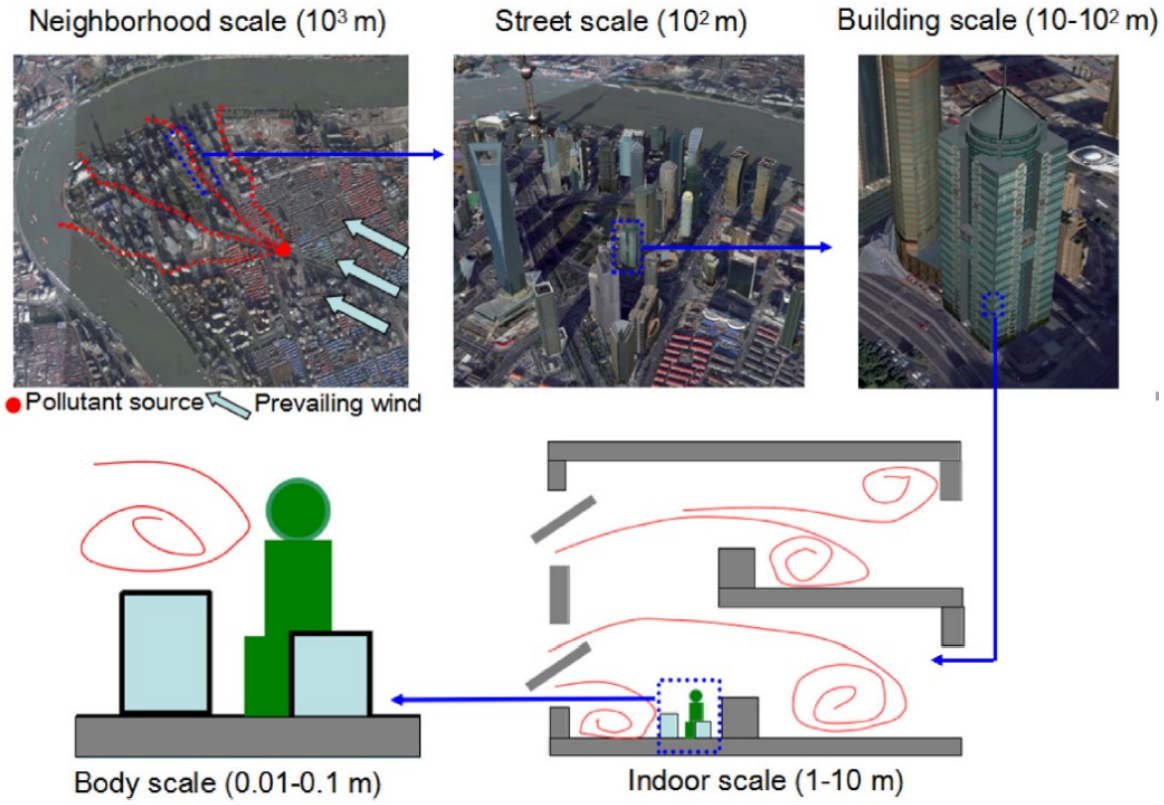


Figure 2-6. Conception of the sub-scale model experiment [49].

Minehiro et al. [50] built a 1:5 sub-scale model of a full-scale horizontal tunnel based on the Froude number to study backlayering distance and critical velocity (Figure 2-7), in which the heat transfer with surrounding envelopes was considered. A new mathematical expression was developed to calculate smoke layering and critical velocity. The study also compared the smoke layering and critical velocity calculated with this new expression to experimental results in five different sub-

scale models and the full-size prototype from previous research. The transient phenomena were modeled using the Biot number and the Fourier number.

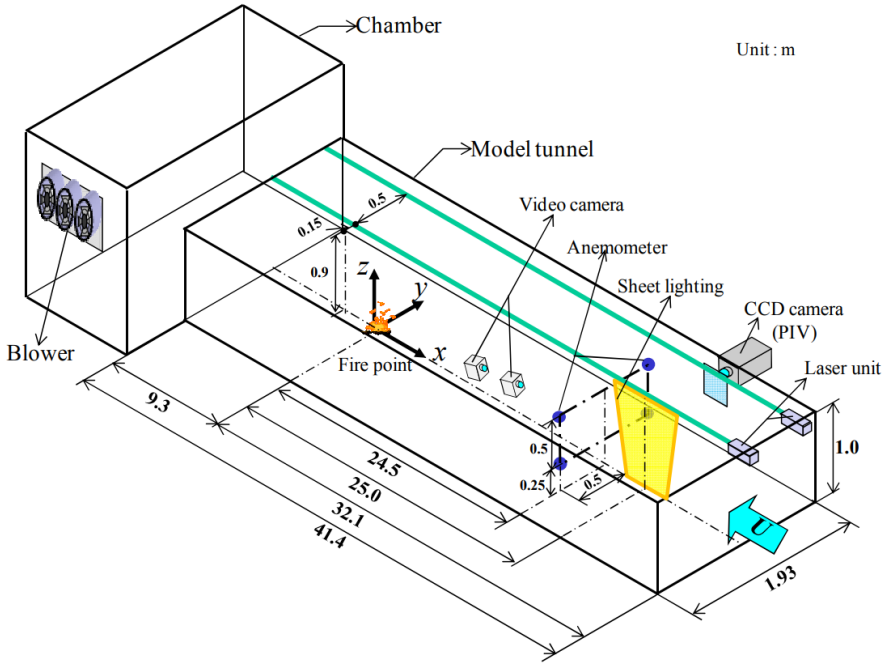


Figure 2-7. Schematics of sub-scale model experiment of backlayering distance and critical velocity [50].

Another study on fire-smoke spread was conducted by Qi et al. [51][52][53] in the vertical shafts of buildings, as shown in Figure 2-8. A new dimensionless number was defined to consider the heat transfer between the fire smoke and the surrounding shaft walls, which had been neglected by Froude modeling, the conventional scaling method. The new dimensionless number ($Fr/C_d$) was derived from the dimensionless forms of analytical conservation equations of heat and mass transfer in building shafts, so that both the buoyancy-driven airflow and the heat-transfer

similarities were conserved. The conclusions were confirmed by multiple sub-scale tests with different construction materials in the study.

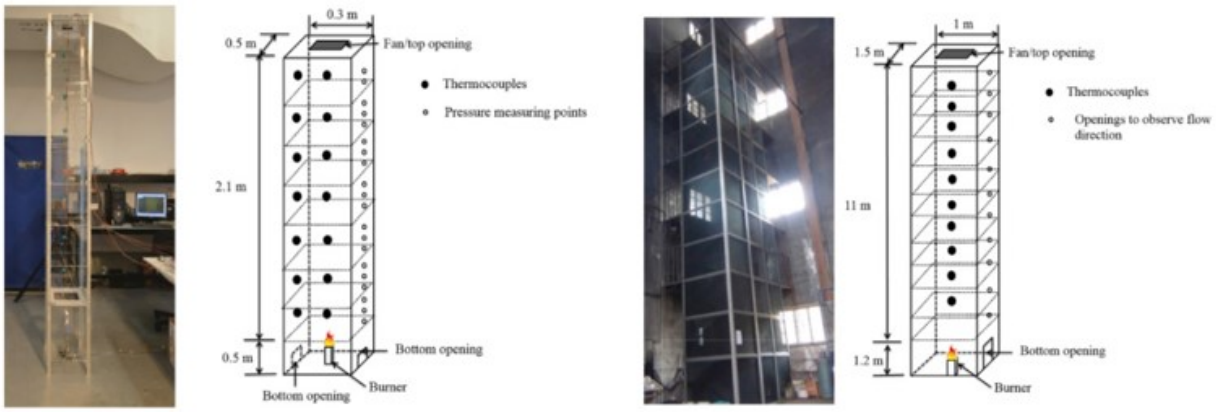


Figure 2-8. Two different scale model of building shafts during fires [52].

Song and Kimura [54] modeled a large industrial building in 1:10 scale for cooling load prediction following the Reynolds number, Prandtl number, and Peclet number. The study compared the energy savings performances of three different air-conditioning systems to find the best system for the building when heating increased.

Ding et al. [21] conducted sub-scale tests and CFD simulations of an eight-story building with an integrated system of double-skin facade, natural ventilation, and a solar chimney, as seen in Figure 2-9. Grashof modeling was applied because natural ventilation was the main phenomenon in the building. However, to conserve the Grashof number, the temperature scaling was cubic value of the length scaling, which was difficult to achieve under lab conditions. As a result, Grashof

independence was forced in the study and results showed that the solar chimney performed well over two floors.

Figure 2-9. Solar chimney tests in a sub-scale eight-story building [21].

Suwa and Tsuchiya [55] built a 1:4 sub-scale model of a data center based on Archimedes number to study 10 different air-conditioning and ventilation modes through various combinations of floor, wall, and ceiling supplies and exhausts, as shown in Figure 2-10. The sub-scale test results showed that the best strategy for data center cooling was to combine the ceiling air supply and ceiling exhaust.

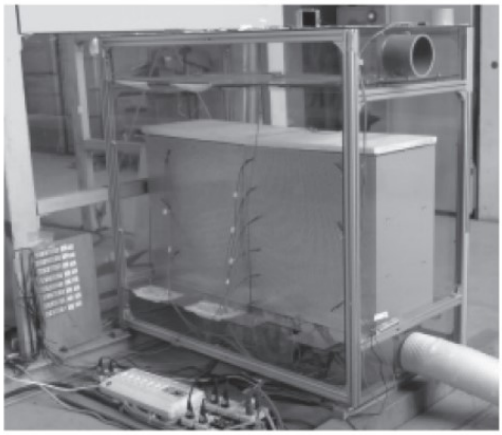

Figure 2-10. A 1:4 sub-scale data center study for the best ventilation strategy [55].

Miura et al. [56] built a 1:10 sub-scale model (Figure 2-11) to study a double-skin and solar chimney based on the Archimedes number. Full-scale CFD simulation results were obtained to be compared to the sub-scale measurements at the steady state. It was found that the sub-scale temperature results were about 4 °C lower than the full-scale CFD results, because heat transfer was neglected in the sub-scale experiment. Therefore, for natural ventilation cases, heat-transfer phenomena can be significant and cannot be ignored.

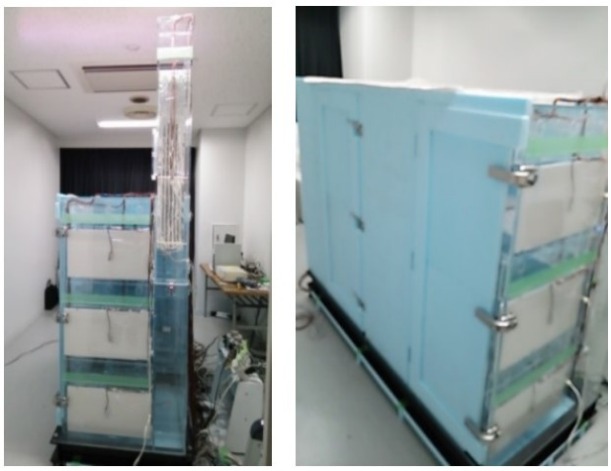

Figure 2-11. A 1:10 sub-scale office building with a solar chimney [56].

To test the thermal performance of glazing, Lirola [23] investigated several multiscale cases (Figure 2-12) based on dimensionless numbers from the Buckingham π theorem. For simplicity, thermal capacity was ignored in the dimensional analysis. The transient temperature measurements compared quite differently among different scales because thermal capacity had been neglected during sub-scaling.

Figure 2-12. Sub-scale experiments with building glazing [23].

Acred and Hunt [18] proposed a general and preliminary design method following a dimensional analysis of natural/hybrid ventilation in multi-floor buildings (Figure 2-13). The performance of the natural ventilation system was evaluated in terms of different vent sizes, mechanical ventilation

rates, and cooling loads by using several newly developed dimensionless numbers based on the analytical solutions of the naturally ventilated building. However, this study also failed to consider heat transfer.

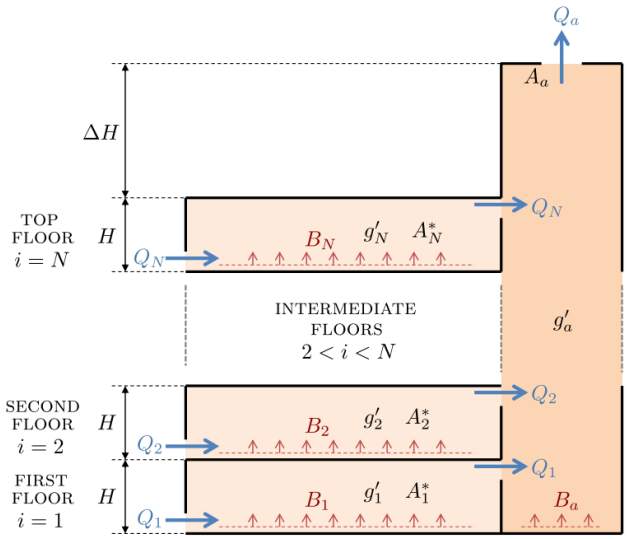


Figure 2-13. A multizone dimensional analysis of an office building [18].

The literature review shows that sub-scale tests are a cost-effective method for making design decisions and optimizing a building's mechanical and control systems, in addition to providing valuable data for the validation and calibration of numerical simulations. To serve different objectives among different cases, various dimensionless numbers have been applied: the Froude number in fire research, the Richardson number in an urban pollutant dispersion study, and the Grashof/Archimedes number for natural/hybrid ventilation research. Besides these commonly recognized numbers, new problem-specific numbers have also been developed from dimensional analysis based on analytical models.

The literature review also shows the limitations of previous research, such as lack of consideration of heat transfer in the envelope and lack of transient-state consideration for thermal mass. The objective of this thesis is to overcome these limitations.

## 2.5. Summary and Thesis Work Introduction

The literature review makes clear the desirability of combining hybrid ventilation with PCM, and it reveals the advantages and disadvantages of CFD, multizone simulation, full-size experiments, and sub-scale model experiments. Clearly, PCM can reduce energy consumption for space cooling with hybrid ventilation, however, quantitative analysis is necessary. For reasons of economy and feasibility, this study will use a coupling of sub-scale models and multizone simulation.

Existing scaling methods consider sub-scale models in adiabatic conditions; in other words, the envelope should be high enough to avoid heat transfer between indoors and outdoors. Furthermore, a lack of consideration of heat transfer makes it impossible to consider thermal mass, which is indispensable for transient state consideration.

To address these issues, this thesis is organized as follows:

Chapter 3 – Conservations of the transient single-zone mass and energy equations are constructed and then made dimensionless to obtain different dimensionless numbers. A transformation of the Fourier number is used for scale reduction. Simultaneously, sub-scale models of different materials are analyzed using previous dimensionless numbers to decide the time scale. Sub-scale tests are then set up for a small single-zone chamber and a scaled high-rise building. In addition, a multizone numerical modeling simulation method is introduced for mass and energy balance equations based on CONTAM and EnergyPlus. The model is built in a self-developed tool coded by the PhD

student, Ali Katal. Construction details, designs, and experimental setups are also detailed in this chapter.

Chapters 4 and 5 – These two chapters summarize the results of the sub-scale experiments and the numerical simulations for the single-zone chamber (Chapter 4) and the sub-scale high-rise building (Chapter 5). Numerical simulations are conducted for the sub-scale models after being calibrated using the sub-scale test data. Full-scale numerical simulations are then performed for both buildings. Lastly, the results are compared between the sub-scale data to the full-size buildings, which are from the full-size simulations.

Chapter 6 – This chapter draws final conclusions from the application methods. It also discusses limitations of the current study and suggests future work accordingly.

Table 2-1. List of limitations in previous research.

| Limitations in previous research |
|---|
| 1. Absence of heat transfer consideration in dimensionless analysis |
| 2. Absence of heat transfer consideration in sub-scale model design |
| 3. Absence of transient state consideration in dimensionless analysis |
| 4. Absence of transient state consideration in sub-scale model design |

# Chapter 3 Methodology

## 3.1. Research Objectives and Framework

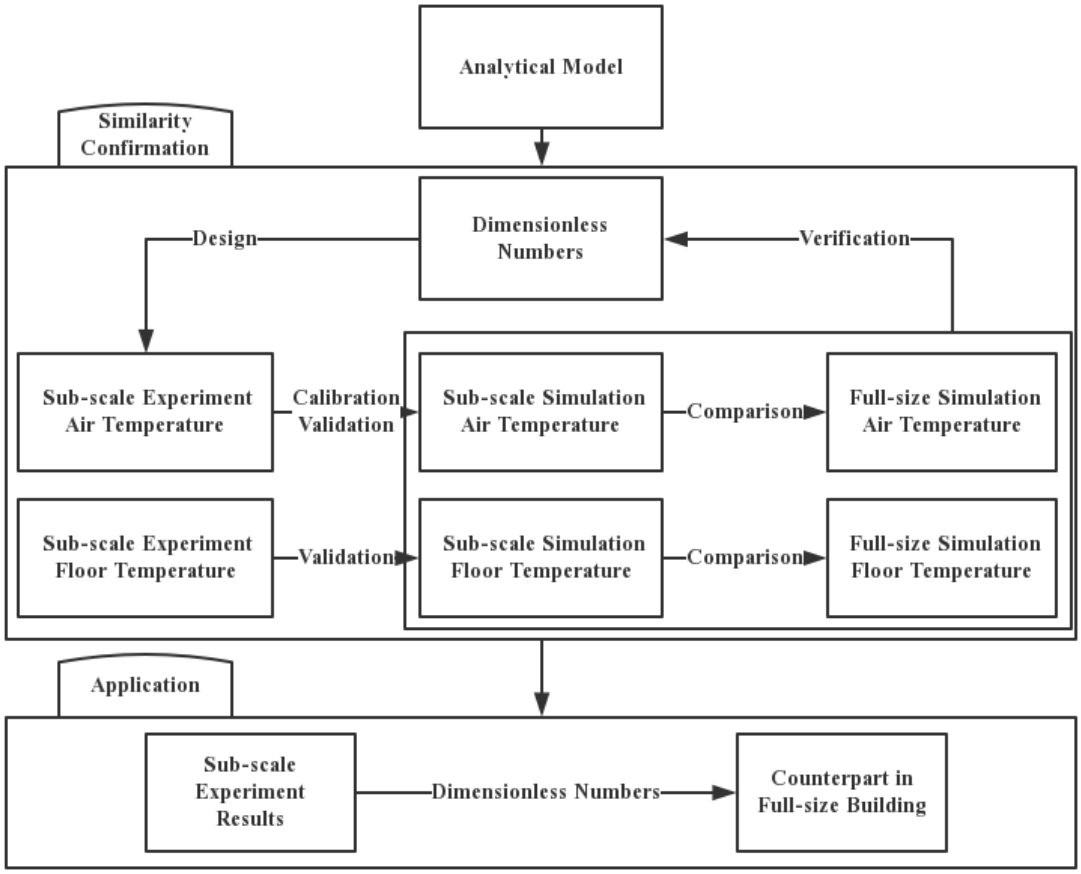


Figure 3-1. The procedure for the dimensional and similarity analysis combining analytical models, sub-scale tests, and numerical simulations.

As discussed previously, this study is based on the combination of analytical analysis, sub-scale tests and numerical simulations at both sub-scale and full-scale buildings. This chapter introduces the proposed process of utilizing the analytical models, sub-scale tests and numerical simulations

for conducting the dimensional and similarity analysis as shown in Fig. 3-1. The whole process includes the part of the similarity confirmation and the application part. The 1st part follows a logical order for the justification and confirmation of the dimensional numbers and their analysis for designs and experiments. The 2nd part of the application applies the direct outcomes from the 1st part including the contributions to initial building designs, construction, and operations and controls.

In the case of the single-zone building model, the dimensional analysis of the analytical model is possible, but it is almost impossible to conduct the analytical analysis for the high-rise building due to its complicated structure and system. Nevertheless, a complicated building may be considered as a group of lumped floors/zones/rooms, each of which the similar single-zone model may apply [18]. Therefore, here there is this assumption that the dimensionless numbers obtained from the single-zone analytical model may be applicable to the multizone building.

There is another assumption that the similarity between the sub-scale and the full-scale models may be confirmed by comparing the full-scale results, which are scaled up from the sub-scale experiments following the proposed scaling laws, with those obtained from the full-scale numerical simulations. The similarity verification can justify the dimensionless numbers with single zone and multizone application. It would be preferred to obtain full-scale test data and/or the test data at different scales from the sub-scale one. However, full-scale tests are often costly and impractical for newly built constructions, so this study relies on the full-scale simulations. To

ensure the accuracy of the numerical simulation model, this study calibrates and validates it against sub-scale test data, which are often effective for the purpose [22].

Both steady-state and transient sub-scale tests were conducted. The transient tests were based on the full-scale outdoor temperature variations over five days—that it, they were five-day data in the full-scale building but scaled down accordingly based on the proposed time-scaling laws to the lab-scale models:

1. Natural ventilation in a single-zone building, which was based on the previous study of "Small Chamber Salt Water Test" [57]

2. Hybrid ventilation in a high-rise building, which was based on the previous studies [5][58] (EV Building, Concordia University, Montreal, QC, Canada)

The five-day weather data were from June 4, 2017, to June 8, 2017, from Montreal, QC, Canada, with a temperature variation from 9 °C to 22 °C, a range in which the temperatures are mostly suitable for the natural and hybrid ventilation system to use free cooling, as suggested by the previous study [9].

### 3.2. Analytical Models and Dimensional Analyses

The analytical models and the dimensional analyses here were based on the methods developed by Qi et al. at the steady state [53][59]. This study focused on the transient state models and analyses. The dimensional analysis was based on the single-zone building model to identify the associated dimensionless numbers, which would then be applied to the multi-zone case.

Table 3-1. List of dimensional analyses assumptions

| Dimensional analyses assumptions |
|---|
| 1. Air, non-PCM envelope, PCM layer are considered as a lump respectively with homogeneous temperature. |
| 2. Air, non-PCM envelope, PCM layer are assumed as a lumped thermal capacitance respectively with homogeneous heat capacity. |
| 3. Air, non-PCM envelope, PCM layer are assumed as a lumped thermal insulation respectively with homogeneous thermal conductivity. |
| 4. Convective coefficient on outside and inside of the envelope are considered as same value ($h_i$=$h_o$). |
| 5. Thermal capacity and density of same material are assumed as same value in both sub-scale and full-size model ($C_p^s = C_p^f,\ C_{pcm}^s = C_{pcm}^f,\ \rho_p^s = \rho_p^f,\ \rho_{pcm}^s = \rho_{pcm}^f$) |

### 3.2.1. Single-layer Envelope

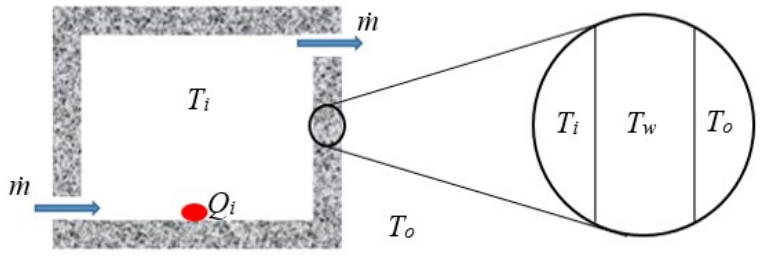


Figure 3-2. The schematic of the single-zone natural ventilation model.

Natural ventilation in a chamber is governed by conservation equations of heat balance (Eq. 3-1 and Eq.3-2) and mass balance (Eq.3-3) in dimensional forms.

The heat balance equations are applied to both the air and the wall:

The indoor air (with the temperature of $T_i$):

$$Q_i + \dot{m}C_p(T_o - T_i) + \frac{A_w}{\frac{1}{h_i} + \frac{1}{2}\frac{L_w}{k_w}}(T_w - T_i) = M_i C_p \frac{dT_i}{dt} \quad 3\text{-}1$$

The walls (with the temperature of $T_w$):

$$\frac{A_w}{\frac{1}{h_o} + \frac{1}{2}\frac{L_w}{k_w}}(T_o - T_w) + \frac{A_w}{\frac{1}{h_i} + \frac{1}{2}\frac{L_w}{k_w}}(T_i - T_w) = M_w C_{pw} \frac{dT_w}{dt} \quad 3\text{-}2$$

Mass flow rate equation [18][59] :

$$\dot{m} = C_d A_e \sqrt{2gH \frac{T_o - T_i}{T_o}} \rho_o = C_d A_e \sqrt{2gH} \rho_o \sqrt{\frac{T_o - T_i}{T_o}}$$

3-3

$$A_e = \frac{A_{top} A_{bottom}}{\sqrt{A_{top}^2 + A_{bottom}^2}}$$

3-4

Merging the energy balance equations of Eq. 3-1 and Eq. 3-2:

$$Q_i + \dot{m} C_p (T_o - T_i) + \frac{A_w}{\frac{1}{h_o} + \frac{1}{2}\frac{L_w}{k_w}} (T_o - T_w) = M_i C_p \frac{dT_i}{dt} + M_w C_{pw} \frac{dT_w}{dt}$$

3-5

When we define the wall heat transfer coefficient, *U*

$$\frac{1}{U} = \frac{1}{h_o} + \frac{1}{2}\frac{L_w}{k_w}$$

3-6

Eq. 3-5 can then be expressed as the following:

$$Q_i + \dot{m} C_p (T_o - T_i) + U A_w (T_o - T_w) = M_i C_p \frac{dT_i}{dt} + M_w C_{pw} \frac{dT_w}{dt}$$

3-7

Dividing Eq. 3-7 by $UA_w$

$$\frac{Q_i}{UA_w} + \frac{\dot{m}C_p}{UA_w}(T_o - T_i) + (T_o - T_w) = \frac{M_i C_p}{UA_w}\frac{dT_i}{dt} + \frac{M_w C_{pw}}{UA_w}\frac{dT_w}{dt}$$

3-8

Substitute Eq. 3-3 into Eq. 3-8:

$$\frac{Q_i}{UA_w} + \frac{C_d A_e \sqrt{2gH}\rho_o C_p}{UA_w}\frac{(T_o - T_i)^{\frac{3}{2}}}{\sqrt{T_o}} + (T_o - T_w) = \frac{M_i C_p}{UA_w}\frac{dT_i}{dt} + \frac{M_w C_{pw}}{UA_w}\frac{dT_w}{dt}$$

3-9

To conserve the dimensional temperature between sub-scale model and full-scale model, we then define the dimensionless temperature and the dimensionless time in which $T_{\max}$ (maximum ambient temperature) and $\tau$ (maximum time duration) are constant in both sub-scale and full-size model in the same case:

$$\theta_o = \frac{T_o}{T_{max}} \quad , \quad \theta_i = \frac{T_i}{T_{max}} \quad , \quad \theta_w = \frac{T_w}{T_{max}} \quad , \quad \hat{t} = \frac{t}{\tau}$$

In different ambient condition or different tests, $T_{\max}$ and $\tau$ are various, however, with the same case, ambient temperature and test time duration are identical in both sub-scale and full-scale model. In other words, with dimensionless temperatures and dimensionless time conserving in a case, dimensional temperatures are also conserved in the same case. Therefore, similarity in the analytical model is based on temperature conservation in multi-scale models.

Eq. 3-9 can then be expressed in the dimensionless form:

$$\frac{Q_i}{UA_w}+\frac{C_dA_e\sqrt{2gH}\rho_oC_p}{UA_w}\frac{(\theta_oT_{max}-\theta_iT_{max})^{\frac{3}{2}}}{\sqrt{\theta_oT_{max}}}+(\theta_oT_{max}-\theta_wT_{max})$$
$$=\frac{M_iC_p}{UA_w}\frac{d(\theta_iT_{max})}{d(\hat{t}\tau)}+\frac{M_wC_{pw}}{UA_w}\frac{d(\theta_wT_{max})}{d(\hat{t}\tau)}$$

3-10

Dividing Eq. 3-10 by $T_{max}$:

$$\frac{Q_i}{UA_wT_{max}}+\frac{C_dA_e\sqrt{2gH}\rho_oC_p}{UA_w}\frac{(\theta_o-\theta_i)^{\frac{3}{2}}}{\sqrt{\theta_o}}+(\theta_o-\theta_w)=\frac{M_iC_p}{UA_w\tau}\frac{d\theta_i}{d\hat{t}}+\frac{M_wC_{pw}}{UA_w\tau}\frac{d\theta_w}{d\hat{t}}$$

3-11

Defining dimensionless numbers as follows:

$$\Pi_1=\frac{Q_i}{UA_wT_{max}}\ ,\ \Pi_2=\frac{C_dA_e\sqrt{2gH}\rho_oC_p}{UA_w}\ ,\ \Pi_3=\frac{M_iC_p}{UA_w\tau}\ ,\ \Pi_4=\frac{M_wC_{pw}}{UA_w\tau}$$

Therefore, Eq. 3-11 can be turned into dimensionless form:

$$\Pi_1+\Pi_2\frac{(\theta_o-\theta_i)^{\frac{3}{2}}}{\sqrt{\theta_o}}+(\theta_o-\theta_w)=\Pi_3\frac{d\theta_i}{d\hat{t}}+\Pi_4\frac{d\theta_w}{d\hat{t}}$$

3-12

With the purpose of conserving dimensionless temperature and time, dimensionless numbers (Π) must be conserved between sub-scale and full-scale model correspondingly.

Mass flow rate Eq. 3-3 can be transferred into dimensionless form:

$$\frac{\dot{m}}{C_d A_e \sqrt{2gH}\rho_o} = \sqrt{\frac{T_o - T_i}{T_o}}$$

3-13

Defining dimensionless number as follow:

$$\Pi_6 = \frac{\dot{m}}{C_d A_e \sqrt{2gH}\rho_o}$$

For the similarity analysis between the sub-scale model and the full-scale model, the goal, therefore, is to conserve these dimensionless numbers:

$\Pi_1^s = \Pi_1^f$

$$Q_i^s = \frac{U^s A_w^s T_{max}^s}{U^f A_w^f T_{max}^f} Q_i^f$$

3-14

$\Pi_2^s = \Pi_2^f$

$$A_e^s = \frac{C_d^f \rho_o^f C_p^f \sqrt{H^f} U^s A_w^s}{C_d^s \rho_o^s C_p^s \sqrt{H^s} U^f A_w^f} A_e^f$$

3-15

$$\Pi_3^s = \Pi_3^f$$

$$\tau_i^s = \frac{M_i^s C_p^s U^f A_w^f}{M_i^f C_p^f U^s A_w^s} \tau_i^f$$

3-16

$$\Pi_4^s = \Pi_4^f$$

$$\tau_w^s = \frac{M_w^s C_{pw}^s U^f A_w^f}{M_w^f C_{pw}^f U^s A_w^s} \tau_w^f$$

3-17

$$\Pi_6^s = \Pi_6^f$$

Submitting equation 3-15 to $\Pi_6$

$$\dot{m}^s = \frac{C_d^f \rho_o^f C_p^f \sqrt{H^f} U^s A_w^s}{C_d^s \rho_o^s C_p^s \sqrt{H^s} U^f A_w^f} \frac{C_d^s \rho_o^s \sqrt{H^s}}{C_d^f \rho_o^f \sqrt{H^f}} \dot{m}^f = \frac{C_p^f U^s A_w^s}{C_p^s U^f A_w^f} \dot{m}^f$$

3-18

For the mechanical, $\dot{m}$ was determined by the mechanical fan. It should follow the same scaling as Eq. 3-18:

$$\dot{m}^s = \frac{C_p^f U^s A_w^s}{C_p^s U^f A_w^f} \dot{m}^f$$

3-19

### 3.2.2. Double layer Envelope with PCM

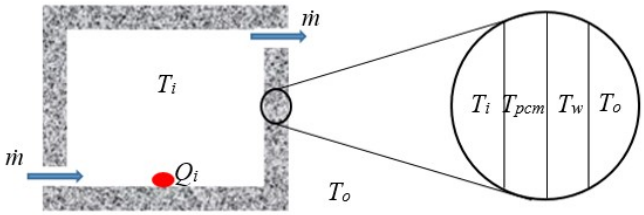


Figure 3-3. The schematic of the single-zone natural ventilation model with PCM.

Similarly, it is possible to develop the analytical model and conduct the analysis when there is PCM in the case.

The energy balance equation of the indoor air ($T_i$):

$$Q_i + \dot{m}C_p(T_o - T_i) + \frac{A_w}{\frac{1}{h_i} + \frac{1}{2}\frac{L_{pcm}}{k_{pcm}}}\left(T_{pcm} - T_i\right) = M_i C_p \frac{dT_i}{dt}$$

3-20

The energy balance of the PCM layer ($T_{pcm}$):

$$\frac{A_w}{\frac{1}{2}\frac{L_{pcm}}{k_{pcm}} + \frac{1}{2}\frac{L_w}{k_w}}\left(T_w - T_{pcm}\right) + \frac{A_w}{\frac{1}{h_i} + \frac{1}{2}\frac{L_w}{k_w}}\left(T_i - T_{pcm}\right) = M_{pcm}C_{pcm}\frac{dT_{pcm}}{dt}$$

3-21

The non-PCM wall layer ($T_w$):

$$\frac{A_w}{\frac{1}{h_o} + \frac{1}{2}\frac{L_w}{k_w}}(T_o - T_w) + \frac{A_w}{\frac{1}{2}\frac{L_{pcm}}{k_{pcm}} + \frac{1}{2}\frac{L_w}{k_w}}\left(T_{pcm} - T_w\right) = M_w C_{pw}\frac{dT_w}{dt}$$

3-22

Mass flow rate equation [18][59] :

$$\dot{m} = C_d A_e \sqrt{2gH \frac{T_o - T_i}{T_o}} \rho_o = C_d A_e \sqrt{2gH} \rho_o \sqrt{\frac{T_o - T_i}{T_o}}$$

3-23

$$A_e = \frac{A_{top} A_{bottom}}{\sqrt{A_{top}^2 + A_{bottom}^2}}$$

3-24

Combining Eqs. 3-20, 3-21, 3-22:

$$Q_i + \dot{m} C_p (T_o - T_i) + \frac{A_w}{\frac{1}{h_o} + \frac{1}{2}\frac{L_w}{k_w}} (T_o - T_w) = M_i C_p \frac{dT_i}{dt} + M_w C_{pw} \frac{dT_w}{dt} + M_{pcm} C_{pcm} \frac{dT_{pcm}}{dt}$$

3-25

Defining

$$\frac{1}{U} = \frac{1}{h_o} + \frac{1}{2}\frac{L_w}{k_w}$$

3-26

Eq. 3-25 can be expressed as the following:

$$Q_i + \dot{m} C_p (T_o - T_i) + U A_w (T_o - T_w) = M_i C_p \frac{dT_i}{dt} + M_w C_{pw} \frac{dT_w}{dt} + M_{pcm} C_{pcm} \frac{dT_{pcm}}{dt}$$

3-27

Dividing Eq. 3-27 by $UA_w$

$$\frac{Q_i}{UA_w}+\frac{\dot{m}C_p}{UA_w}(T_o-T_i)+(T_o-T_w)=\frac{M_iC_p}{UA_w}\frac{dT_i}{dt}+\frac{M_wC_{pw}}{UA_w}\frac{dT_w}{dt}+\frac{M_{pcm}C_{pcm}}{UA_w}\frac{dT_{pcm}}{dt}$$

3-28

Substituting Eq. 3-23 into Eq. 3-28:

$$\frac{Q_i}{UA_w}+\frac{C_dA_e\sqrt{2gH}\rho_oC_p}{UA_w}\frac{(T_o-T_i)^{\frac{3}{2}}}{\sqrt{T_o}}+(T_o-T_w)$$
$$=\frac{M_iC_p}{UA_w}\frac{dT_i}{dt}+\frac{M_wC_{pw}}{UA_w}\frac{dT_w}{dt}+\frac{M_{pcm}C_{pcm}}{UA_w}\frac{dT_{pcm}}{dt}$$

3-29

With same logic of section 3.2.1, defining dimensionless temperature and time as following:

$$\theta_o=\frac{T_o}{T_{max}}\ ,\quad \theta_i=\frac{T_i}{T_{max}}\ ,\quad \theta_w=\frac{T_w}{T_{max}}\ ,\quad \theta_{pcm}=\frac{T_{pcm}}{T_{max}}\ ,\quad \hat{t}=\frac{t}{\tau}$$

All of the dimensionless temperature and time are the same, furthermore, an additional dimensionless temperature of PCM is defined.

Eq. 3-29 can be rewritten as:

$$\frac{Q_i}{UA_w}+\frac{C_dA_e\sqrt{2gH}\rho_oC_p}{UA_w}\frac{(\theta_oT_{max}-\theta_iT_{max})^{\frac{3}{2}}}{\sqrt{\theta_oT_{max}}}+(\theta_oT_{max}-\theta_wT_{max})$$
$$=\frac{M_iC_p}{UA_w}\frac{d(\theta_iT_{max})}{d(\hat{t}\tau)}+\frac{M_wC_{pw}}{UA_w}\frac{d(\theta_wT_{max})}{d(\hat{t}\tau)}+\frac{M_{pcm}C_{pcm}}{UA_w}\frac{d(\theta_{pcm}T_{max})}{d(\hat{t}\tau)}$$

3-30

Dividing Eq. 3-30 by $T_{max}$:

$$\frac{Q_i}{UA_w T_{max}} + \frac{C_d A_e \sqrt{2gH}\rho_o C_p}{UA_w}\frac{(\theta_o - \theta_i)^{\frac{3}{2}}}{\sqrt{\theta_o}} + (\theta_o - \theta_w) = \frac{M_i C_p}{UA_w \tau}\frac{d\theta_i}{d\hat{t}} + \frac{M_w C_{pw}}{UA_w \tau}\frac{d\theta_w}{d\hat{t}} + \frac{M_{pcm} C_{pcm}}{UA_w \tau}\frac{d\theta_{pcm}}{d\hat{t}}$$

3-31

Defining dimensionless numbers as following:

$$\Pi_1 = \frac{Q_i}{UA_w T_{max}} \ , \ \Pi_2 = \frac{C_d A_e \sqrt{2gH}\rho_o C_p}{UA_w} \ , \ \Pi_3 = \frac{M_i C_p}{UA_w \tau} \ ,$$

$$\Pi_4 = \frac{M_w C_{pw}}{UA_w \tau} \ , \ \Pi_5 = \frac{M_{pcm} C_{pcm}}{UA_w \tau}$$

Therefore, Eq. 3-31 in the dimensionless form is:

$$\Pi_1 + \Pi_2 \frac{(\theta_o - \theta_i)^{\frac{3}{2}}}{\sqrt{\theta_o}} + (\theta_o - \theta_w) = \Pi_3 \frac{d\theta_i}{d\hat{t}} + \Pi_4 \frac{d\theta_w}{d\hat{t}} + \Pi_5 \frac{d\theta_{pcm}}{d\hat{t}}$$

3-32

With the purpose of conserving dimensionless temperature and time, dimensionless numbers (Π) must be conserved between sub-scale and full-scale model correspondingly.

Mass flow rate Eq. 3-23 can be transferred into dimensionless form:

$$\frac{\dot{m}}{C_d A_e \sqrt{2gH}\rho_o} = \sqrt{\frac{T_o - T_i}{T_o}}$$

3-33

Defining dimensionless number as follow:

$$\Pi_6 = \frac{\dot{m}}{C_d A_e \sqrt{2gH}\rho_o}$$

Compared with Section 3.2.1, all the dimensionless numbers are same to single-layer envelope dimensional analysis. $\Pi_5$ is additional dimensionless number for PCM.

To conserve the similarities between the sub-scale and the full-scale models:

$\Pi_1^s = \Pi_1^f$

$$Q_i^s = \frac{U^s A_w^s T_{max}^s}{U^f A_w^f T_{max}^f} Q_i^f$$

3-34

$\Pi_2^s = \Pi_2^f$

$$A_e^s = \frac{C_d^f \rho_o^f C_p^f \sqrt{H^f} U^s A_w^s}{C_d^s \rho_o^s C_p^s \sqrt{H^s} U^f A_w^f} A_e^f$$

3-35

$\Pi_3^s = \Pi_3^f$

$$\tau_i^s = \frac{M_i^s C_p^s U^f A_w^f}{M_i^f C_p^f U^s A_w^s} \tau_i^f$$

3-36

$$\Pi_4^s = \Pi_4^f$$

$$\tau_w^s = \frac{M_w^s C_{pw}^s U^f A_w^f}{M_w^f C_{pw}^f U^s A_w^s} \tau_w^f$$

3-37

$$\Pi_5^s = \Pi_5^f$$

$$\tau_{pcm}^s = \frac{M_{pcm}^s C_{pcm}^s U^f A_w^f}{M_{pcm}^f C_{pcm}^f U^s A_w^s} \tau_{pcm}^f$$

3-38

$$\Pi_6^s = \Pi_6^f$$

Submitting equation 3-35 to $\Pi_6$

$$\dot{m}^s = \frac{C_d^f \rho_o^f C_p^f \sqrt{H^f} U^s A_w^s}{C_d^s \rho_o^s C_p^s \sqrt{H^s} U^f A_w^f} \frac{C_d^s \rho_o^s \sqrt{H^s}}{C_d^f \rho_o^f \sqrt{H^f}} \dot{m}^f = \frac{C_p^f U^s A_w^s}{C_p^s U^f A_w^f} \dot{m}^f$$

3-39

For the mechanical, $\dot{m}$ was determined by the mechanical fan. It should follow the same scaling as Eq. 3-39:

$$\dot{m}^s = \frac{C_p^f U^s A_w^s}{C_p^s U^f A_w^f} \dot{m}^f$$

3-40

### 3.2.3. Discussions of Dimensionless Numbers

For the conduction heat transfer in envelope, $\Pi_1$ is defined as dimensionless heat transfer coefficient.

$$\Pi_1 = \frac{Q_i}{UA_w T_{max}}$$

3-41

For a typical dimensional analysis in thermal airflow, Stanton and Grashof numbers are used widely:

$$\mathrm{St} = \frac{h}{\rho u C_p}$$

3-42

$$\mathrm{Gr} = \frac{g\beta(T_s - T_0)L^3}{\nu^2}$$

3-43

$\Pi_2$ is a transformed parameter to consider both Stanton and Grashof dimensionless numbers:

$$\Pi_2 = \frac{C_d A_e \sqrt{2gH}\rho_o C_p}{UA_w}$$

3-44

For a typical transient state dimensional analysis, Fourier number is one of the most significant parameters to characterize the freezing and melting process [60]:

$$\mathrm{Fo} = \frac{kt}{C_p \rho L^2}$$

3-45

The time dimensionless number depending on dimensional analysis above:

$$\Pi_3 = \frac{M_i C_p}{U A_w \tau} \ , \ \Pi_4 = \frac{M_w C_{pw}}{U A_w \tau} \ , \ \Pi_5 = \frac{M_{pcm} C_{pcm}}{U A_w \tau}$$

Compared with the Fourier Number, defined new time dimensionless number is a transformed parameter to consider the total heat transfer of envelope instead of only thermal conductivity in the envelope. Therefore, it considers both conduction and convection, which is more appropriate in multi-zone simulation model.

When the sub-scale and the full-scale model have the same wall materials, e.g. the same PCM envelopes are used, the time scaling becomes:

For the indoor air:

$$\frac{\tau_i^s}{\tau_i^f} = \frac{M_i^s C_p^s U^f A_w^f}{M_i^f C_p^f U^s A_w^s} = \frac{U^f L_w^s}{U^s L_w^f}$$

3-46

For the PCM layer:

$$\frac{\tau_{pcm}^s}{\tau_{pcm}^f} = \frac{M_{pcm}^s C_{pcm}^s U^f A_w^f}{M_{pcm}^f C_{pcm}^f U^s A_w^s} = \frac{U^f L_w^s}{U^s L_w^f} = \frac{\tau_i^s}{\tau_i^f}$$

3-47

For the non-PCM wall layer:

Therefore, the wall time scaling is the same as that of the indoor air. On the other hand, it is common to use different materials of the walls in the sub-scale model from the full-scale ones. For example, the sub-scale is made from acrylic glasses to model a full-scale concrete building. Then, the time scaling for the non-PCM wall will be different from that of the indoor air.

The non-PCM wall time scaling:

$$\frac{\tau_w^s}{\tau_w^f} = \frac{M_w^s C_{pw}^s U^f A_w^f}{M_w^f C_{pw}^f U^s A_w^s} = \frac{\rho_w^s C_{pw}^s L_w^s U^f}{\rho_w^f C_{pw}^f L_w^f U^s}$$

3-48

### 3.2.4. Experiment Parameter Settings

Based on the scaling law presented earlier, Table 3-2 shows the Atrium Test input and output with sub-scale and full-size models. It also shows the sources of the parameters and boundary conditions.

Table 3-2. Summary of the parameter settings in the 1:50 naturally ventilated single-zone building.

| | **Sub-scale** | **Source** | **Full-scale** | **Source** |
|---|---|---|---|---|
| $Q$ (W) | 5 | Calculated by Scaling Law | 10424 | Input |
| $\tau$ | 5400 s | Calculated by Scaling Law | 5 days | Input |
| $A_{opening}$ ($m^2$) | 0.001125 | Input | 1.55 | Calculated by Scaling Law |
| $C_d$ | 3 | Calibration by Experiment | 0.64 | Calculated by Scaling Law |
| Air and Slab $T$ (°C) | Output | Measurement or Calculated by simulation | Output | Calculated by Simulation |
| $\dot{m}$ (kg/s) | Output | Calculated by simulation | Output | Calculated by simulation |

Similarly, Table 3-3 shows the High-Rise Building Test input and output, however, it assumes there is no heat source in the hybrid ventilation space and all heat is coming from envelope heat transfer from connected office space (set-point temperature 21 °C).

Table 3-3. Summary of the parameter settings of the 1:100 hybrid-ventilated high-rise building model.

| | **Sub-scale** | **Source** | **Full-size** | **Source** |
|---|---|---|---|---|
| $\dot{m}$ *(kg/s)* | $0.003\rho_o$ | Calculated by Scaling Law | $15\rho_o$ | Input |
| $\tau$ | 1800 s | Calculated by Scaling Law | 5 days | Input |
| $A_{opening}$ $(m^2)$ | 0.00014 | Input | 0.55 | Calculated by Scaling Law |
| $C_d$ | 3 | Calibration by Experiment | 0.4 | Actual Measurement |
| Air and Slab $T$ $(°C)$ | Output | Measurement or Calculated by simulation | Output | Calculated by simulation |

Discharge coefficients in both cases were calibrated by sub-scale experiments, which were assumed to be 0.65 in the real building case and will be calculated in a range of 0.5 to 1.0. However, the sub-scale model is different from the real-size building due to the reduction of geometry scale. Research [61] calibrated a discharge coefficient in natural ventilation of the sub-scale shaft as 2.187, therefore, in the sub-scale model, the discharge coefficient became extremely large because of the small opening.

Due to accuracy of anemometer, it is impossible to measure airflow velocity and airflow rate in sub-scale model in which velocity and airflow rate become extremely small.

### 3.3. Experimental Design and Setup

#### 3.3.1. Natural Ventilation in a Single-Zone Space

The main concept underlying the naturally ventilated single-zone case was to create a 1:50-scale model with an internal heat source and two natural ventilation openings, which could be considered to represent a typical large open space, such as an atrium [57][62]. In this study, the sub-scale model was 200 mm (length) × 100 mm (width) × 200 mm (height) with different wall materials to be tested, including the 3D-printed material PLA, acrylic glasses, and PCM. The material properties are illustrated in Table 3-4.

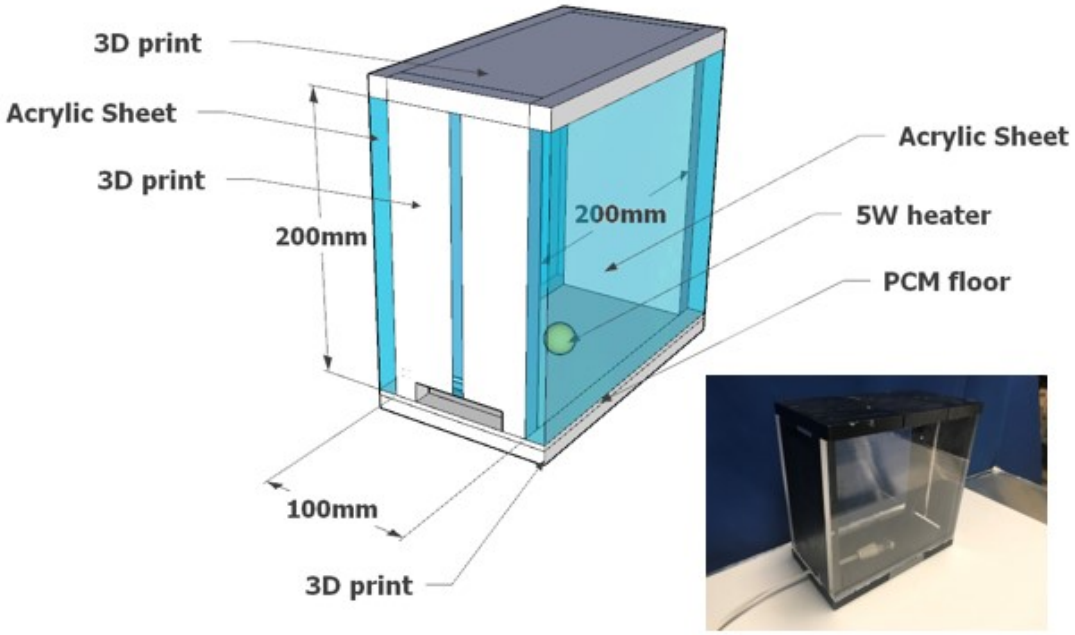


Figure 3-4. Schematics of the 1:50-scale naturally ventilated building model.

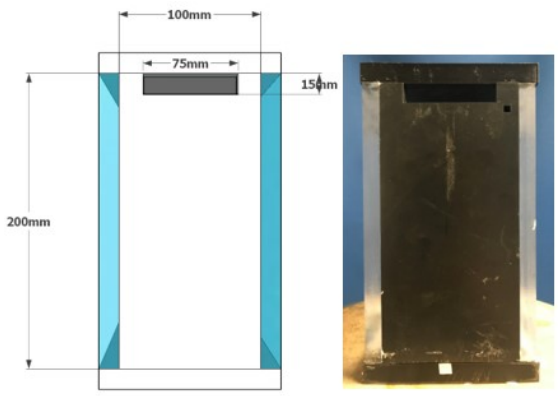


Figure 3-5. Schematics of the atrium sub-scale model on one side opening.

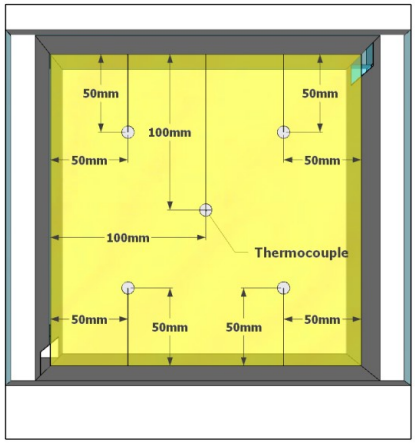


Figure 3-6. Schematics of thermocouple locations in the interior space.

Table 3-4. Properties of model materials.

| | *k* | ρ | *C* | |
|---|---|---|---|---|
| | W/m·K | kg/m3 | J/kg·K | |
| PLA | 0.25 | 1150 | 1700 | 3D print Material |
| Air | 0.0257 | 1.2 | 1005 | 3D print Material |
| Acrylic | 0.189 | 1190 | 1500 | |
| PCM [17][63] | 0.18–0.22 | 855.5 | 2500 (average) | Latent heat (18–24 °C) 70,000 J/kg |

Each 3D-printed wall section was 14.1 mm thick, including the PLA materials, with 2.1 mm on each side of the wall and the 12.1-mm-thick interior net-structures filled with air (i.e., the air layer). There were four 3D-printed sections to the sub-scale model: the left and right walls, the ceiling, and the floor. The front and back walls were made from 11-mm acrylic glass, as shown in Figures 3-4 and 3-5. The acrylic wall sections allowed for particle image velocimetry (PIV) measurements and observations. A constant 5-W heater was buried in the middle of the floor. The two wall openings were both 15 mm × 75 mm. For internal air temperature measurements, five thermocouples were installed at locations indicated in Figure 3-6, and readings were later averaged to obtain the air temperature. The wall temperatures were measured by two thermocouples attached on both sides of each wall.

3D printing technology can reduce fabrication time of experiment model, simultaneously, it also can increase experiment model complexity. Traditionally, complicated model has to be fabricated by mold, however, 3D printing saves the time and cost of mold making. Therefore, 3D printing becomes preferred fabrication technology of experiment model.

The single-zone model was placed inside an environmental chamber to simulate ambient temperature variations. The environmental chamber was equipped with a mechanical system of the ESPEC SCP-22 temperature and humidity chamber walk-in series, which controlled the temperature by multiple steps with straight-line changing. Thus, actual ambient temperature variations could be simulated when the time step was small enough. For this study, the ambient

temperature was taken from real weather data recorded between June 4, 2017, and June 8, 2017, measured locally by a weather station placed at the top of the Concordia University EV Building, Montreal, QC, Canada (more details can be found in Appendix 8). When time-scaled, the five-day ambient temperature data record corresponded to a total of 5,400 seconds for the sub-scale model (Table 3-2).

The first series of tests were conducted using walls without the PCM installed. The second series measured the impact of installing a 5.2-mm-thick PCM floor section placed on the top of the 3D-printed PLA section to form a two-layer floor section. Two thermocouples were installed on each side of the PCM layer.

### 3.3.2. Hybrid Ventilation in a Sub-scale Model of a Highrise Building

The full-scale high-rise building of interest is the Concordia University EV Building, which is equipped with a whole-building hybrid ventilation system (Figure 3-7). The building includes 16 floors above the ground and two underground floors. Above the 16th floor are several mechanical rooms. Starting at the second floor, each group of three floors is connected by a central, three-story atrium onto which all corridors open. Each three-story atrium is, in turn, connected to the one above it via a set of dampers.

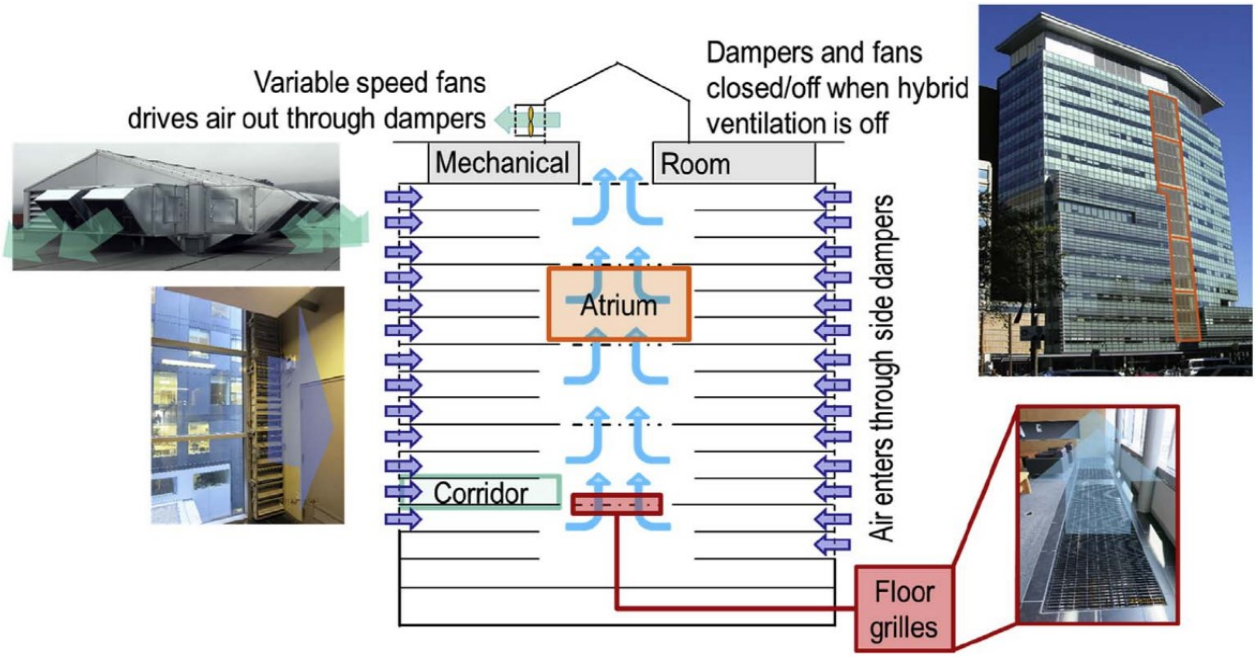


Figure 3-7. Hybrid ventilation system in the EV Building [9].

In the ceiling of the top atrium, there is an auxiliary exhaust fan, the airflow through which is commonly measured at 18.117 $m^3/s$. The operation strategy is based on the outside temperature. The dampers at the end of each corridor and the rooftop fan are triggered when the outside

temperature falls within the range of 15 °C to 22 °C. Because there are sensitive experimental devices located on the top three floors of the building, however, the dampers on those floors do not open. The sub-scale model experiment replicated these conditions. The operational temperature, however, was decreased from 15 °C to 9 °C during the night to aid in space cooling during the following day [9].

The sub-scale model (1:100) was built of 3.2-mm-thick acrylic plastic sheet having properties shown in Table 3-4. A central processing unit (CPU) fan served as the model's exhaust fan. The model was separated into two zones—a ventilation zone with atrium and corridor, and a sealed office zone with heater. The ventilation zone followed the space pattern of the full-size building, while the office zone was simplified into several lumped spaces. For the free-cooling mode, office zones were kept at a constant temperature of 22 °C for the boundary condition by the heater [9]. The sub-scale model is shown in Figure 3-8.


Figure 3-8. Sub-scale EV Building model.

The EV Building model was put into the environmental chamber to simulate the weather conditions from June 4, 2017, to June 8, 2017. The sub-scale model test time was 360 s, which was calculated from 1 real day using the scaling law (Table 3-3). The exhaust CPU fan was installed on the top of the atrium, and airflow rate was measured at 0.003 $m^3/s$. The corresponding full-size airflow rate would have been 15 $m^3/s$, which was very similar to real-life data. The corridor dampers were opened on one side of the third floor and on both sides from the fourth floor to 13th floor. Five thermocouples were installed in the center of each atrium space to record the local temperature in the model.

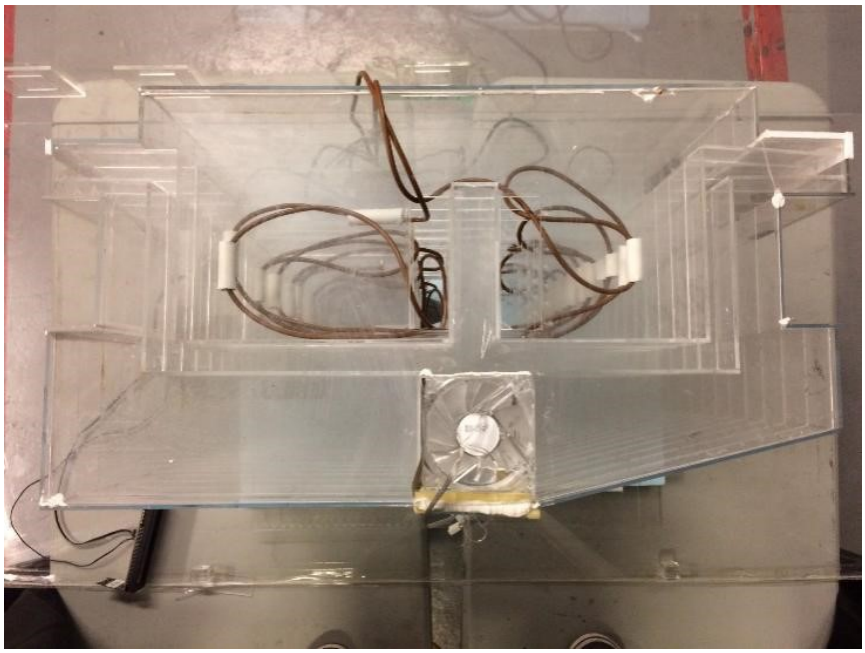

Figure 3-9. Top view of EV Building sub-scale model.

The first case study (Ex s.3) was baseline, which ran for 360 s to model 1 day. One piece of PCM (80 mm × 80 mm × 5.2 mm) was then inserted on each atrium floor, covering the floor area to the edge of the damper openings. Test Ex s.4 was then performed under the same conditions used for Ex s.3. Both sides of the plastic floors and the additional PCM floor inserts in each atrium had thermocouples attached to record the surface floor temperature to estimate the thermal mass average temperature. The EV Building sub-scale model is shown in Figure 3-10. The yellow rectangle shows the shaft of the five atriums, and the blue rectangles show the locations of the PCM floor panels. Red points indicate the thermocouple locations.

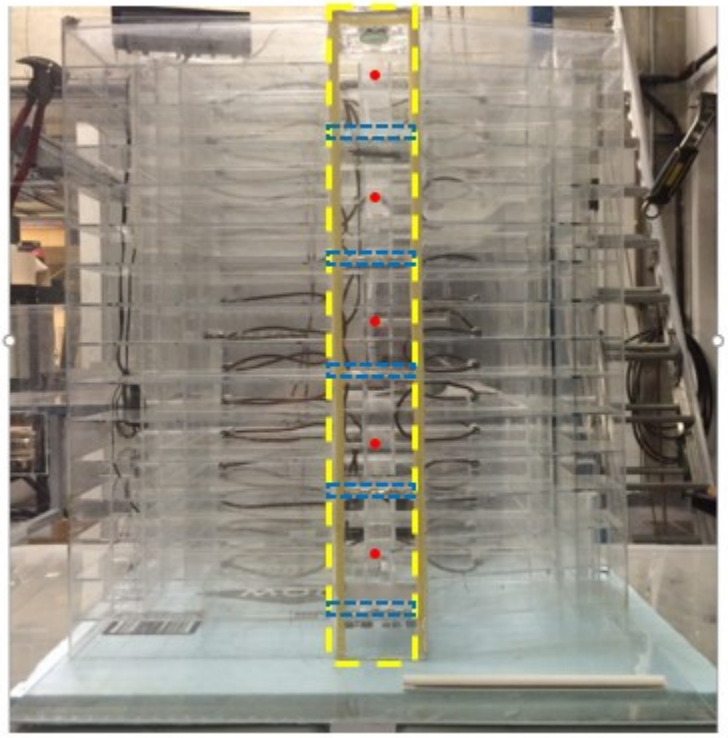

Figure 3-10. Atrium zones of EV Building.

### 3.3.3. Table of Experiment Case Names and Main Setup

Table 3-5. Experiment case names and main setup.

| Case Name | Space Type | Ventilation Type | Floor Type |
|---|---|---|---|
| Ex s.1 | Atrium | Natural | Without PCM |
| Ex s.2 | Atrium | Natural | With PCM |
| Ex s.3 | High-Rise Building | Hybrid | Without PCM |
| Ex s.4 | High-Rise Building | Hybrid | With PCM |

## 3.4. Multizone Numerical Simulation Model

### 3.4.1. Numerical Simulation Model Equations

In the multizone network simulation model, temperature and pressure distribution was assumed to be well-mixed as a homogeneous state in each control volume. The mass and energy balance equations are presented in this section.

Mass balance equation:

$$\sum_{z=1}^{N_{zones}} \dot{m}_{zi} + S_i = \frac{dM_i}{dt}$$

3-49

The equation shows the summing of airflow rate between zones *z* and the interior air of object zone *i*, and the sources and sinks of air are blown in and out of zone *i*.

Energy balance equation:

1.Zone air.

$$M_i C_p \frac{dT_i}{dt} = \sum_{z=1}^{N_{zones}} \dot{m}_{zi} C_p (T_z - T_i) + \sum_{w=1}^{N_{surfaces}} h_w A_w (T_s - T_i) + Q_i$$

3-50

2.Transient heat conduction in envelopes.

$$M_w C_{pw} \frac{dT_w}{dt} = U_w A_w (T_i - T_o)$$

3-51

$$U_w = \frac{1}{\frac{1}{h_i} + \frac{L_w}{k_w} + \frac{1}{h_o}}$$

3-52

The thermal mass of each envelope was divided into five layers with same thickness for the simulation model. The PCM's various capacities were defined using the manufacturer's information (Appendix 1).

Interior node connection equation:

$$\dot{m}_{zi} = C(\Delta P_{zi})^n$$

3-53

Pressure difference through each connection:

$$\Delta P_{zi} = (P_z - \rho_z g H_z) - (P_i - \rho_i g H_i) + \frac{\rho_z + \rho_i}{2} g(Z_z + H_z - Z_i - H_i) + P_{zi,wind}$$

3-54

Orifice equation:

$$\dot{m} = C_d A_{open} \sqrt{2\rho\Delta P}$$

3-55

### 3.4.2. Numerical Simulation Model

The atrium simulation model, illustrated in Figure 3-11, was built as a single-zone model with two openings on the top and bottom in the transient state. The model was heated by a heat source in the middle of the floor. Building material information was introduced in section 3.3.1. above.

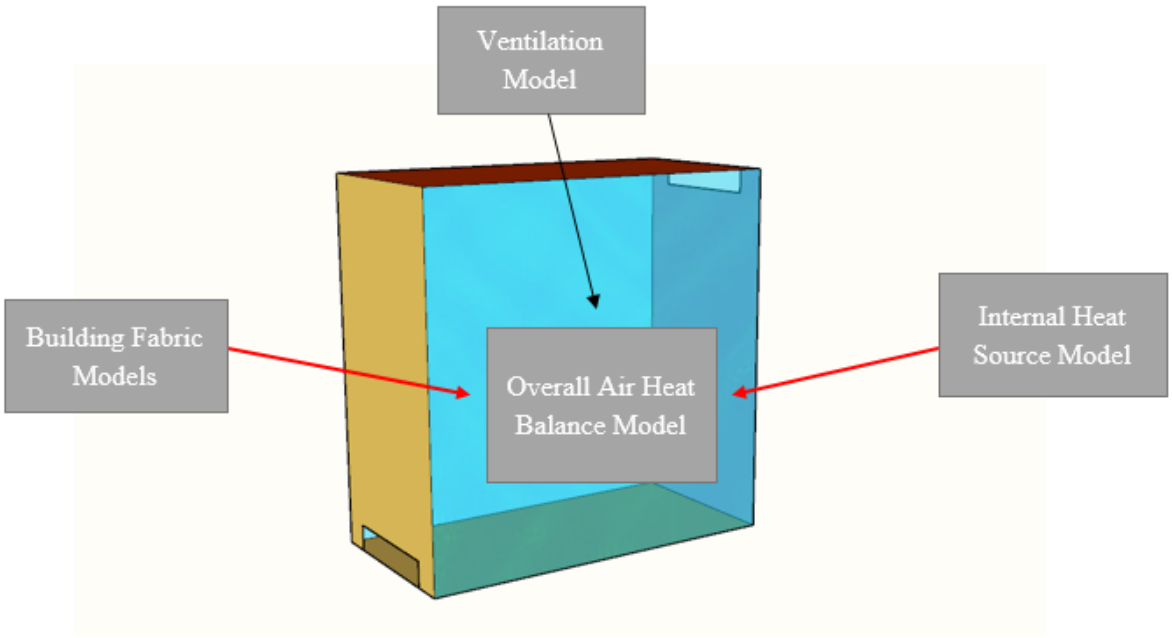


Figure 3-11. Atrium simulation model.

The building model is illustrated in Figures 3-12 and 3-13. Model fabric information was introduced in section 3.3.2. The EV Building was built as a multizone model with hybrid ventilation, with an exhaust fan located on the top of atriums. Airflow path is illustrated in Figure 3-13.

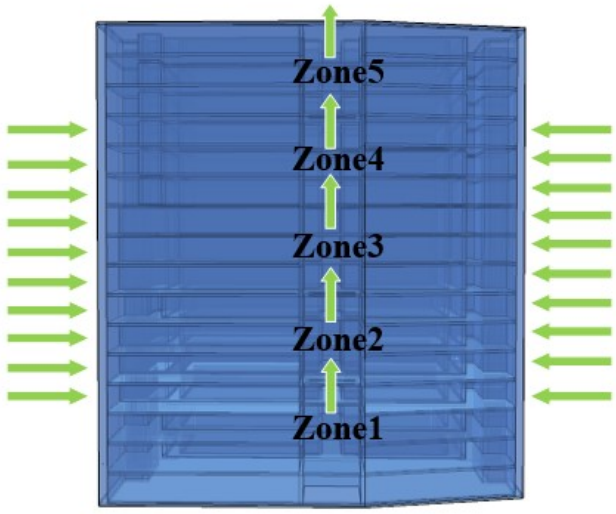


Figure 3-12. Airflow concept in vertical view.

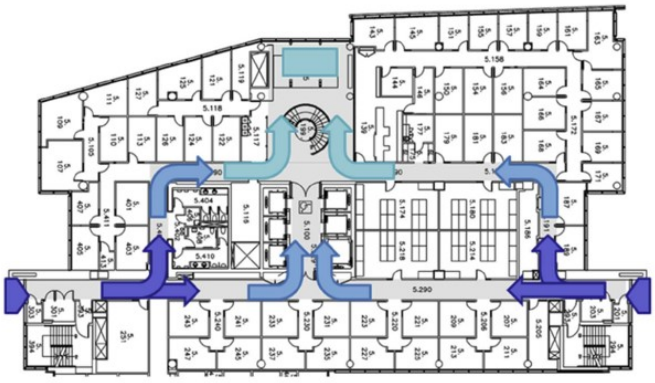

Figure 3-13. Airflow path in top view.

Due to simulation uncertainty, validation is indispensable, i.e., the numerical simulation model accuracy cannot be guaranteed without validation. Validation is a way to bridge the gap between computational simulation data and experiments data, furthermore, simulation data validated will be more convincing.

# Chapter 4 Natural Ventilation in Atrium

## 4.1. Simulations Validation of Atrium

The atrium sub-scale experiment model was built in the environmental room, which simulated temperature variation using outdoor weather data. The experiments did not consider wind or solar irradiation.

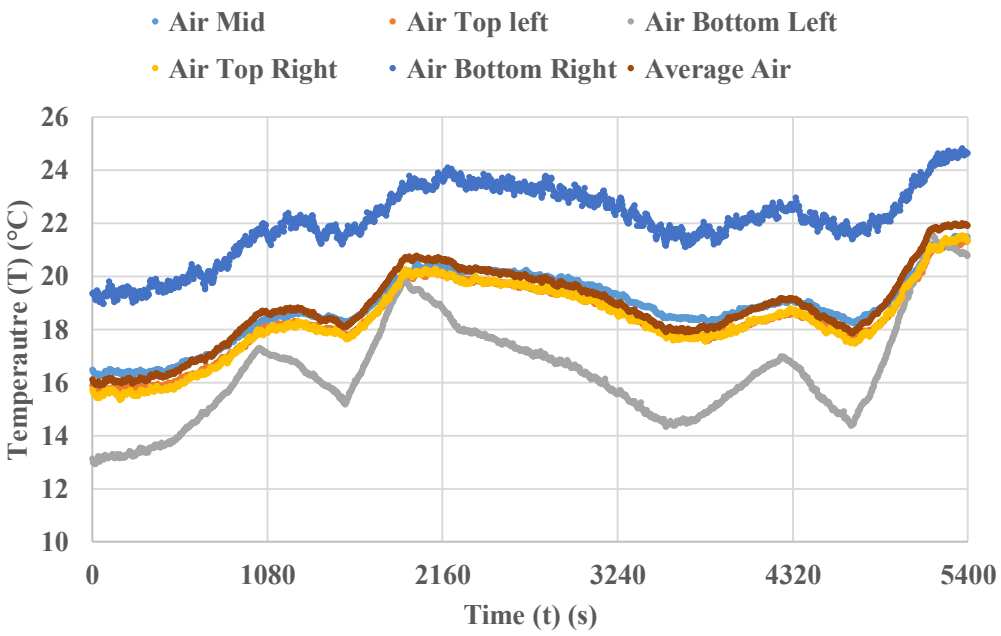


Figure 4-1. Measured air temperature and average air temperature in Ex s.1.

Figure 4-1 shows measured air temperature in five locations and average air temperature at those five points. Air temperature near the top opening was much higher than in other locations, and air temperature near the bottom opening was much lower than in other locations. Air stratification was obvious, with an 8-°C difference between top and bottom. Furthermore, each location's

temperature fluctuated within a range of 6 °C, except for air temperature at the bottom left (grey line). Air temperature near the bottom opening had the greatest variation, depending on airflow from outside within a range of 8 °C.

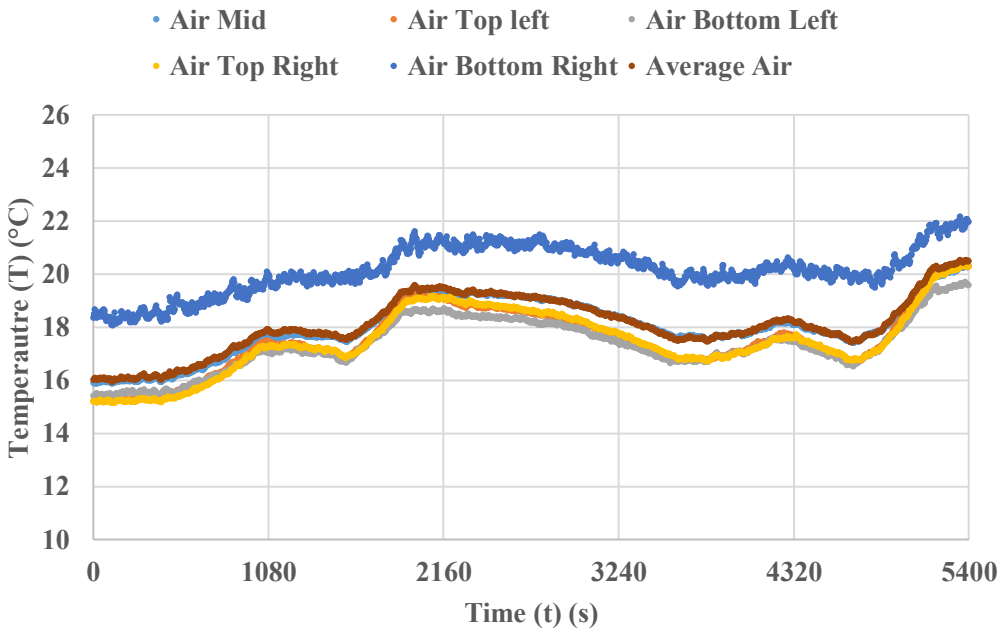


Figure 4-2. Measured air temperature and average air temperature in Ex s.2.

Figure 4-2 shows air temperature of Ex s.2, however, air temperature near the bottom opening was close to the air temperature in middle compared with Ex s.1. Air temperature near the top opening was higher than air temperature measured at other locations. It is supposed that the decrease in air stratification between top and bottom (within a 3-°C difference) was an effect of the PCM.

In terms of air stratification, in both cases average air temperature across five locations was close to the air temperature measured in the middle. Therefore, the middle air temperature was used as average temperature in the thermal zone to reduce the number of sensors.

Ex s.1 was the baseline for the atrium test, the prototype of which was the whole concrete fabrication, and the sub-scale model was built with 3D-printed materials and acrylic sheets. Therefore, dimensionless numbers were calculated by average thermal conduction and capacity in the sub-scale model. The fabrication information of Ex s.2 was the same for Ex s.1, however, a PCM sheet was inserted as a layer between baseline floor and atrium air.

Before verifying dimensional analysis by simulation model, the simulation model must be calibrated and validated by sub-scale experimental model. The discharge coefficient for the sub-scale model was unknown; therefore, it was calibrated from air temperature in Ex s.1, and the same discharge coefficient was used for other experiments. Slabs of wall and floor also were validated in Figure 4-3 (Ex s.1) and Figure 4-4 (Ex s.2).

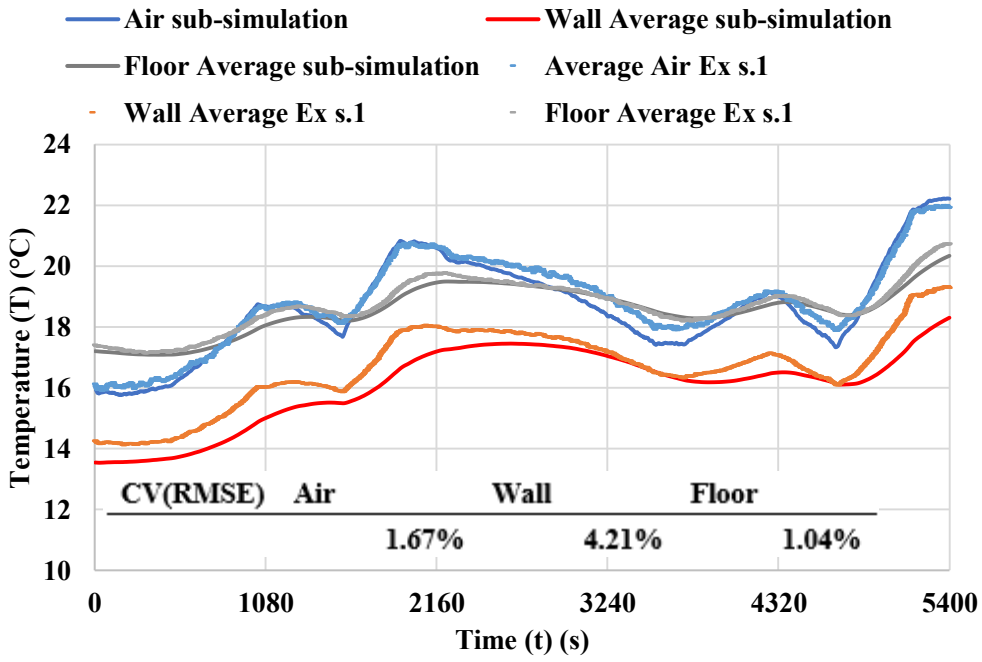


Figure 4-3. Validation of Ex s.1 (baseline without PCM).

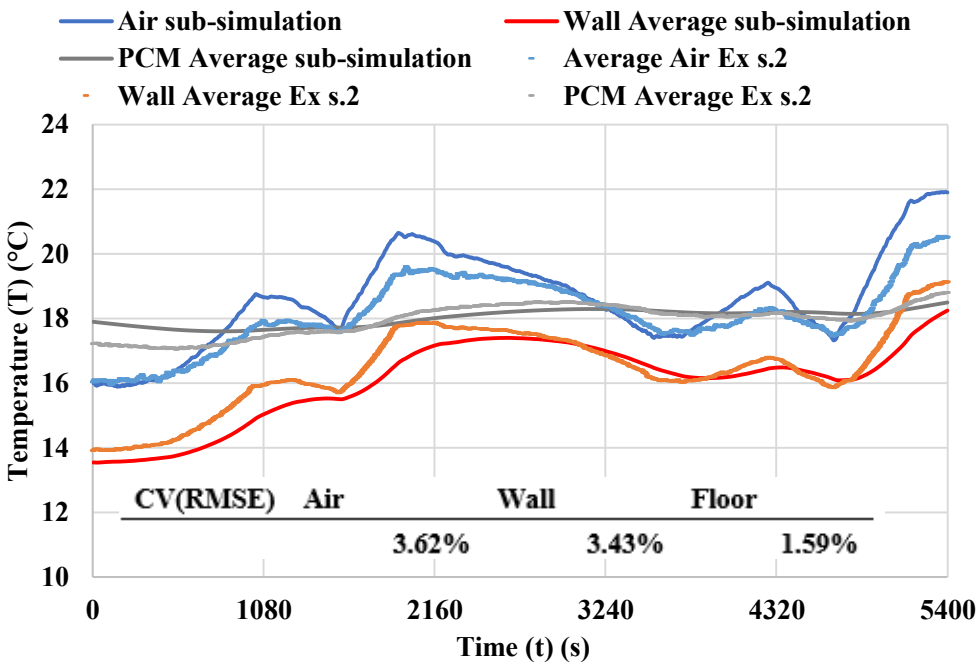


Figure 4-4. Validation of Ex s.2 (with PCM floor).

The experiment and simulation air and envelope temperatures were in good agreement, with CV (root-mean-square error) (RMSE) less than 4% in total. However, with deficiency of simulation model coding, initial thermal mass temperature was calculated by the average temperature between adjacent thermal zones, therefore, error is larger in initial temperature of thermal mass.

Clearly, the floor simulation error can be expected to be better than those for the air and wall—within 1.6%. Meanwhile, Ex s.2 simulation results showed differences for air and floor that were larger than those in Ex s.1 It was supposed that this was because the PCM simulation required more assumptions and approximations, which can decrease accuracy in simulations.

Using the validated simulation model, it was possible to build a full-size model to compare with the sub-scale simulation model and verify the dimensionless number for dimensional analysis. An

analytical model was built based on the same equation used in the simulation models, therefore, it was a good verification of both sub-scale and full-size models. However, the full-size simulation model was not calibrated and validated by full-size experiment and measurement.

### 4.2. Results and Discussion

Temperature profiles of cases are compared in Figures 4-5 and 4-6 by dimensionless temperature (θ) and dimensionless time ($\hat{t}$). The scaling law considers heat transfer between the thermal zone and the outdoor environment in the transient state. Results of the sub-scale simulation and full-size simulation were similar, with CV (RMSE) of less than 2.1% in total.

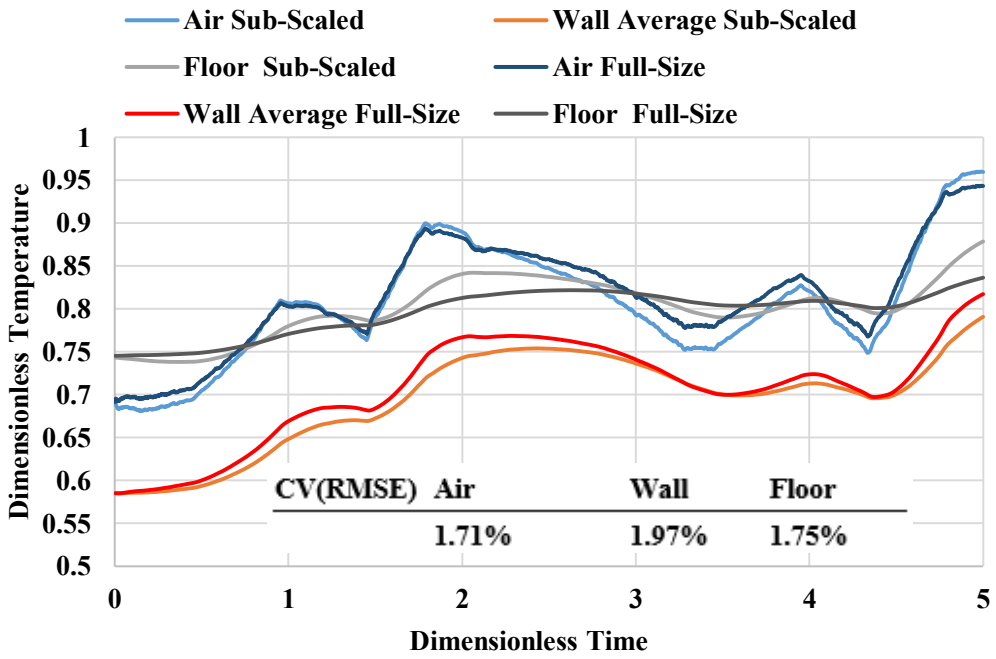


Figure 4-5. Dimensionless comparison of simulation results in Ex s.1.

Figure 4-5 compares sub-scale and full-size simulation results of baseline average temperature in air, wall and floor, with differences between 1.7% and 2%. The difference for wall temperature (1.97%) was larger than those for air (1.71%) and floor (1.75%). With variation of the outdoor temperature, air and wall temperature were affected more than floor, however, a larger fluctuation had no impact on similarity.

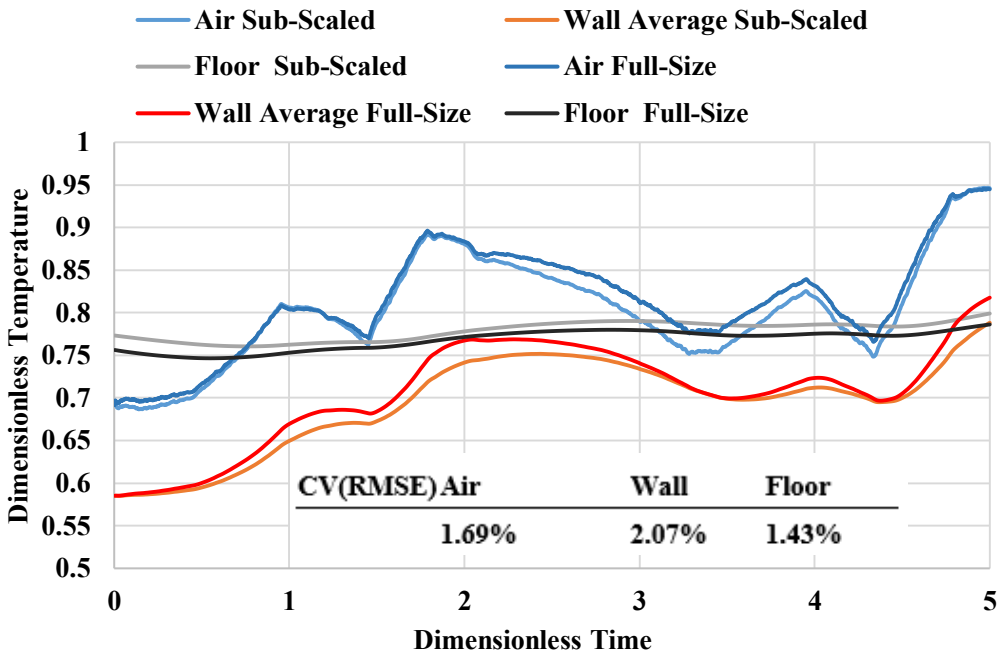


Figure 4-6. Dimensionless comparison of simulation results in Ex s.2.

Figure 4-6 illustrates the comparison between sub-scale simulation and full-size simulation with the PCM floor, with differences from 1.4% to 2.1%. The difference of average wall temperature is again larger than those of air and floor, as was seen in Figure 4-5.

Overall, in the atrium comparison between sub-scale and full-size simulation, there was good agreement, with a difference of less than 2.1%. Therefore, dimensionless numbers derived by a simplified analytical model can be verified by simulation results. By conserving dimensionless temperature between sub-scale and full-size models in the transient state, corresponding energy consumption in a full-size building can be calculated from sub-scale experiment results.

Using dimensionless numbers, the full-size temperature profile can be calculated. Additionally, with different setups in Ex s.1 and Ex s.2, the effects of PCM can be quantified. Diurnal

temperature variation can improve thermal-mass efficiency by pre-cooling in a natural ventilation system. PCM can expand this advantage by increasing thermal capacity and reducing temperature fluctuation.

### 4.3. Application

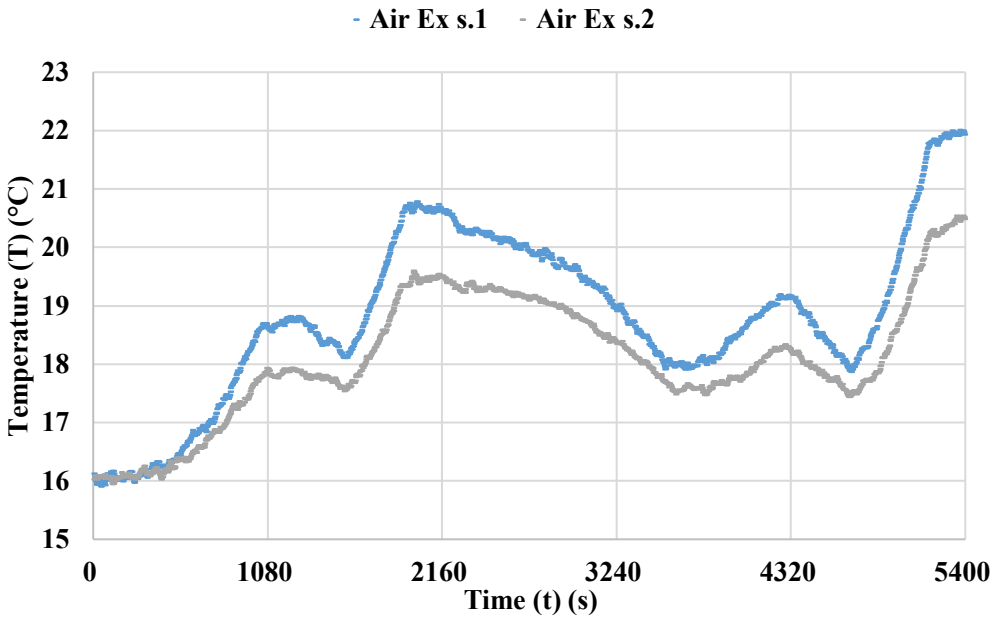


Figure 4-7. Comparison of air temperature between Ex s.1 and Ex s.2.

Figure 4-7 shows the indoor air temperature variation between Ex s.1 and Ex s.2, which illustrates the influence of PCM on air temperatures. Ex s.2 peak temperature was about 2 °C lower than that in Ex s.1. Furthermore, real-time temperature was also less under the same boundary condition. Clearly, Ex s.2 showed PCM was effective in reducing fluctuations of indoor air temperature when natural ventilation was performed. Higher thermal capacity also can cut peak-cooling energy consumption.

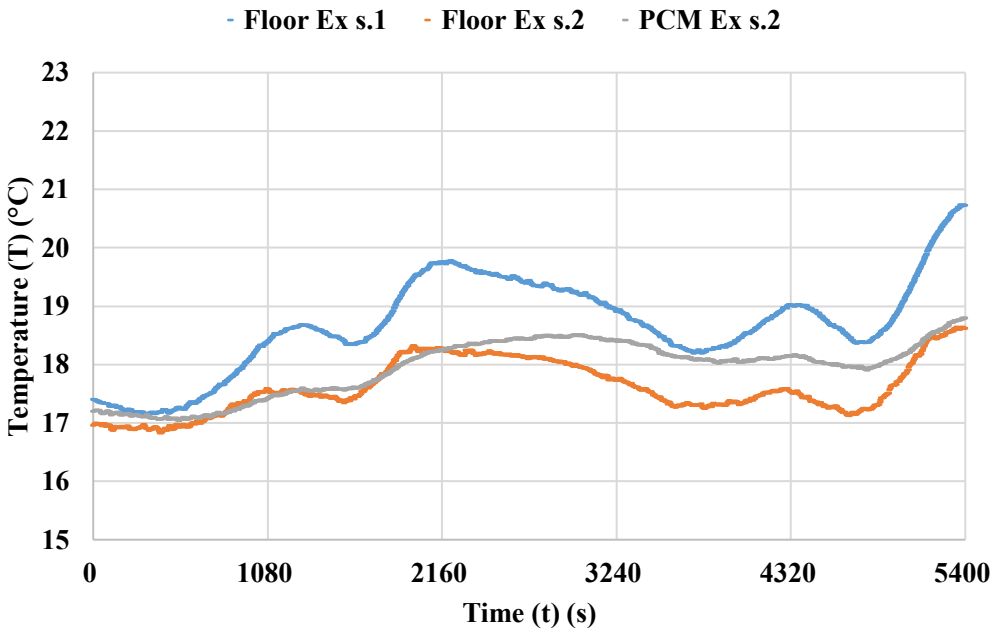


Figure 4-8. Comparison of floor temperature between Ex s.1 and Ex s.2.

Figure 4-8 shows the thermal mass temperature variation in the floors. Clearly, the PCM temperature fluctuation was smaller than the others, also affecting the floor that was covered with the PCM. The floor temperature variation trend was almost same, however, the temperature of the floor in Ex s.2 was lower than that in Ex s.1. Therefore, by influencing the attached envelope and thermal air, PCM can charge and discharge more thermal energy, while also reducing temperature variation to reduce discomfort for occupants.

The daily results of thermal charge and discharge in different floors are presented in Figure 4-9, which describes daily total thermal contribution in a typical atrium. The PCM has 30% to 50% higher daily thermal charge and discharge than concrete. The outside temperature increased overall

in these five days, however, it decreased on day 3. Therefore, the discharge difference is higher than the charge difference on four of the five days, with 2017/6/6 being the exception.

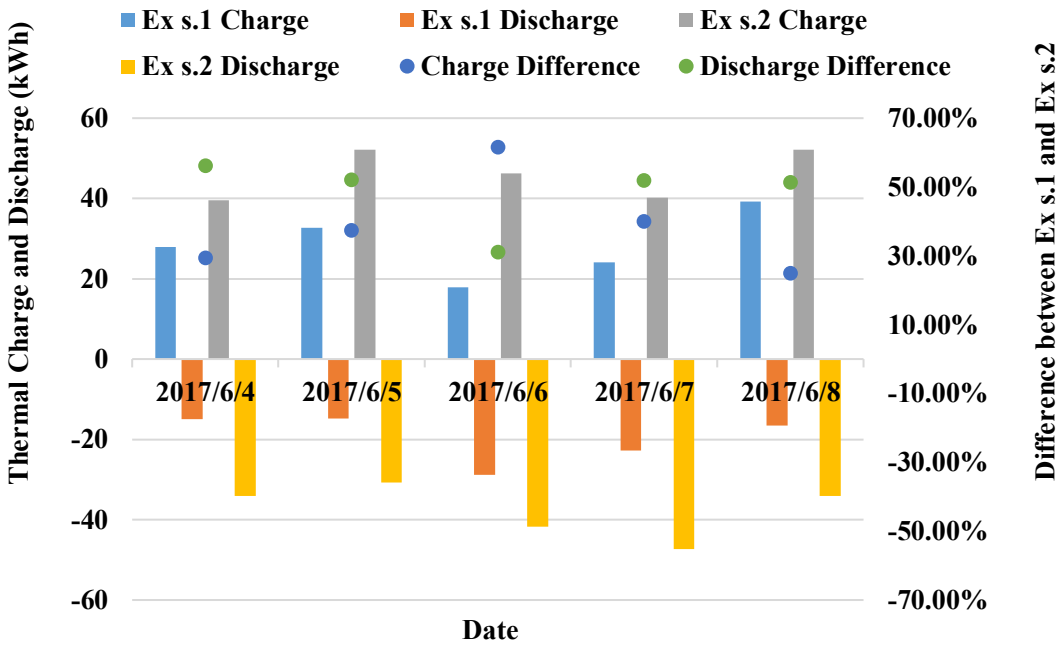


Figure 4-9. Comparison between Ex s.1 and Ex s.2 in full-size counterparts.

Thermal charge and discharge had a large difference in value depending on natural ventilation, with the lowest value less than 20 kWh and the greatest more than 50 kWh. Therefore, higher thermal mass can increase the energy savings of natural ventilation, with natural ventilation determining how the thermal mass can be activated.

# Chapter 5 Hybrid Ventilation in High-Rise Building

## 5.1. Simulations Validation of Multizone Modeling in EV Building

The EV Building was tested under the same weather conditions as the atrium. Results of sub-scale simulation of the five atriums in the EV Building were validated by sub-scale experiments. Table 5-1 shows the difference of air and floor temperature in CV (RMSE) between sub-scale experiments and simulations. The discharge coefficient was used in the same number of Ex s.1.

Zone 1 to zone 5 were arranged from the second floor to the 16th floor, with each zone including three floors and their integrated atrium in the middle of building. Zone 1 included floors 2 to 4, and openings in floors 2 and 3 were closed, which reflected the conditions in the real building. Openings in zone 5 were all closed because of the presence on those floors of a precise-instrument laboratory that must avoid strong airflow.

Table 5-1. CV (RMSE) for air and floor between experiment and sub-scale simulation.

| **CV (RMSE)** | **Zone 1** | **Zone 2** | **Zone 3** | **Zone 4** | **Zone 5** |
|---|---|---|---|---|---|
| Air | | | | | |
| Ex s.3 | 3.16% | 2.10% | 2.84% | 7.06% | 3.44% |
| Ex s.4 | 2.53% | 2.31% | 3.68% | 6.58% | 3.28% |
| Floor | | | | | |
| Ex s.3 | 5.90% | 4.50% | 5.23% | 4.90% | 4.80% |
| Ex s.4 | 7.51% | 7.58% | 7.18% | 1.83% | 2.93% |

In validation results, the difference for zone 4 air temperatures was larger than those in the other zones. Conversely, the difference for zone 4 floor temperatures was among the smallest. The range of differences is from 1.83% to 7.58%, which is greater than the range of differences for the atrium simulation in the single-zone model. This shows that simulation models are less accurate for more complicated models.

Overall, in zone 1 to zone 3, the difference for floor temperatures was greater than those for air temperatures. Conversely, in zone 4 and zone 5 the difference for floor temperatures was better than those for air temperature. It is supposed that the higher airflow rate in zone 4 and zone 5 may have increased the complexity of variation in air temperature.

## 5.2. Results and Discussion

Dimensional analysis was built on a simplified single-zone model. This section discusses application of those dimensionless number to a more complicated model. Time and fan flow rate were scaled by dimensionless numbers, and dimensionless temperature (θ) and dimensionless time ($\hat{t}$) were conserved for comparison between sub-scale and full-size simulation models.

The comparison between sub-scale and full-size simulation results are shown in Figure 5-1 through Figure 5-20. Ex s.3 (Figure 5-1 to Figure 5-10) is the baseline experiment case without the PCM, and Ex s.4 (Figure 5-11 to Figure 5-20) is the case with PCM installed in the atriums. Air temperature and floor slab temperature are compared in both cases with dimensionless temperature and time. In figure legends, "S" represents the sub-scale simulation and "F" is the full-size simulation. Thermal zones are numbered 1 to 5 from bottom to top.

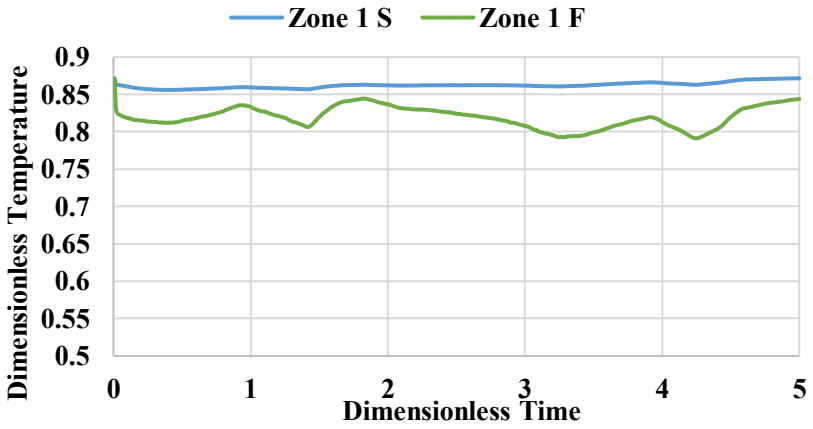


Figure 5-1. Comparison in zone 1 of Ex s.3 air.

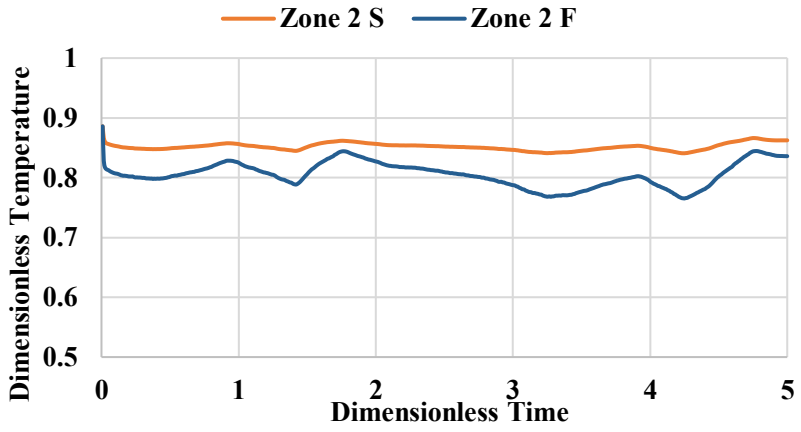


Figure 5-2. Comparison in zone 2 of Ex s.3 air.

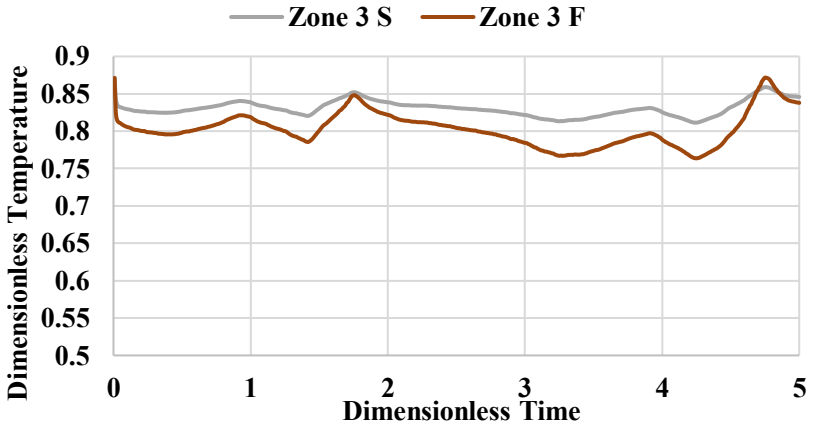


Figure 5-3. Comparison in zone 3 of Ex s.3 air.

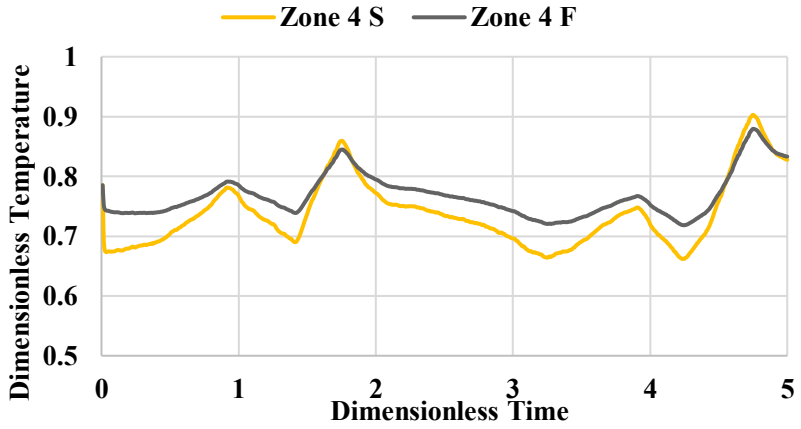


Figure 5-4. Comparison in zone 4 of Ex s.3 air.

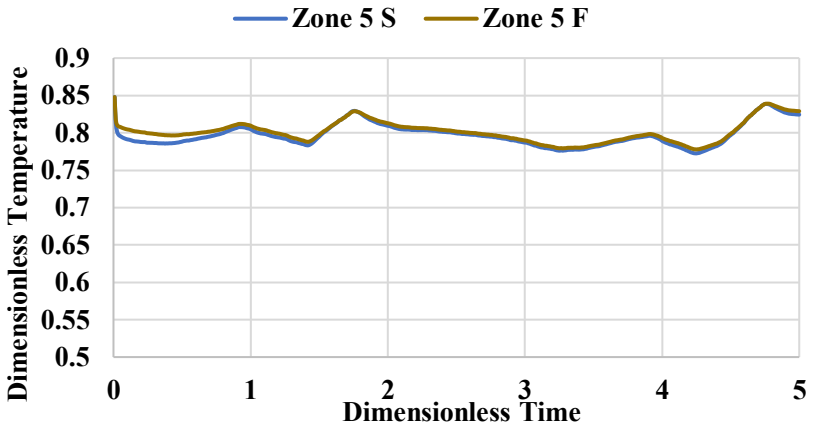


Figure 5-5. Comparison in zone 5 of Ex s.3 air.

Figures 5-1 to 5-5 show comparisons of air temperature between sub-scale and full-size simulations in Ex s.3 as a baseline. From zone 1 to zone 3, air temperatures in the full-size simulation fluctuates more widely and were lower than those in the sub-scale simulation. Conversely, zone 4 air temperature in the full-size simulation was higher than that in the sub-scale simulation. Zone 5 air temperatures for sub-scale and full-size simulations were very similar, because corridor openings were closed in this thermal zone.

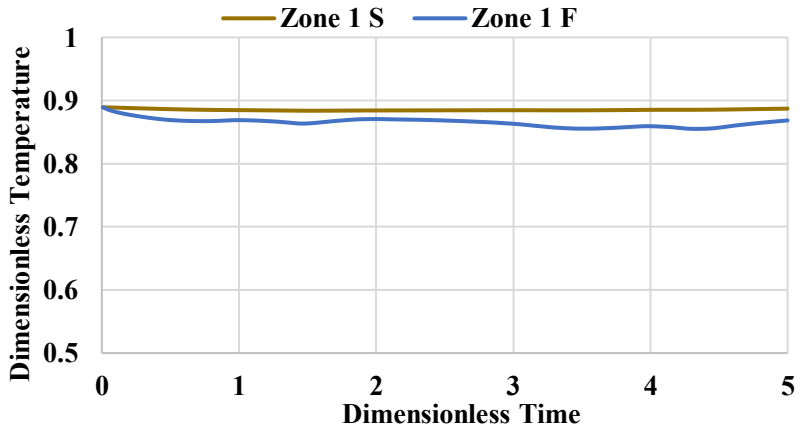


Figure 5-6. Comparison in zone 1 of Ex s.3 floor.

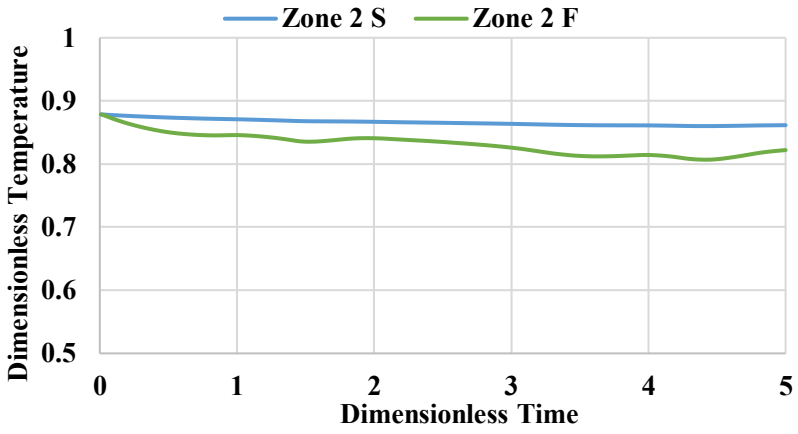


Figure 5-7. Comparison in zone 2 of Ex s.3 floor.

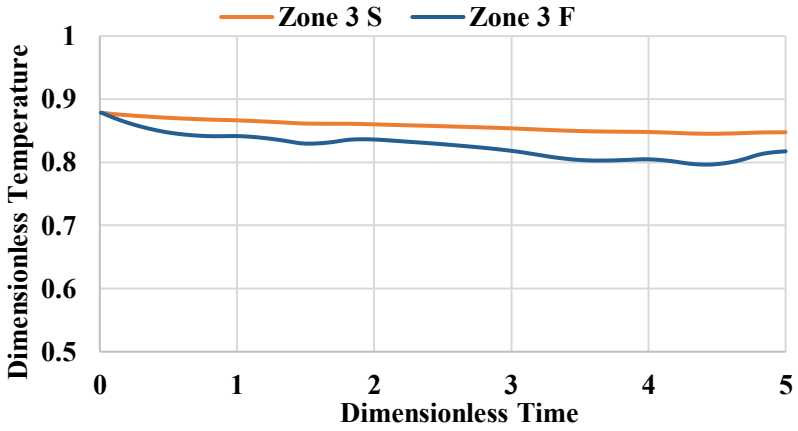


Figure 5-8. Comparison in zone 3 of Ex s.3 floor.

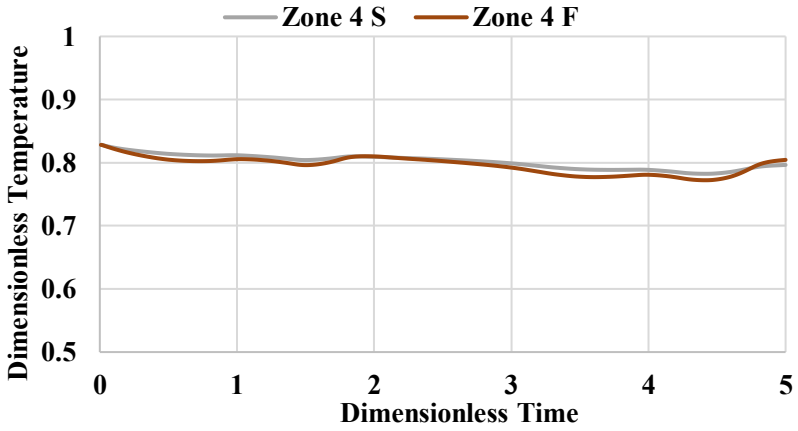


Figure 5-9. Comparison in zone 4 of Ex s.3 floor.

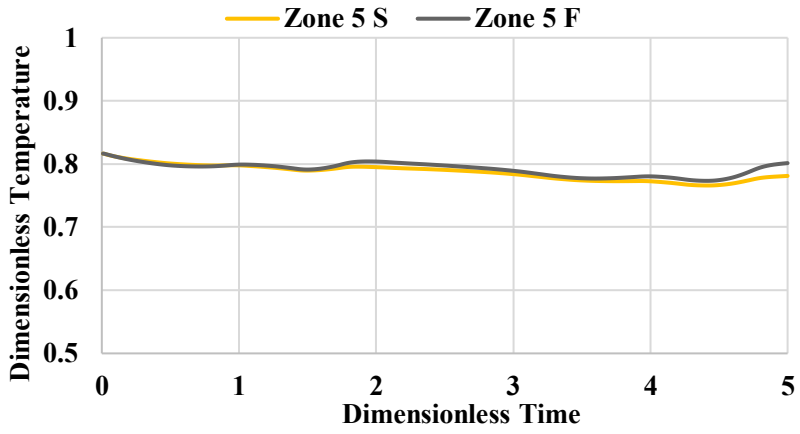


Figure 5-10. Comparison in zone 5 of Ex s.3 floor.

Figures 5-6 to 5-10 illustrate temperature variation in floor slabs. Because of the thermal-mass effect, floor slab temperatures changed only within a small range of from 0.8 to 0.9 on the dimensionless temperature scale. Correspondingly, differences for floor slab temperatures were similar to those for air temperatures from zone 1 to zone 3. Zone 5 floor slab temperatures for sub-scale and full-size simulations were also very similar.

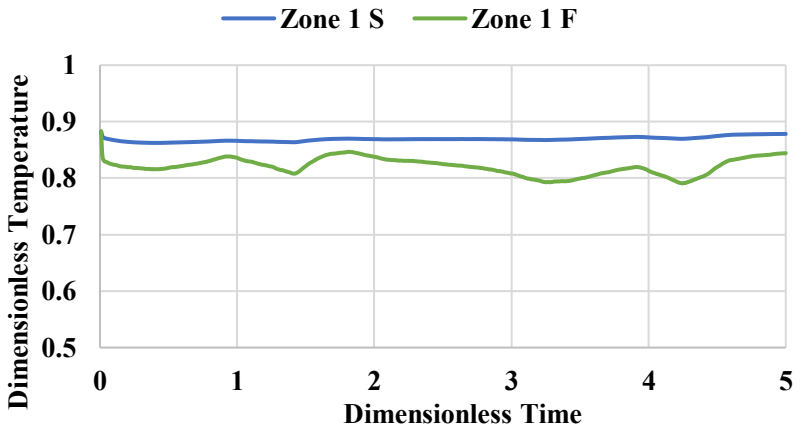


Figure 5-11. Comparison in zone 1 Ex s.4 air.

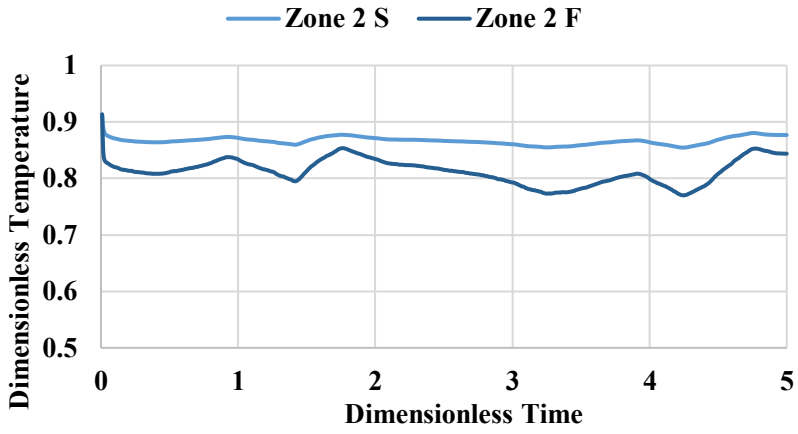


Figure 5-12. Comparison in zone 2 Ex s.4 air.

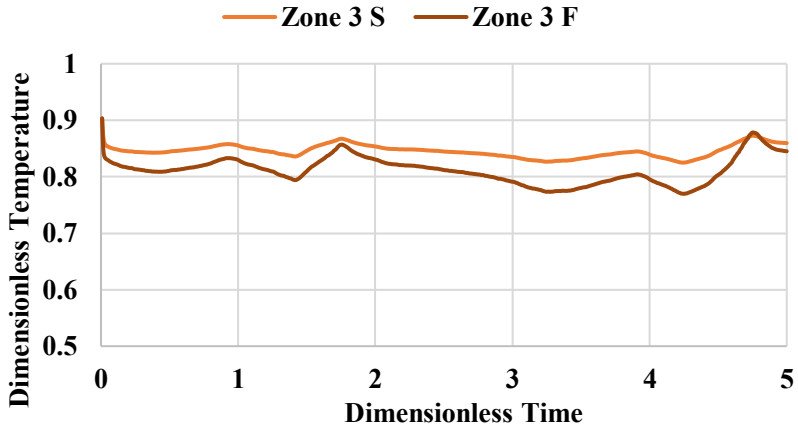


Figure 5-13. Comparison in zone 3 Ex s.4 air.

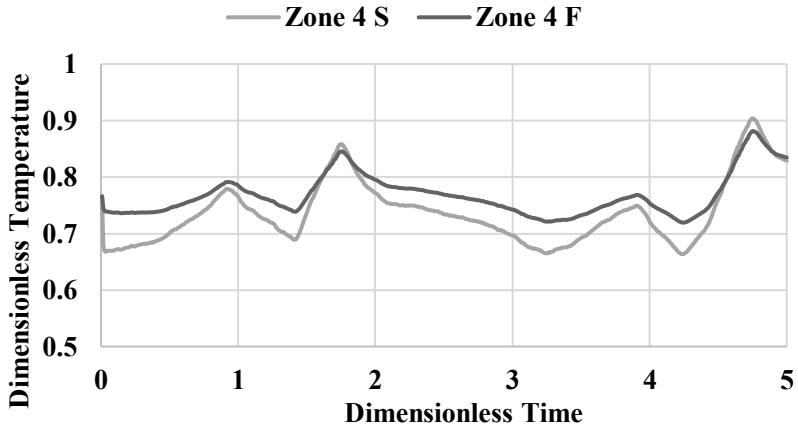


Figure 5-14. Comparison in zone 4 Ex s.4 air.

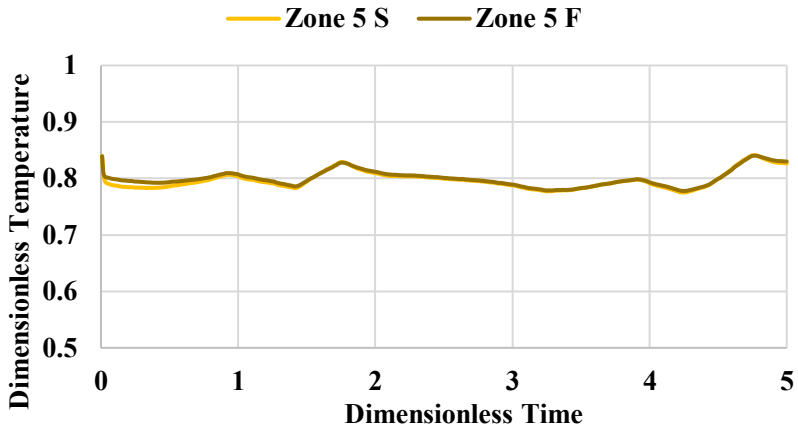


Figure 5-15. Comparison in zone 5 Ex s.4 air.

Figures 5-11 to 5-15 show dimensionless air temperature differences between sub-scale and full-size simulations in Ex s.4 with a PCM floor in each atrium. The similarity was comparable to that seen for Ex s.3, because airflow was controlled by a mechanical fan, which had a certain fan flowrate. With hybrid ventilation, however, which included mechanical ventilation and natural ventilation, maintaining a steady airflow was more difficult. Comparing air temperatures, there was no obvious difference between sub-scale and full-size results.

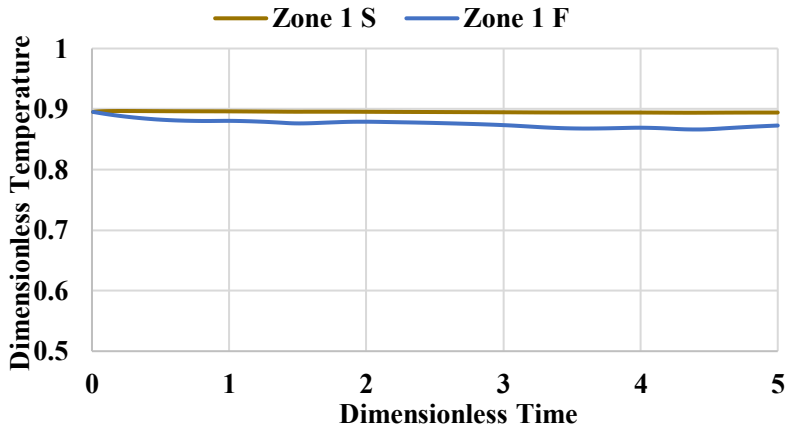


Figure 5-16. Comparison in zone 1 of Ex s.4 floor.

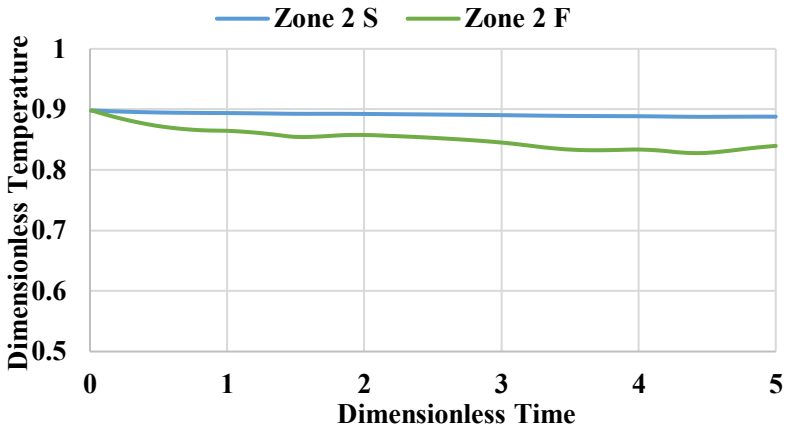


Figure 5-17. Comparison in zone 2 of Ex s.4 floor.

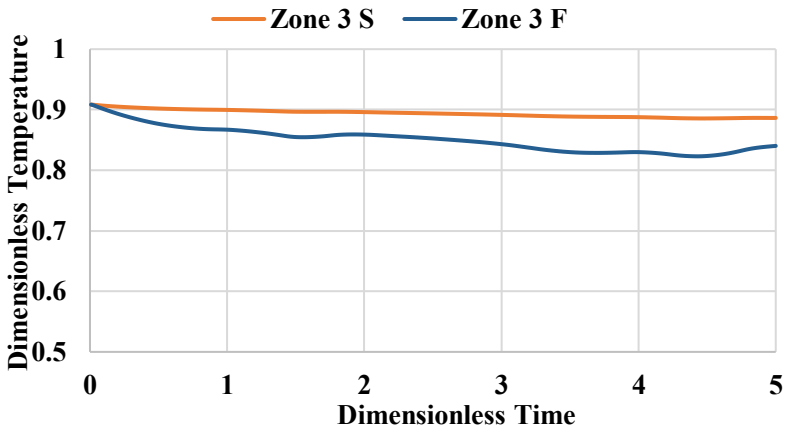


Figure 5-18. Comparison in zone 3 of Ex s.4 floor.

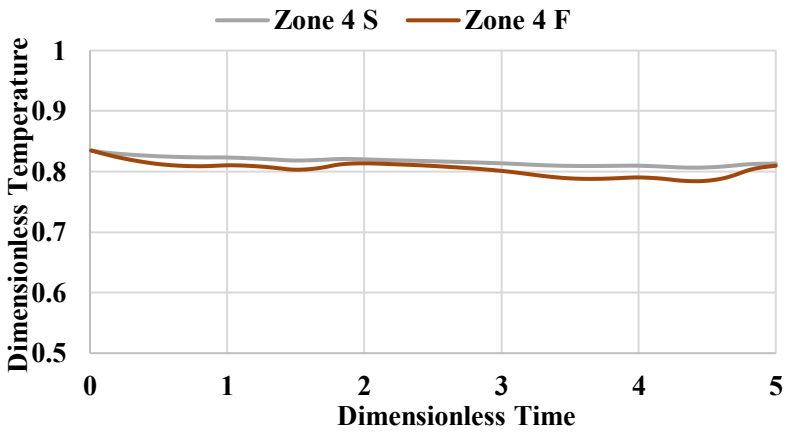


Figure 5-19. Comparison in zone 4 of Ex s.4 floor.

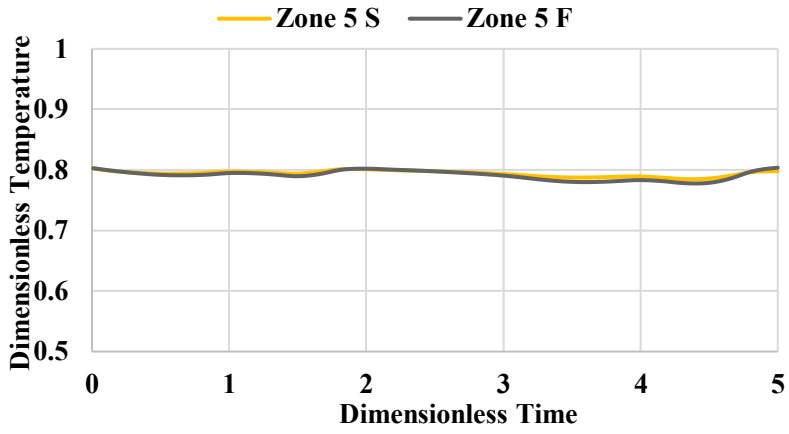


Figure 5-20. Comparison in zone 5 of Ex s.4 floor.

Figures 5-16 to 5-20 show comparisons of PCM floor temperatures between sub-scale and full-size simulations for Ex s.4. Compared with Ex s.3, the temperature fluctuation for each floor is smoother. However, the temperature differences in zone 1 to zone 3 were larger than those for zone 4 and zone 5, and it is supposed that those differences were the result of air temperature differences.

Overall, there were larger differences in a range of 0.1 dimensionless temperature units between sub-scale and full-size simulation results for both air and floor slab items for Ex s.4. Dimensionless temperature differences for air in zone 4 were also large, however, the corresponding floor slab temperature has a smaller CV (RMSE) difference.

Table 5-2. CV (RMSE) for air and floor between sub-scale and full-size simulation.

| CV (RMSE) | **Zone 1** | **Zone 2** | **Zone 3** | **Zone 4** | **Zone 5** |
|---|---|---|---|---|---|
| Ex s.3 air | 5.22% | 5.75% | 3.69% | 4.91% | 0.64% |
| Ex s.4 air | 5.80% | 6.52% | 4.32% | 5.00% | 0.49% |
| Ex s.3 floor | 2.37% | 4.22% | 3.96% | 0.90% | 0.88% |
| Ex s.4 floor | 2.28% | 4.82% | 5.08% | 1.76% | 0.51% |

Table 5-2 introduces CV (RMSE) differences between sub-scale and full-size simulation results in both air and floor slabs. Zone 5 has the best similarity, with both air and floor slab differences of less than 1%. Roughly speaking, air differences were larger than floor slab differences, which may have been a result of distorted airflow between the sub-scale and full-size models. Overall, differences from 0.49% to 6.52% can be seen as good agreement of the scaling law to verify the dimensionless numbers.

## 5.3. Application

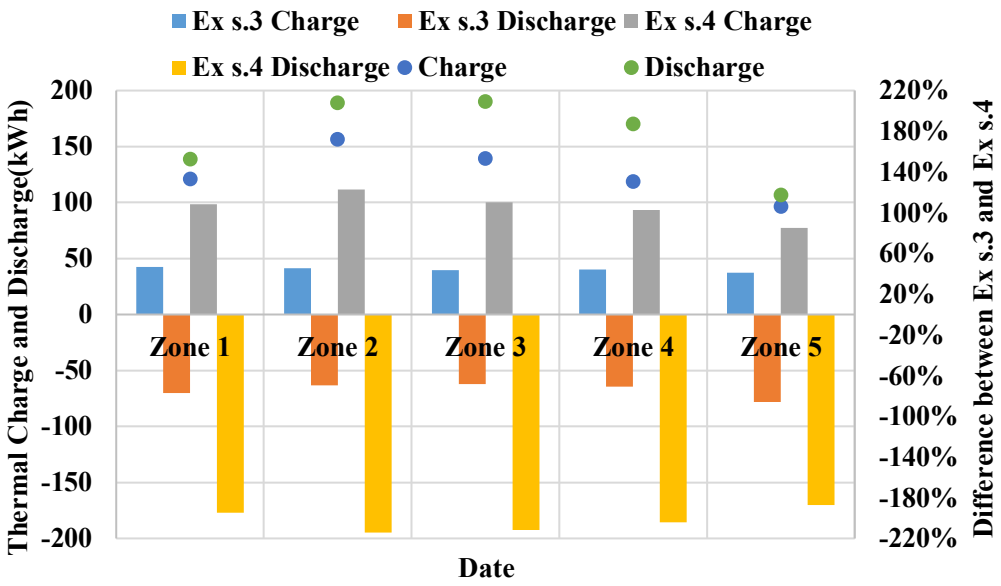


Figure 5-21. Comparison between Ex s.3 and Ex s.4 in full-size counterpart.

Figure 5-21 illustrates total thermal charge and discharge in each zone, which was calculated from sub-scale model experiment results through conserving dimensionless temperature and time. The differences between Ex s.3 (baseline) and Ex s.4 (PCM) are also introduced. PCM in hybrid ventilation had a much higher percentage increase in thermal charge and discharge than it did under natural ventilation, because mechanical fan can increase more airflow, resulting in greater heat exchange.

Comparing Ex s.3 and Ex s.4 shows that the PCM increased thermal charge and discharge efficiency more than 100%, and that at best this improvement in efficiency could reach 200%. Comparing this to the average 50% efficiency improvement that resulted from PCM when it was used with natural ventilation, it becomes clear that hybrid ventilation can increase the effectiveness of PCM.

# Chapter 6 Conclusion and Future Work

## 6.1. Conclusion

This study considers heat transfer, thermal capacity, and airflow similarity in a transient state through dimensional analysis, which includes energy balance and mass flow equations. Depending on the dimensionless numbers used, similarity between the sub-scale model and full-size model is established.

Transformation of Fourier numbers can be used to scale down in a transient state. Sub-scale modeling not only reduces the geometric scale, but also shortens experiment time by using a dimensionless time scale. Five days in full-size measurement can be scaled to 1800 s in a 1:100-scale model and to 5400 s in a 1:50-scale model, meaning that a one-year test can be completed in 36.5 h (1:100 scale) or 109.5 h (1:50 scale).

Dimensionless numbers derived by dimensional analysis are verified for the atrium case simulation by comparison between the sub-scale model and full-size model, which show less than a 2% difference with a natural ventilation system in a transient state. Not only air temperature but also thermal-mass temperature can be scaled by dimensional analysis through the use of dimensionless numbers in a transient state with integrated consideration of heat transfer and airflow.

Dimensionless numbers from the simplified atrium model can be applied to a more complicated high-rise building to establish an appropriate sub-scale experiment model. Although in the high-

rise case the difference between the sub-scale and full-size models increases to about 7%, it has difficulties similar to those of building a full-size simulation model of a complicated building.

The installation of PCM can slow fluctuations of thermal air and can charge and discharge more energy for cutting peak energy load. PCM thermal efficiency can be improved by a factor of three by using it with a hybrid ventilation system rather than a natural ventilation system, given the greater heat exchange that comes with mechanical airflow.

Sub-scale experiments can be a good way to test a preliminary design that includes complicated geometry or difficult-to-determine property inputs for a simulation, such as phase-change process properties for a PCM. In an atrium experiment test, average temperature of a space can be represented as measured air temperature in the middle of the space. Furthermore, thermal stratification of the air can be reduced by the use of PCMs.

## 6.2. Limitations of This Study

This study focused on sub-scale experiment similarity, however, it has several limitations.

- Limited weather data are used in the tests. The outside temperature used is too low to open the windows if there are occupants in the atriums. Also, there are no separate winter and summer tests for similarity verification.
- Full-size calibration for the discharge coefficient is limited. In the atrium case, the discharge coefficient used for full-size is the default number in ASHRAE, which needs to be calibrated in a full-size experiment. In the EV Building, the same discharge coefficient is used for each opening, while in reality the discharge coefficient would vary depending on differences in height and other conditions.
- Full-size simulation results need to be validated by a full-size experiment or measurement. Given differences in conditions between the lab and the real building, a full-size simulation model is difficult to validate by real measurement.
- Wind and solar irradiation are not considered. In a real case, wind and solar irradiation will significantly affect ventilation and thermal mass.
- Lack of multiscale model experiment for justification. The simulation model basically is the same equation used for the analytical model, and it can only verify dimensionless numbers.

### 6.3. Recommendations for Future Work

This study verifies dimensionless numbers in an analytical model to qualify thermal-mass effect in natural and hybrid ventilation systems. For future work, a few items can be considered:

- A multiscale experiment with both the atrium and EV Building experiments to justify the method.
- Investigating more cases to consider winter and summer operation strategies and conditions without natural and hybrid ventilation.
- Developing a theoretical equation in wind and solar cases to discuss similarity in more particular conditions.
- Based on CFD simulations, justifying the scaling law in more cases under different conditions.
- Investigating the discharge coefficient in openings of different scales.
- Investigating similarity cases in horizontal space construction such as a tunnel or a large factory space.
- Investigating a sub-scale model experiment for operation strategy decisions or tests such as for Model Protective Control (MPC).

## Reference


[1] Minister of Natural Sources, "Energy Use Data Handbook – 1990 to 2015," 2018, [Online], Available: http://oee.nrcan.gc.ca/corporate/statistics/neud/dpa/data_e/downloads/handbook/pdf/2015/HB2015e.pdf

[2] International Energy Agency, "The Future of Cooling. Opportunities for energy-efficient air conditioning.," 2018, [Online], Available: https://www.iea.org/publications/freepublications/publication/The_Future_of_Cooling.pdf

[3] O. Saadatian, L. C. Haw, K. Sopian, and M. Y. Sulaiman, "Review of windcatcher technologies," *Renew. Sustain. Energy Rev.*, vol. 16, no. 3, pp. 1477–1495, Apr. 2012.

[4] G. Carrilho da Graça and P. Linden, "Ten questions about natural ventilation of non-domestic buildings," *Build. Environ.*, vol. 107, pp. 263–273, Oct. 2016.

[5] J. Cheng, "An Experimental and Computational Study of Natural and Hybrid Ventilation in Buildings," MASc Thesis, Department of Building, Civil, and Environmental Engineering, Concordia University, 2017.

[6] Burge, S., Hedge, A., Wilson, S., Bass, J. H., & Robertson, A, "Sick Building Syndrome: A study of 4,373 office workers," *The Annals of Occupational Hygiene,* Volume 31, Issue 4A, 1 January 1987, Pages 493–504, 1987.

[7] J. Chen, G. Augenbroe, and X. Song, "Evaluating the potential of hybrid ventilation for small to medium sized office buildings with different intelligent controls and uncertainties in US climates," *Energy Build.*, vol. 158, pp. 1648–1661, Jan. 2018.

[8] S. Ezzeldin and S. J. Rees, "The potential for office buildings with mixed-mode ventilation and low energy cooling systems in arid climates," *Energy Build.*, vol. 65, pp. 368–381, Oct. 2013.

[9] S. Yuan, C. Vallianos, A. Athienitis, and J. Rao, "A study of hybrid ventilation in an institutional building for predictive control," *Build. Environ.*, vol. 128, pp. 1–11, Jan. 2018.

[10] N. Artmann, H. Manz, and P. Heiselberg, "Climatic potential for passive cooling of buildings by night-time ventilation in Europe," *Appl. Energy*, vol. 84, no. 2, pp. 187–201, Feb. 2007.

[11] B. M. Diaconu, "Thermal energy savings in buildings with PCM-enhanced envelope: Influence of occupancy pattern and ventilation," *Energy Build.*, vol. 43, no. 1, pp. 101–107, Jan. 2011.

[12] S. Takeda, K. Nagano, T. Mochida, and K. Shimakura, "Development of a ventilation system utilizing thermal energy storage for granules containing phase change material," *Sol. Energy*, vol. 77, no. 3, pp. 329–338, Sep. 2004.

[13] K. Nagano, S. Takeda, T. Mochida, K. Shimakura, and T. Nakamura, “Study of a floor supply air conditioning system using granular phase change material to augment building mass thermal storage—Heat response in small scale experiments,” *Energy Build.*, vol. 38, no. 5, pp. 436–446, May 2006.

[14] S. E. Kalnaes, B. Petter, and J. Ab, “Phase Change Materials for Building Applications: A State-of-the-Art Review and Future Research Opportunities,” *Energy Build.*, vol. 42, no. 9, pp. 1361–1368, Sep. 2010.

[15] M. Iten, S. Liu, and A. Shukla, “A review on the air-PCM-TES application for free cooling and heating in the buildings,” *Renew. Sustain. Energy Rev.*, vol. 61, pp. 175–186, Aug. 2016.

[16] Q. Chen, “Ventilation performance prediction for buildings: A method overview and recent applications,” *Build. Environ.*, vol. 44, no. 4, pp. 848–858, Apr. 2009.

[17] F. Kuznik, J. Virgone, and K. Johannes, “Development and validation of a new TRNSYS type for the simulation of external building walls containing PCM,” *Energy Build.*, vol. 42, no. 7, pp. 1004–1009, Jul. 2010.

[18] A. Acred and G. R. Hunt, “Stack ventilation in multi-storey atrium buildings: A dimensionless design approach,” *Build. Environ.*, vol. 72, pp. 44–52, 2014.

[19] D. Coakley, P. Raftery, and M. Keane, "A review of methods to match building energy simulation models to measured data," *Renew. Sustain. Energy Rev.*, vol. 37, pp. 123–141, 2014.

[20] M.-L. Persson, A. Roos, and M. Wall, "Influence of window size on the energy balance of low energy houses," *Energy Build.*, vol. 38, no. 3, pp. 181–188, Mar. 2006.

[21] W. Ding, Y. Hasemi, and T. Yamada, "Natural ventilation performance of a double-skin façade with a solar chimney," *Energy Build.*, vol. 37, no. 4, pp. 411–418, 2005.

[22] J. M. Lirola, E. Castañeda, B. Lauret, and M. Khayet, "A review on experimental research using scale models for buildings: Application and methodologies," *Energy Build.*, vol. 142, pp. 72–110, 2017.

[23] J. M. Lirola, "Simulation of thermal performance of glazing in the architecture using scale models," PhD. Thesis, Department of Construction and Building Technology, Technical University of Madrid, 2015.

[24] W. Tian, X. Han, W. Zuo, and M. D. Sohn, "Building energy simulation coupled with CFD for indoor environment: A critical review and recent applications," *Energy Build.*, vol. 165, pp. 184–199, Apr. 2018.

[25] E. Djunaedy, J. Hensen, T. U. Eindhoven, T. U. Eindhoven, and P. Climate, "Toward external coupling of building energy and airflow modeling programs," *ASHRAE Trans.*, vol. 109, no. 2, pp. 771–787, 2003.

[26] A. K. Athienitis and L. (William) O'Brien, "Modeling, design, and optimization of net-zero energy buildings. " Book, 2015 .

[27] A. Foucquier, S. Robert, F. Suard, L. Stéphan, and A. Jay, "State of the art in building modelling and energy performances prediction: A review," *Renew. Sustain. Energy Rev.*, vol. 23, pp. 272–288, Jul. 2013.

[28] A. W. W. J.M.Holford, "On the thermal buffering of naturally ventilated buildings through internal thermal mass," *J. Fluid Mech*, vol. 580, pp. 3–29, 2018.

[29] G. Brager, S. Borgeson, and Y. Lee, "Summary Report: Control Strategies for Mixed-Mode Buildings," Report, UC Berkeley, Oct. 2007.

[30] G. Brager and L. Baker, "Occupant satisfaction in mixed-mode buildings," *Build. Res. Inf.*, vol. 37, no. 4, pp. 369–380, Aug. 2009.

[31] H. C. Spindler and L. K. Norford, "Naturally ventilated and mixed-mode buildingsdPart I: Thermal modeling," *Build. Environ.*, vol. 44, pp. 736–749.

[32] M. Simonetti, V. Gentile, L. Liggieri, G. V. Fracastoro, and M. G. Carrabba, "Experimental analysis of 'NAC-wall' for hybrid ventilation mode," *Energy Build.*, vol. 152, pp. 399–408, Oct. 2017.

[33] D. Yang and P. Li, "Dimensionless design approach, applicability and energy performance of stack-based hybrid ventilation for multi-story buildings," *Energy*, 93, pp.128-140. 2015.

[34] W. J. N. Turner and H. B. Awbi, "Experimental investigation into the thermal performance of a residential hybrid ventilation system," *Applied Thermal Engineering,* 77, pp.142-152. 2015.

[35] P. Karava, A. K. Athienitis, T. Stathopoulos, and E. Mouriki, "Experimental study of the thermal performance of a large institutional building with mixed-mode cooling and hybrid ventilation," *Build. Environ.*, vol. 57, pp. 313–326, Nov. 2012.

[36] M. Telkes, "thermal energy storage using sodium sulfate decahydrate and water," *Sol. Energy*, vol. 20, no. 1, p. 107, Jan. 1978.

[37] M. M. Farid, A. M. Khudhair, A. K. Razack, and S. Al-Hallaj, "A review on phase change energy storage: materials and applications," *Energy Convers. Manag.*, vol. 45, pp. 1597–1615, 2004.

[38] F. Guarino, A. Athienitis, M. Cellura, and D. Bastien, “PCM thermal storage design in buildings: Experimental studies and applications to solaria in cold climates,” *Appl. Energy*, vol. 185, pp. 95–106, Jan. 2017.

[39] K. Yanbing, J. Yi, and Z. Yinping, “Modeling and experimental study on an innovative passive cooling system—NVP system,” *Energy Build.*, vol. 35, no. 4, pp. 417–425, May 2003.

[40] J. Axley, “Multizone Airflow Modeling in Buildings: History and Theory,” *HVAC&R Res.*, vol. 13, no. 6, pp. 907–928, Nov. 2007.

[41] Z. Zhai, Q. Chen, P. Haves, and J. H. Klems, “On approaches to couple energy simulation and computational fluid dynamics programs,” *Build. Environ.*, vol. 37, no. 8–9, pp. 857–864, Aug. 2002.

[42] M. L. Hosain and R. B. Fdhila, “Literature Review of Accelerated CFD Simulation Methods towards Online Application,” *Energy Procedia*, vol. 75, pp. 3307–3314, Aug. 2015.

[43] W. Zuo and Q. Chen, “Real-time or faster-than-real-time simulation of airflow in buildings,” *Indoor Air*, vol. 19, no. 1, pp. 33–44, Feb. 2009.

[44] A. Katal, L. Wang, W. S. Dols, and B. J. Polidoro, "An Investigation of Different Strategies For Solving Coupled Thermal Airflows By Multi-Zone Network Method," Conference of COBEE, pp.614-619, 2018.

[45] Y.-H. Lim, H.-W. Yun, and D. Song, "Indoor Environment Control and Energy Saving Performance of Hybrid Ventilation System for a Multi-residential Building," *Energy Procedia*, vol. 78, pp. 2863–2868, 2015.

[46] Z. Zhai, M.-H. Johnson, and M. Krarti, "Assessment of natural and hybrid ventilation models in whole-building energy simulations," *Energy Build.*, vol. 43, pp. 2251–2261, 2011.

[47] G. Astarita, "Dimensional analysis, scaling, and orders of magnitude," *Chem. Eng. Sci.*, vol. 52, no. 24, pp. 4681–4698, 1997.

[48] H. Hossdorf and C. Hernández, "Modelos reducidos: métodos de cálculo," Instituto Eduardo Torroja de la Construcción y del Cemento, 1972.

[49] P. Y. Cui, Z. Li, and W. Q. Tao, "Wind-tunnel measurements for thermal effects on the air flow and pollutant dispersion through different scale urban areas," *Build. Environ.*, vol. 97, pp. 137–151, 2016.

[50] T. Minehiro, K. Fujita, N. Kawabata, M. Hasegawa, and F. Tanaka, "Backlayering Distance of Thermal Fumes in Tunnel Fire Experiments Using a Large-Scale Model*," *J. Fluid Sci. Technol.*, vol. 7, no. 3, 2012.

[51] D. Qi, L. Wang, and R. Zmeureanu, "An analytical model of heat and mass transfer through non-adiabatic high-rise shafts during fires," *Int. J. Heat Mass Transf.*, vol. 72, pp. 585–594, May 2014.

[52] D. Qi, L. (Leon) Wang, J. Ji, and M. Li, "Dimensionless analytical solutions for steady-state fire smoke spread through high-rise shaft," *Fire Saf. J.*, vol. 93, pp. 12–20, Oct. 2017.

[53] D. Qi and D. Qi, "Analytical Modeling of Fire Smoke Spread in High-rise Buildings," PhD. Thesis, Department of Building, Civil, and Environmental Engineering, Concordia University, 2016.

[54] S.-K. SONG and K. KIMURA, "Experimental study on the prediction of cooling load of large factory space using three dimensional model," *J. Archit. Plan. (Transactions AIJ)*, vol. 67, no. 553, pp. 77–83, 2002.

[55] Y. SUWA and T. TSUCHIYA, "Experimental study using a shrink model on highperformance airflow design for air-conditioning system in data centers," *J. Environ. Eng. (Transactions AIJ)*, vol. 77, no. 675, pp. 365–374, May 2012.

[56] T. Miura, Y. Ito, Y. Murae, S. Kuriki, and K. Sasagase, "Study on Natural Ventilation System of Office Building by Double Skin and Solar Chimney Part 1 Outline of Natural Ventilation System and Measurement Result of Ventilation Volume by Experimental Scaled-down Model," *Soc. Heating, Air-Conditioning Sanit. Eng. Japan*, p. B-41, 2015.

[57] Y. Li *et al.*, "Some examples of solution multiplicity in natural ventilation," *Build. Environ.*, vol. 36, no. 7, pp. 851–858, 2001.

[58] J. Cheng, D. Qi, L. Wang, and A. Athienitis, "Whole-Building Simulation of Hybrid Ventilation based on Full-scale Measurements in an Institutional High-rise Building for Predictive Control," Proceedings of 15th International Conference of IBPSA. 2017.

[59] D. Qi, W. Li, J. Cheng, and L. Wang, "Scale Modelling of Thermal Airflows in Buildings, " Coference of COBEE, pp.609-613, 2018.

[60] F. Agyenim, N. Hewitt, P. Eames, and M. Smyth, "A review of materials, heat transfer and phase change problem formulation for latent heat thermal energy storage systems (LHTESS)," *Renewable and sustainable energy reviews*, 14(2), pp.615-628, 2010.

[61] H. Kotani, R. Satoh, and T. Yamanaka, "Natural ventilation of light well in high-rise apartment building," *Energy and Buildings*, 35(4), pp.427-434, 2003.

[62] Y. Andersen, A.; Bjerre, M.; Chen, Z. D.; Heiselberg, Per Kvols; Li, "Experimental Study of Wind-Opposed Buoyancy-Driven Natural Ventilation," Proceedings 21 st AIVC Annual Conference of Innovations in Ventilation Technology, pp. 26-29, 2000.

[63] M. Ahmad, A. Bontemps, H. Sallée, and D. Quenard, "Thermal testing and numerical simulation of a prototype cell using light wallboards coupling vacuum isolation panels and phase change material," *Energy Build.*, vol. 38, no. 6, pp. 673–681, Jun. 2006.

# Appendix

Appendix 1 PCM thermal capacity

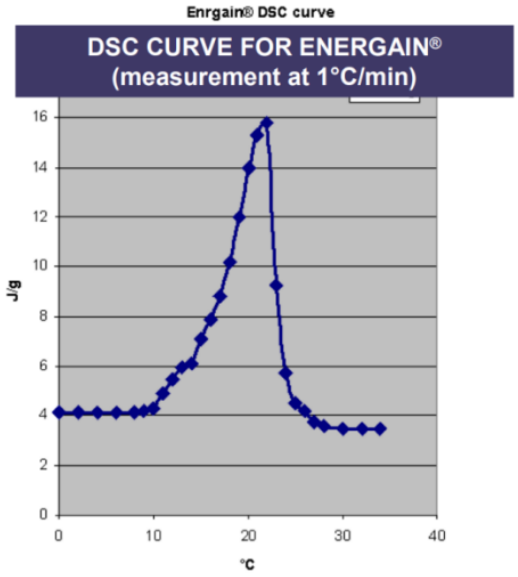


Appendix 2 Experiment data of atrium

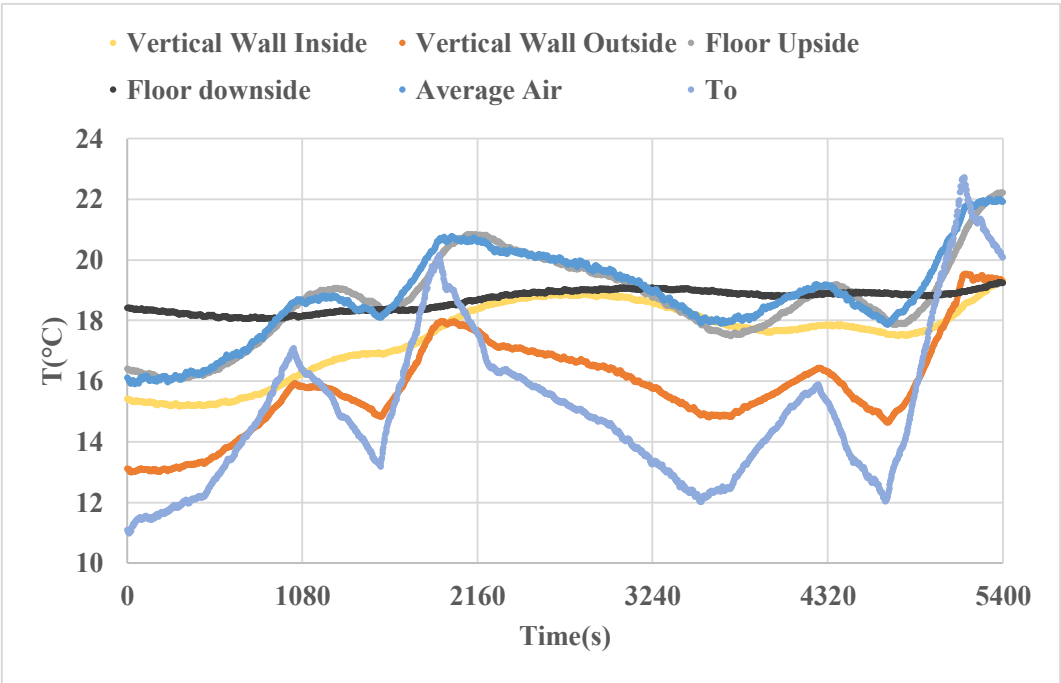

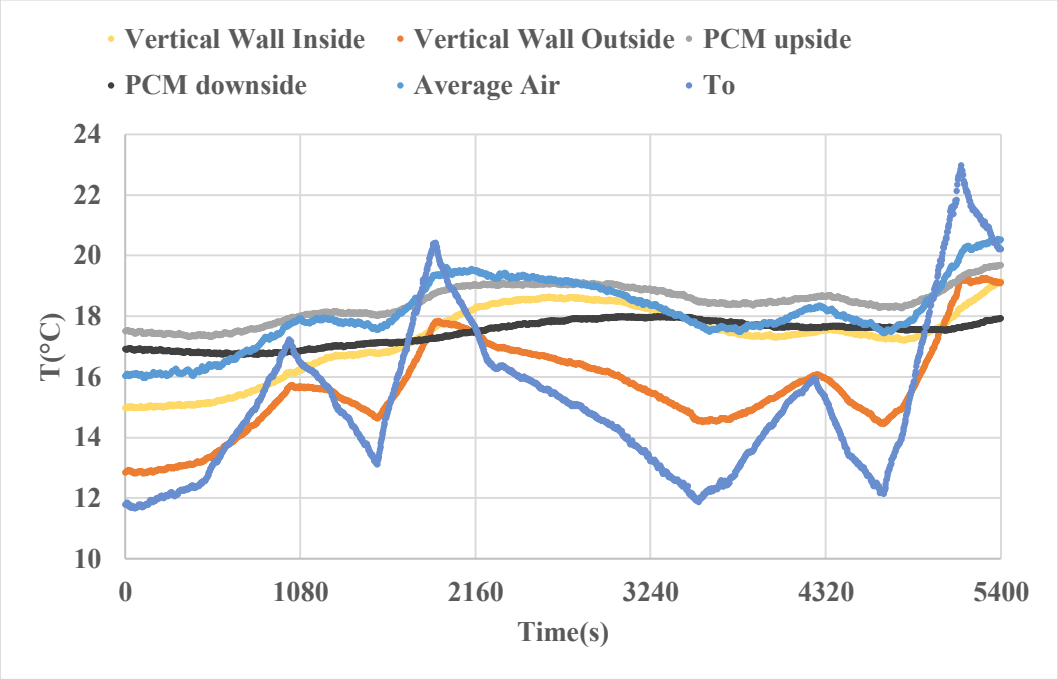


Appendix 3 Air temperature validation of sub-scale simulation in Ex s.3

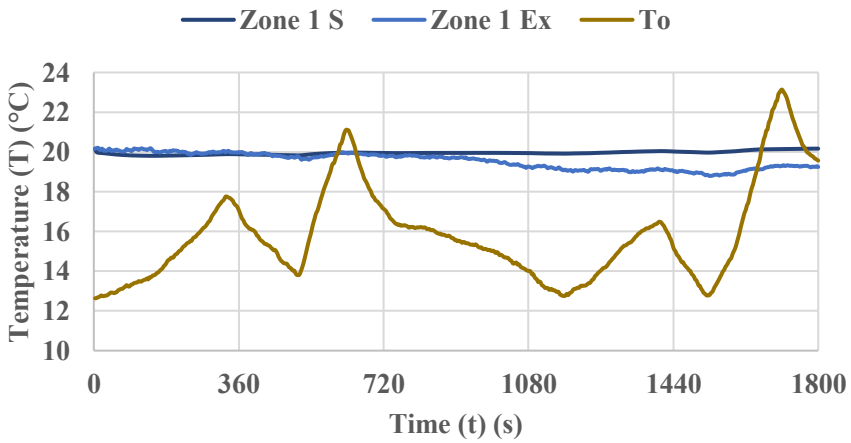

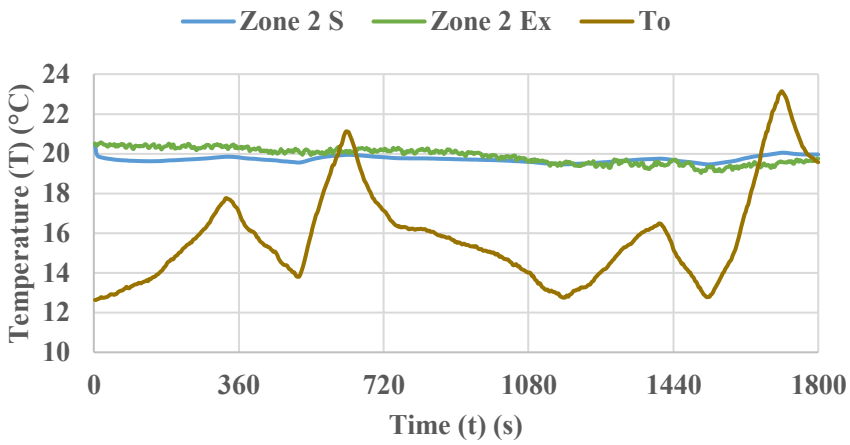
Zone 2 S
Zone 2 Ex
To
Temperature (T) (°C)
24
22
20
18
16
14
12
10
0
360
720
1080
1440
1800
Time (t) (s)

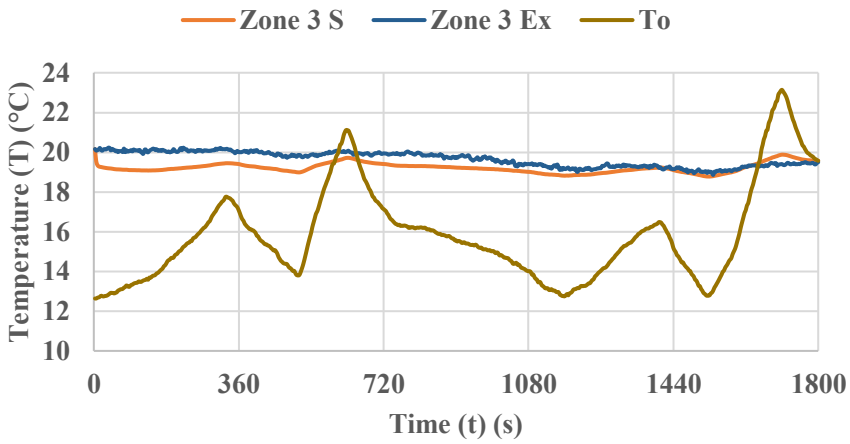
Zone 3 S
Zone 3 Ex
To
Temperature (T) (°C)
24
22
20
18
16
14
12
10
0
360
720
1080
1440
1800
Time (t) (s)

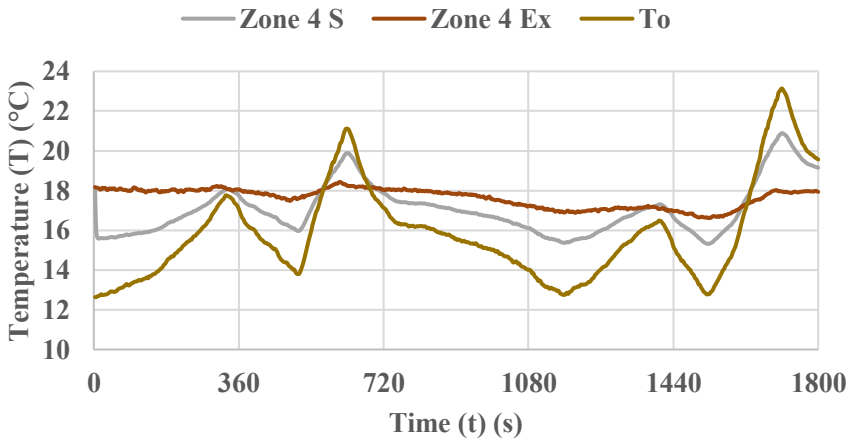
Zone 4 S
Zone 4 Ex
To
Temperature (T) (°C)
24
22
20
18
16
14
12
10
0
360
720
1080
1440
1800
Time (t) (s)

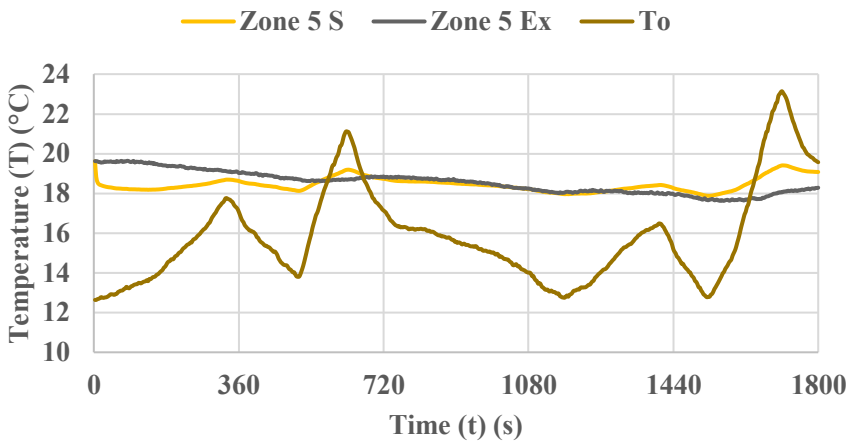


Appendix 4 Air temperature validation of sub-scale simulation in Ex s.4

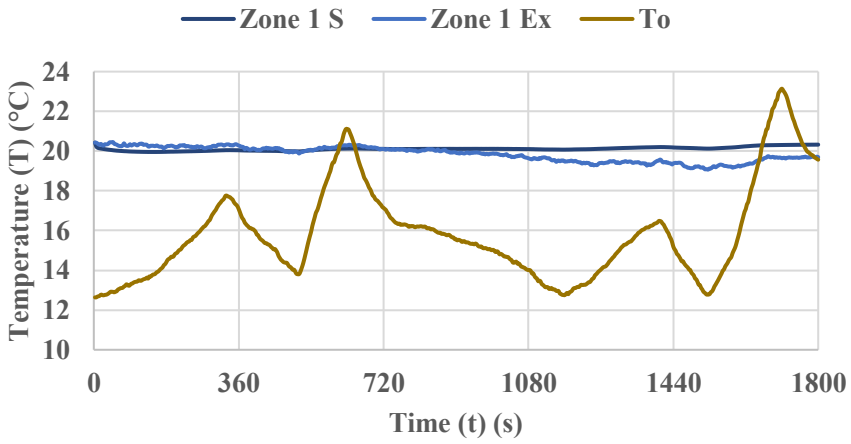

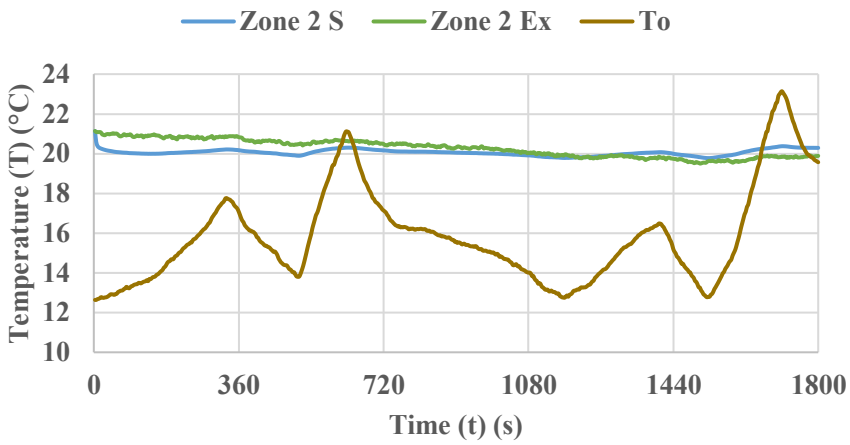
Zone 2 S
Zone 2 Ex
To
Temperature (T) (°C)
24
22
20
18
16
14
12
10
0
360
720
1080
1440
1800
Time (t) (s)

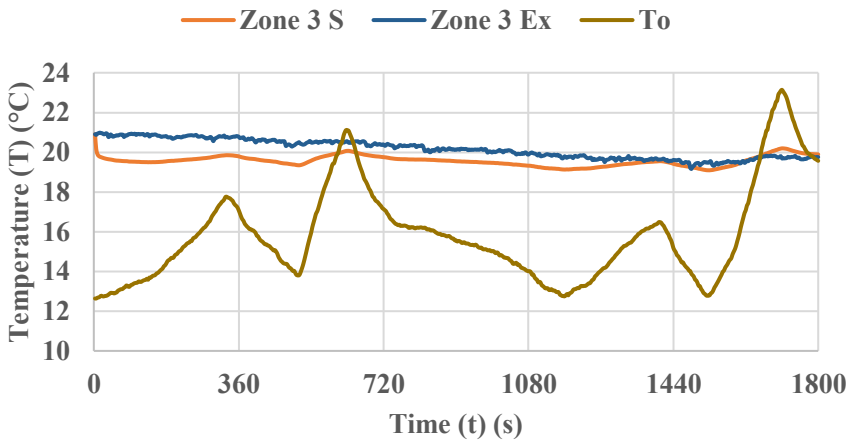
Zone 3 S
Zone 3 Ex
To
Temperature (T) (°C)
24
22
20
18
16
14
12
10
0
360
720
1080
1440
1800
Time (t) (s)

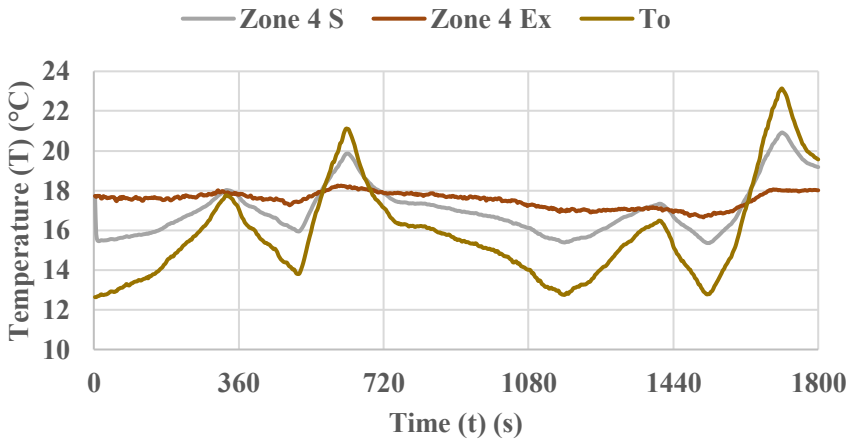
Zone 4 S
Zone 4 Ex
To
Temperature (T) (°C)
24
22
20
18
16
14
12
10
0
360
720
1080
1440
1800
Time (t) (s)

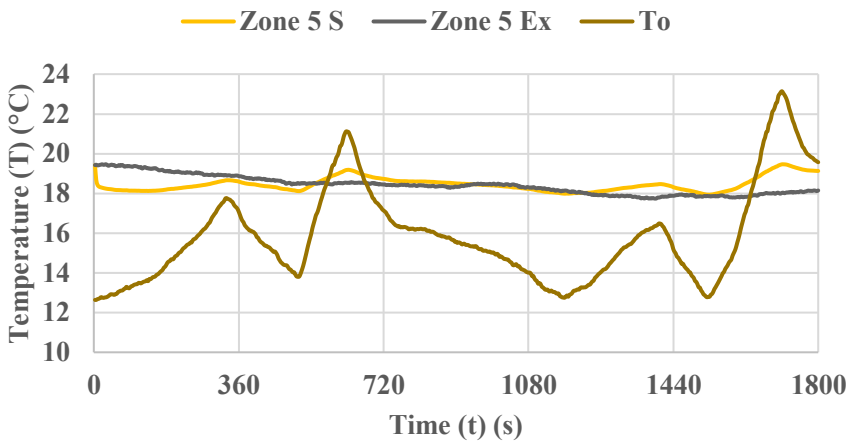


Appendix 5 Floor slab temperature validation of sub-scale simulation in Ex s.3

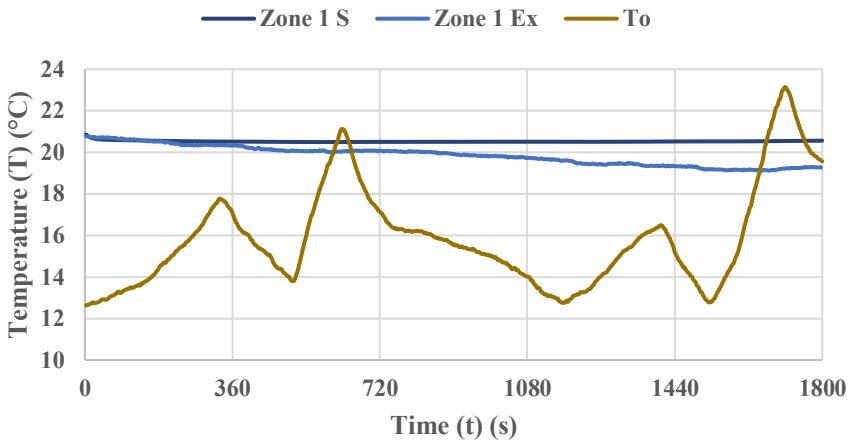

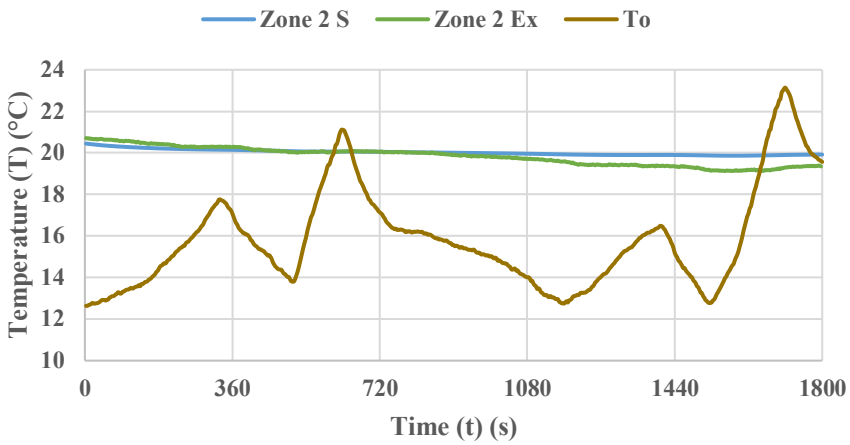
Zone 2 S
Zone 2 Ex
To
Temperature (T) (°C)
24
22
20
18
16
14
12
10
0
360
720
1080
1440
1800
Time (t) (s)

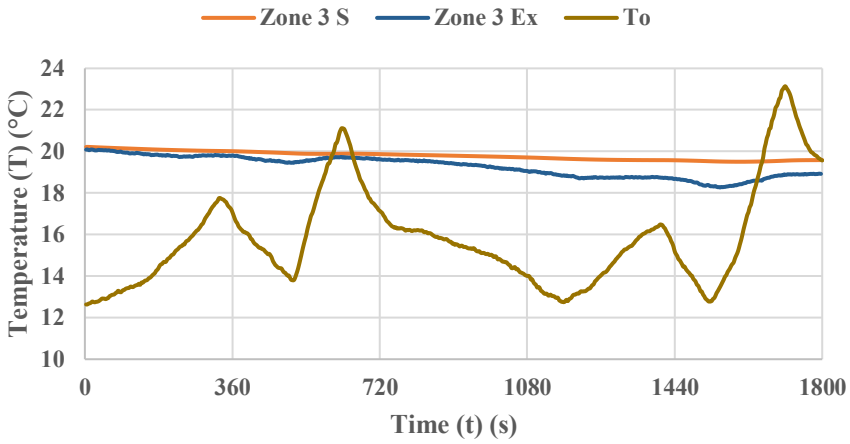
Zone 3 S
Zone 3 Ex
To
Temperature (T) (°C)
24
22
20
18
16
14
12
10
0
360
720
1080
1440
1800
Time (t) (s)

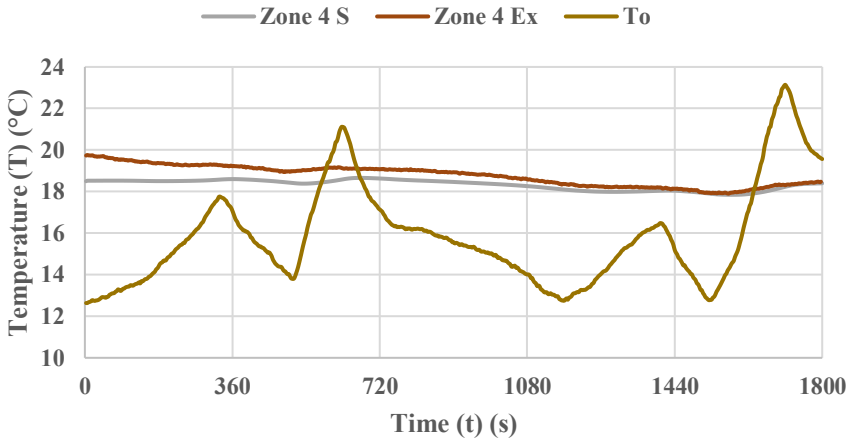
Zone 4 S
Zone 4 Ex
To
Temperature (T) (°C)
24
22
20
18
16
14
12
10
0
360
720
1080
1440
1800
Time (t) (s)

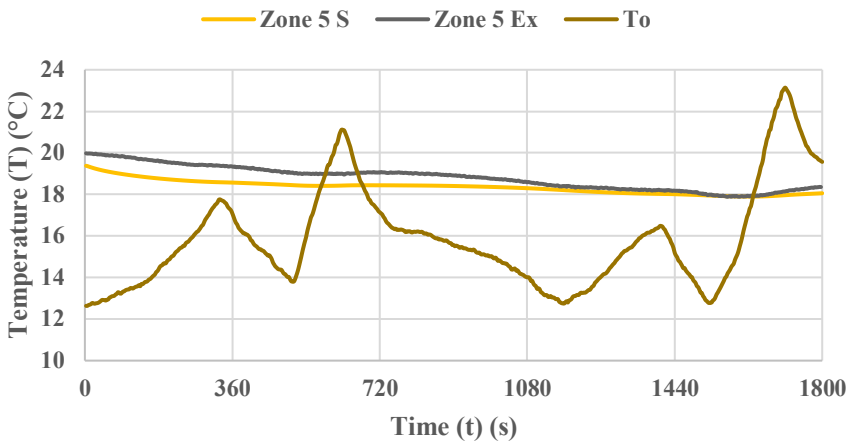


Appendix 6 Floor slab temperature validation of sub-scale simulation in Ex s.4

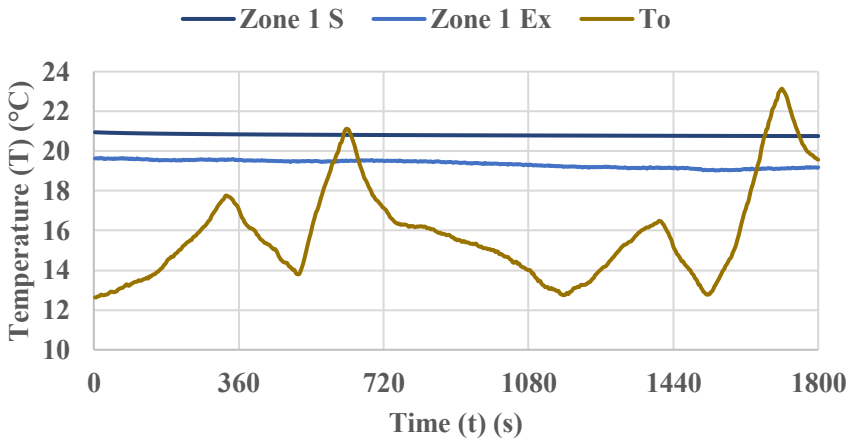

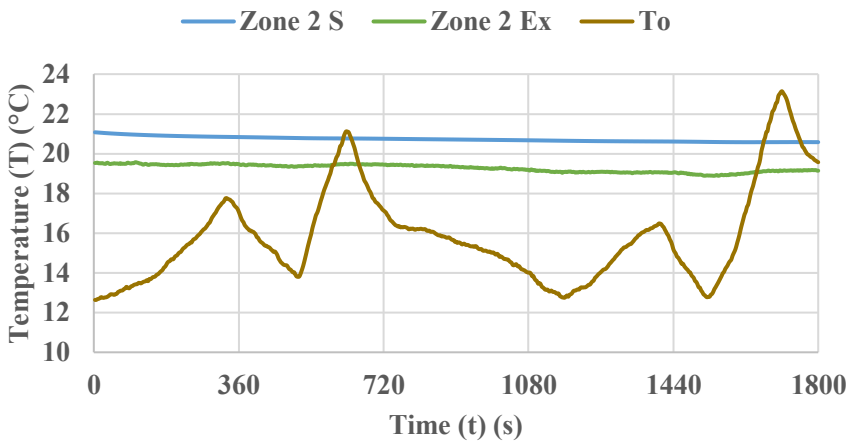
Zone 2 S
Zone 2 Ex
To
Temperature (T) (°C)
24
22
20
18
16
14
12
10
0
360
720
1080
1440
1800
Time (t) (s)

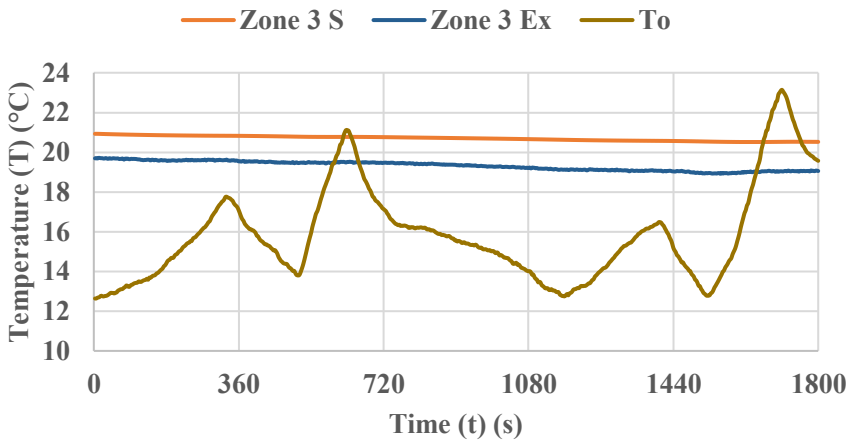
Zone 3 S
Zone 3 Ex
To
Temperature (T) (°C)
24
22
20
18
16
14
12
10
0
360
720
1080
1440
1800
Time (t) (s)

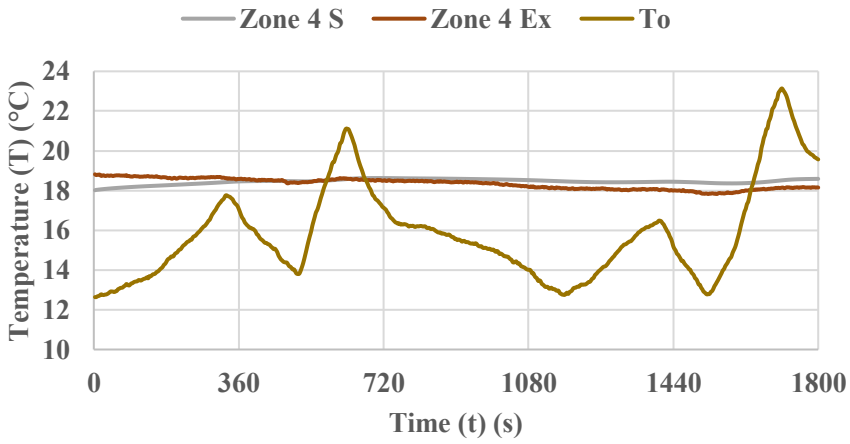
Zone 4 S
Zone 4 Ex
To
Temperature (T) (°C)
24
22
20
18
16
14
12
10
0
360
720
1080
1440
1800
Time (t) (s)

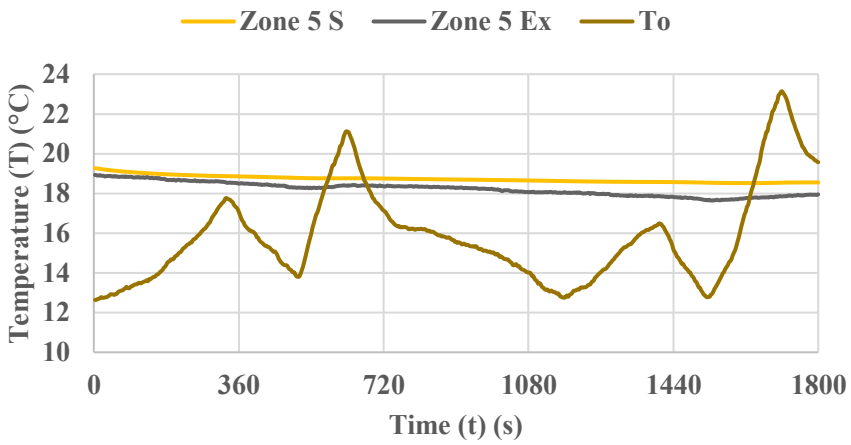


Appendix 7 Floor charge and discharge in experiments

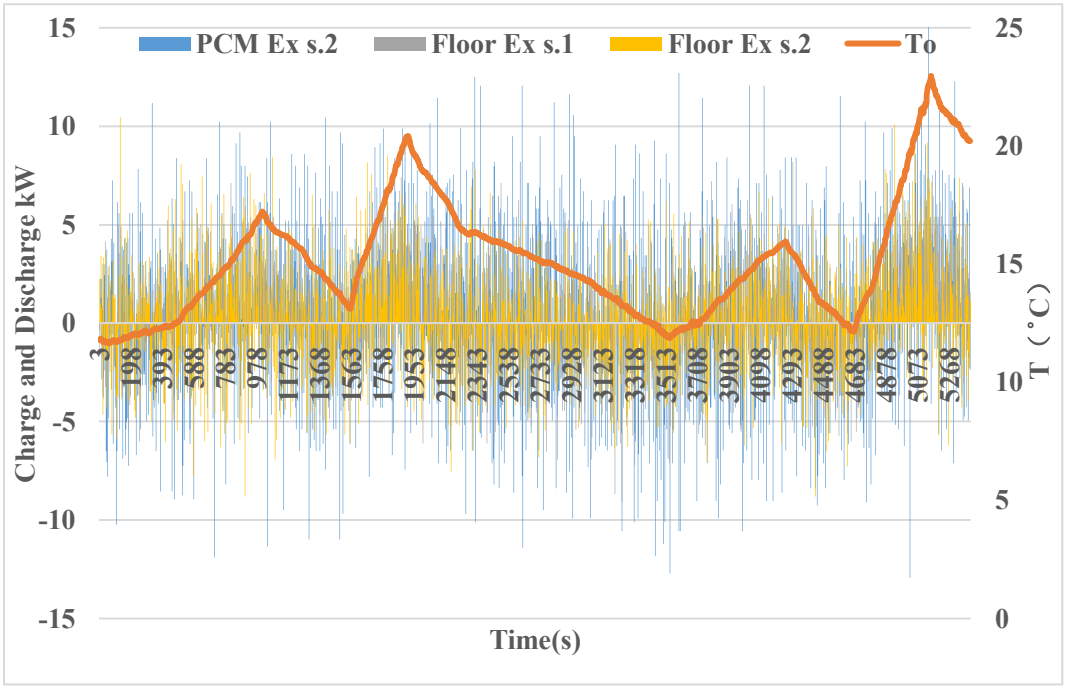

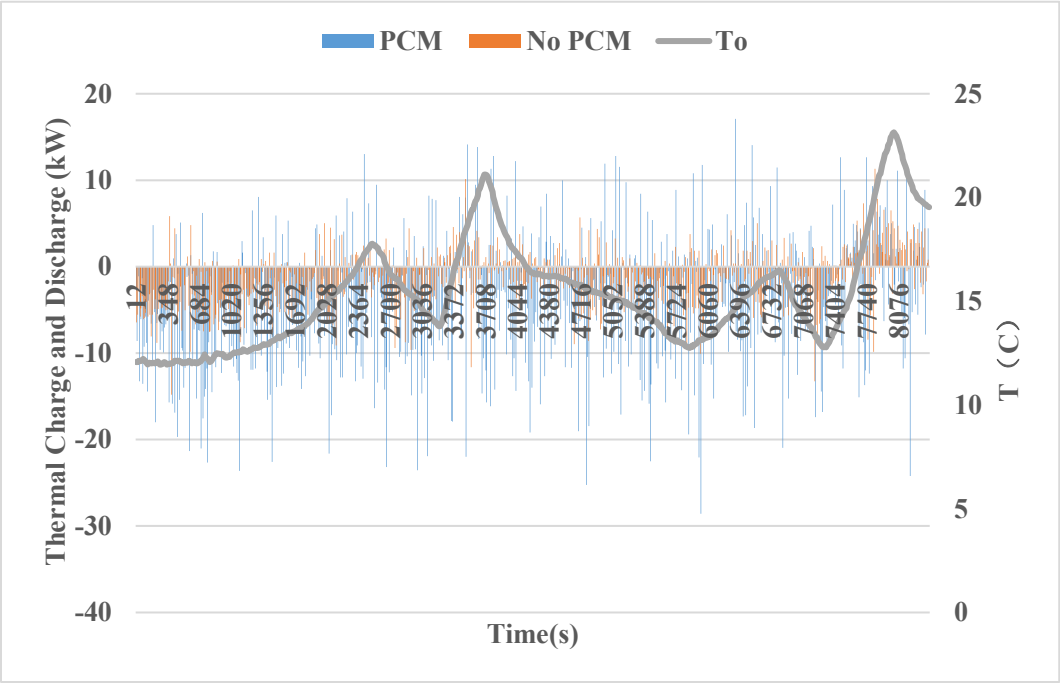
PCM
No PCM
To
Thermal Charge and Discharge (kW)
T（C）
Time(s)
20
10
0
-10
-20
-30
-40
25
20
15
10
5
0
12
348
684
1020
1356
1692
2028
2364
2700
3036
3372
3708
4044
4380
4716
5052
5388
5724
6060
6396
6732
7068
7404
7740
8076

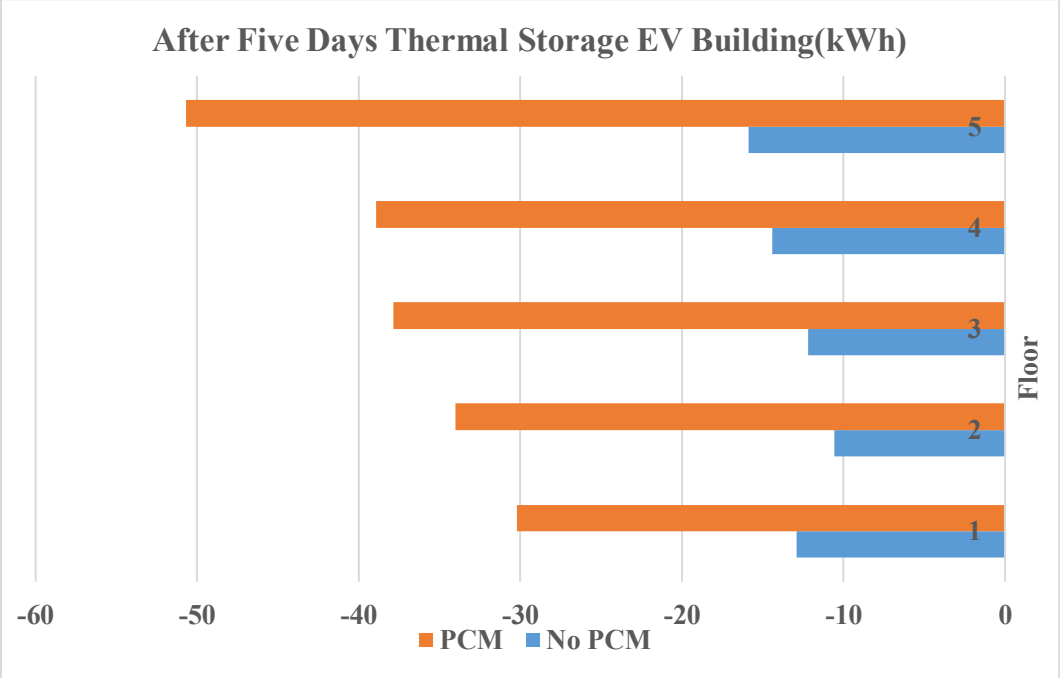
After Five Days Thermal Storage EV Building(kWh)
Floor
5
4
3
2
1
-60
-50
-40
-30
-20
-10
0
PCM
No PCM

Appendix 8 Ambient Temperature in Montreal.